UNIVERSITY OF SIENA

DEPARTMENT OF BIOTECHNOLOGY, CHEMISTRY AND PHARMACY

PhD School in Biochemistry and Molecular Biology

XXXIV Cycle

Coordinator: Prof.ssa Lorenza Trabalzini

Protein post translational modifications and diabetes.

Pro-inflammatory cytokines reshape lysin acetylome of rat clonal β cells and human pancreatic islets.

Candidate

Lorenzo Zallocco

Supervisor

Prof. Maria Rosa Mazzoni

SSD BIO/10

Academic Year 2021-2022

Index

I. List of Figures

shown. Each islet preparation was analyzed in duplicate. Statistical analysis was performed using a parametric paired t test. *, p<0.05.

Figure 13. A) Morphological change of INS-1E β cells after cytokine treatment. B) Growth ratio calculated as number of cells after treatment with (Cyto) or without (CTRL) cytokines/number of cells seeded. C) Total insulin content in treated (Cyto) and untreated (CTRL) cells. D) Insulin release after 19.7 mM glucose stimulation of Cyto and CTRL cells. Cyto and CTRL data were compared by parametric t test. *, p<0.05; ***, p<0.001.

Figure 14. Volcano plot of differentially expressed proteins with a cut-off of 1.3 for -$\log_{10}$ p-values and ± 0.584 for $\log_2$ Cyto/CTRL ratio values. The red dots represent the curated list of proteins showing significant changes.

Figure 15. Metascape enrichment analysis. Network of enriched terms are coloured by cluster ID. Nodes that share the same cluster ID are typically close to each other.

Figure 16. A) Volcano plot of differentially soluble proteins with a cut-off of 1.3 for -$\log_{10}$ p-values and ± 0.584 for $\log_2$ Cyto/CTRL ratio values. The red dots represent the curated list of proteins showing significant changes. B) Graphical representation of the correlation between significant variations of protein solubility and expression reported as $\log_2$ Cyto/CTRL ratio values with a cut-off of ± 0.584.

Figure 17. Metascape enrichment analysis. Bar graph of enriched terms coloured according to -$\log_{10}$ p-value.

II.   List of Table

III. List of acronymus

Diabete mellitus (DM)

Type I/II diabete mellitus (T1DM/T2DM)

Glucose transporter (GLUT)

Lactate dehydrogenase (LDH)

Tricarboxilic acid (TCA)

Dihydroxyacetone phosphate (DHAP)

Glycerol-3-phosphate (Gly3P)

Diacylglycerol (DAG)

Reactive oxygen species (ROS)

Nitric oxide (NO)

Interleukin (IL)

Interferon (INF)

Tumor necrosis factor (TNF)

Transforming growth factor β (TGF-β)

Nuclear factor-κ-light chain enancher of activated B cells (NF- κB)

Pancreas/duodenum homeobox protein 1 (PDX1)

Insulin gene enhancher protein 1, islet 1 (ISL-1)

Inducible nitric oxide synthase (iNOS)

Endoplasmatic reticulum (ER)

Signal transducer and activator of transcription 1 (STAT1)

Heat shock protein (HSP)

Apoptotic protease-activating factor 1 (APAF1)

BCL-2 interacting mediator (BIM)

Unfolded protein response (UPR)

Inositol-requiring enzyme 1α (IRE-1α)

PKR-like ER kinase (PERK)

Activating transcriprion factor 4 (ATF4)

X-BOX binding protein 1 (XBP-1)

C/EBP-homologous protein (CHOP)

Lysine acetyltransferase (KAT)

Lysine deacetylase (KDAC)

NAD^+-dependent deacetylase (SIRT)

Cyclin dependent deacetylase (CDK1)

Ataxia telangiectasia mutated (ATM)

Phosphatase and tensin homolog (PTEN)

RAC-α-serine/threonine protein kinase (AKT)

Pyruvate dehydrogenase acetyl transferring kinase isozyme 1 (PDK1)

Mechanicistic target of rapamycin complex (mTORC)

Rapamycin-insensitive companion of mTOR (RICTOR)

Superoxide dismutase (SOD)

TAR DNA-binding protein 43 (TDP43)

Acetyl-CoA synthase (ACSS)

Endoplasmic reticulum aminopeptidase 2 (ERAP2)

γ-interferon-inducible lysosomal thiol reductase (IFI30)

Transcription factor p65 (RELA)

Interferon regulatory factor 1 (IRF1)

Nuclear factor erythroid 2-related factor 2 (NRF2)

Peroxisome proliferator-activated receptor α (PPARα)

Retinoic acid receptor RXR α (RXRα)

Bone marrow stromal antigen 2 (BST2)

Antigen peptide transporter (TAP)

Reactive nitrogen species (RNS)

Peroxiredoxin 1 (PRDX1)

Thioredoxin reductase 1 (TXNRD1)

Thioredoxin interacting protein (TXNIP)

Voltage-dependent anion-selective channel protein (VDAC)

Hydroxyacyl-CaA dehydrogenase (HADH)

Endoplasmic reticulum chaperone BiP (GRP78/HSPA5)

High mobility group box 1 (HMGB1)

Post translational modification (PTM)

Nα-Acetyltransferase (NAT)

Histone acetyltransferase (HAT)

Histone deacetylase (HDAC)

Succinate dehydrogenase flavoprotein (SDHA)

DEAD-box RNA helicases (DDX)

Ubiquitin-fold modifier (UMF)

Interferon-induced protein with tetracopeptide repeats 2 (IFIT2)

ATP-binding cassette (ABC)

IV. Abstract

Type I diabetes mellitus (T1DM) is characterized by insulin deficiency due to β cells death caused by inflammation and immune reaction. Pro-inflammatory cytokines play a key role in T1DM pathogenesis by activating the pro-apoptotic pathway. Cytokine-activated NF-κB and STAT1 signalling also leads to oxidative stress and triggers the antigen presentation pathway. Stressful stimuli and self-defence responses combined cause mitochondrial dysfunction and endoplasmic reticulum (ER) stress, which progress to β cell functional impairments and death. Some molecular mechanisms involved in the progressive loss of functions are still unknown. In this contest, a study, which analyses proteomic changes of β cells upon cytokine prolonged exposure, can be useful.

The global effects of pro-inflammatory cytokines, IL-1β and INF-γ, on protein expression, Nε-acetylation, and thermal stability was studied using different proteomic approaches and β cell models (rat INS-1E cells and human pancreatic islets). At first, the impact of cytokines on β cell insulin secretion, survival and apoptosis activation was examined to confirm functional impairment. Differential expression proteomics showed that cytokines dysregulated the expression of many proteins, which are components of pathways involved in T1DM pathogenesis. The study of protein lysine acetylome highlighted 83 and 242 differentially modified proteins in human islets and INS-1E cells, respectively. Most proteins are related to metabolic, mitochondrial dysfunction, inflammation, and insulin secretion pathways. In INS-1E cells, an analysis of Proteome Integral Solubility Alteration (PISA) was also performed. This technique allowed to identify 504 proteins, which thermal stability was modified by cell exposure to cytokines. Many of these proteins participate to protein synthesis, protein trafficking, and antigen presentation or are directly involved in mediating cytokine effects. Overall, this multi-level proteomic analysis unveiled new potential players of cytokine-induced β cells dysfunction.

1. Introduction

1.1.   Diabetes Mellitus

Diabetes Mellitus (DM), which is a complex metabolic disease characterized by an inadequate control of glucose blood levels, represents a serious long-term condition impacting patient and family lives but also societies. In 2019, it was estimated that 450 million people were affected worldwide, and this number will double in the next 15-20 years [1]. Although the term DM collectively include a heterogenous group of metabolic disorders with chronic hyperglycaemia, the most prevalent forms are type 1 DM (T1DM) and type 2 DM (T2DM), which differ for pathogenetic mechanisms, presentation, and management. Whereas T2DM, which accounts for more than 90% of DM cases in adults, is characterized by insulin resistance and reduction of its secretion up to complete deficiency in T1DM insulin is absent or extremely low as consequence of β cell destruction in the pancreatic islets. The current notion is that in both DM types β cell dysfunction and death are pivotal processes albeit T1DM and T2DM pathogenetic mechanisms are completely different [2]. In fact, β cell dysfunction in T2DM is driven by metabolic unbalances while it is mediated by autoimmune mechanisms in T1DM, and the final β cell fate is also different with mild to moderate cell loss in the former and massive loss in the later.

Genetic, lifestyle and environmental factors concur to create a predisposition to DM development although the importance of each single factor varies depending on disease type. In T2DM, the genetic susceptibility in concert with lifestyle and diet is important for developing the disease. On the other hand, the genetic predisposition is the major factor involved in T1DM development. Genetic susceptibility of both DM types has a polygenic nature albeit with distinct genes implicated. Class II HLA alleles contribute to approximately 50% of T1DM genetic risk while the insulin gene (INS) and variable number tandem repeat loci transmit the next highest genetic risk [3; 4]. Other genetic loci or SNPs, mostly implicated in gene regulation, provide a small risk for the disease. The most recent data indicate that some loci directly affect β cell response to inflammation or cytokines whereas the previous prevalent idea was that they were exclusively involved in regulating immune cell functions [3; 4].

T2DM is mostly an adult disease linked to unhealthy lifestyles with a devious onset while T1DM typically affects children and adolescents, and the first clinical manifestations are often dramatic. However, young adults can also develop T1DM as well as T2DM has been diagnosed in overweight children and adolescents. The differential diagnosis relies upon two distinctive features of T1DM: 1) insulin deficiency and requirement of insulin therapy; 2) presence of anti-islet antigen autoantibodies, which are not pathogenic but present at the onset of hyperglycaemia in more than 90% of patients with the classical disease phenotype, (pediatric and adolescent patients). Anyway, T1DM presentation phase, which can range from modest hyperglycaemia to diabetic ketoacidosis, is preceded by two additional progressive phases of which the first one is initiated by a single or multiple events involving β cells followed by an autoimmune response [4].

1.2. Pancreas – anatomy and physiology

The pancreas, an organ of endodermal origin, is located behind the stomach in the upper left abdomen. It is surrounded by other organs including the small intestine, liver, and spleen. The wide part, called the head, is located at the junction between stomach and duodenum. Indeed, pancreas head occupies the concave part of the duodenal curve where it releases digestive enzymes (Figure 1). The central portion of the pancreas is formed by the neck and body while the thin end, which extends to the left side, is called the tail (Figure 1). Approximately 95% of pancreas consists of exocrine tissue that produces pancreatic enzymes needed for food digestion. The remaining tissue consists of endocrine cells, which form the islets of Langerhans. These clusters of cells, produce hormones regulating glycaemia but also pancreatic secretions [5].
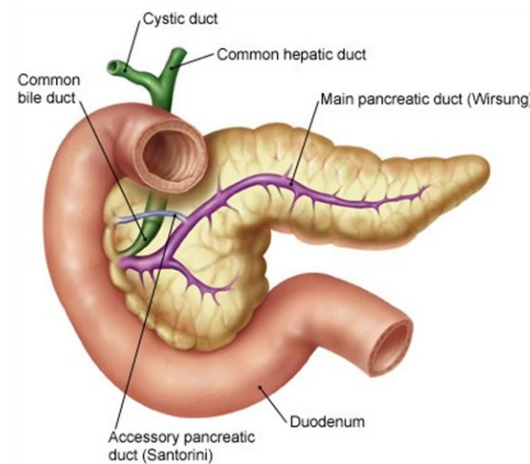
Figure 1. Graphical representation of human pancreas and its position within the duodenal curve

In humans, the pancreatic islets are spherical or ellipsoid with a mean diameter of approximately 100 μm, highly vascularised and surrounded by a collagen capsule (Figure 2). The estimated total number of islets in human pancreas ranges between 3.2 and 14.8 million [6]. Each islet consists of glucagon-producing α cells (~ 30%), insulin producing β cells (~ 60%), and a remaining ~ 10% that is made up of somatostatin-producing δ cells, pancreatic polypeptide-producing γ or PP cells, and ghrelin-producing ε cells. These different endocrine cells are randomly disturbed in human islets while rodent islets, which are broadly used in biomedical research, show a β cell core encircled by the other endocrine cells. The islet cells have distinct functions, but they operate within a complex network regulated by paracrine and neuronal signals to maintain energy homeostasis. Figure 3 shows a schematic representation of the paracrine interplay between human islet cells. More detailed information concerning the function of each cell type can be found in Da Silva Xavier (2018) [6].
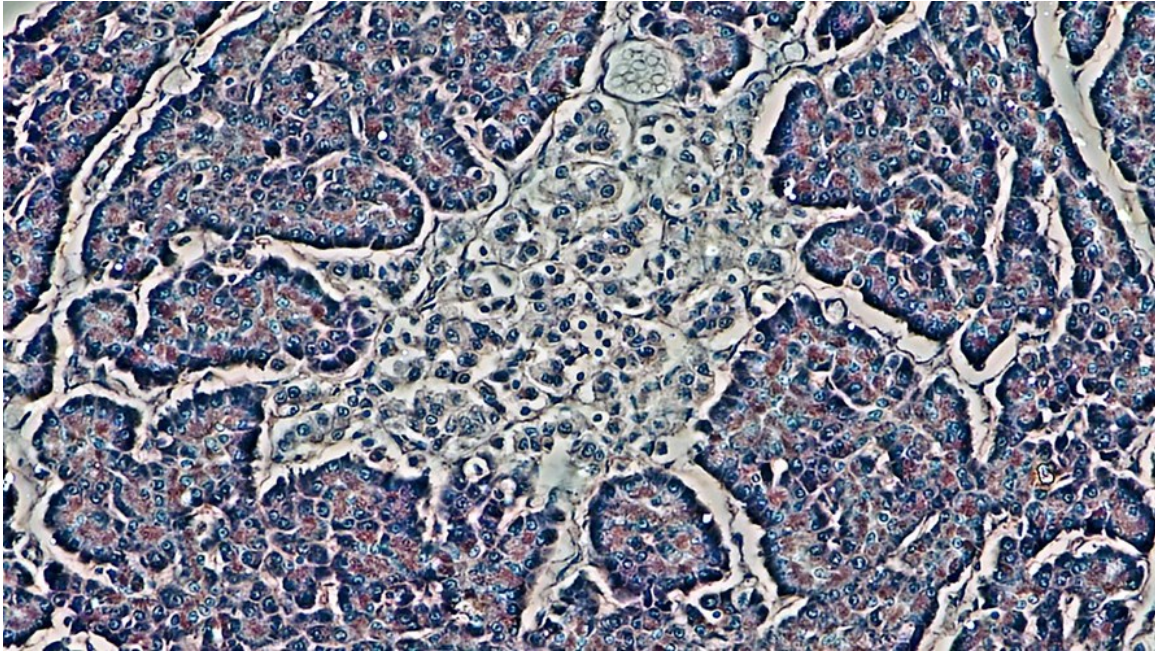
Figure 2. Histochemical image of a human pancreatic islet
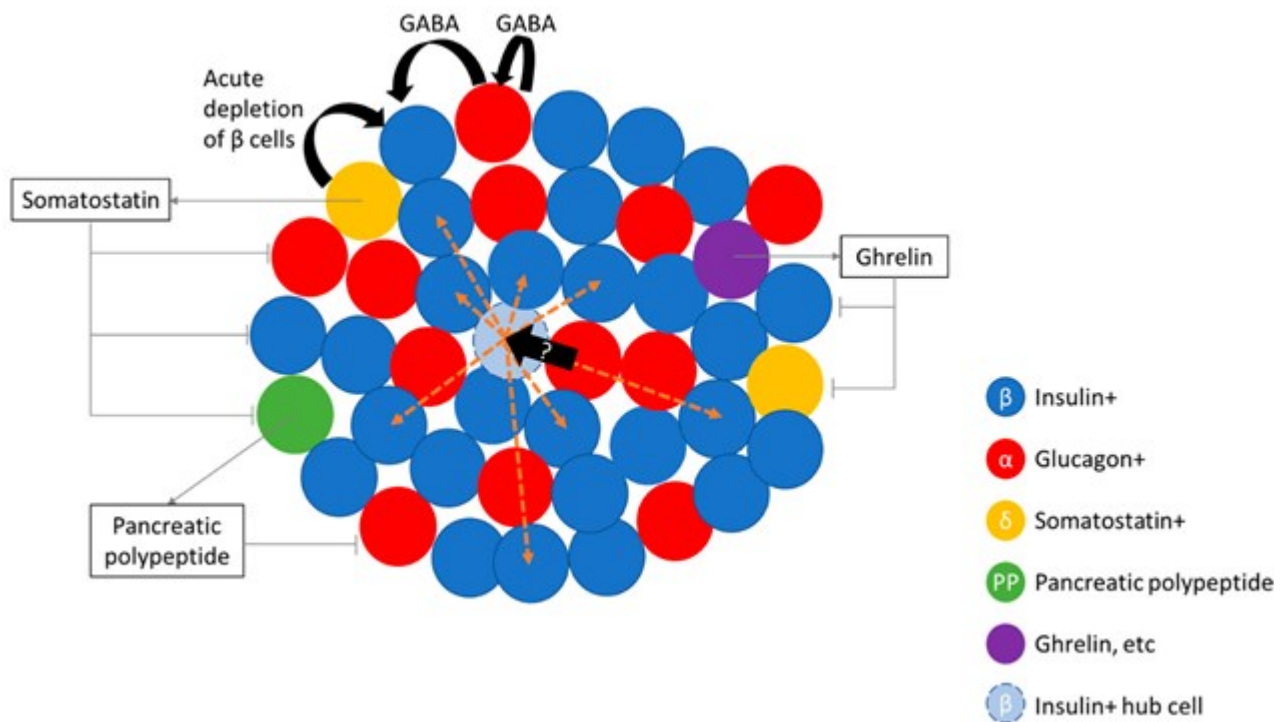
Figure 3. Schematic representation of the interplay between islet cells. Literature data suggest the possibility of α- and δ-cells transdifferentiation (solid black arrows) into β (like)-cells. The specialized hub β-cells influence (yellow arrows) the function of other β-cells [6].

1.2.1. β cells and insulin secretion

The secretory activity of β cells is mainly, but not exclusively, regulated by blood glucose levels. Insulin, packaged into secretory granules in a complex with zinc, is released in

response to high glucose concentrations although high concentrations of other organic molecule, such as fatty acids (mainly palmitate) and some amino acids, and stimulation by neurotransmitters can also induce the release. Incretins also enhance insulin secretion. On the other hand, somatostatin, secreted by δ cells, inhibits insulin secretion (Figure 3) as adrenalin, galanin, ghrelin, and leptin also do.

The β cells express the low affinity, high transport capacity glucose transporter 2, GLUT2 (also GLUT1 in human β cells), which is not regulated by insulin and allows a high flow of glucose into the cell. In the β cell cytoplasm, glucose is promptly phosphorylated to glucose-6-phosphate by glucokinase, a hexokinase subtype also expressed in liver cells, which has a low affinity for glucose (K_m, 6 mM) and is not inhibited by its product. These two properties allow the enzyme to function as a glucose sensor and maintain its activity even at high glycolysis load, linking the flow through the pathway to glucose extracellular levels [7].

Unlike liver cells, which also express GLUT2 and glucokinase, pancreatic β cells do not express lactate dehydrogenase (LDH) and so pyruvate, the endpoint of glycolysis, cannot be reduced to lactate and NADH oxidised to NAD^+ allowing the metabolic pathway to continue. At this point, pyruvate must take another route and enters mitochondria where it is converted into acetyl-CoA by pyruvate dehydrogenase and metabolized through the tricarboxylic acid (TCA) or Krebs cycle coupled with oxidative phosphorylation. This metabolic route ensures ATP production allowing an increase of intracellular ATP/ADP ratio that is required for the closer of ATP sensitive potassium channels (K_{ATP} channels), plasma membrane depolarization, opening of voltage dependent Ca^{2+} channels and influx of the ion with the increased intracellular Ca^{2+} concentration eventually leading to activation of exocytosis of insulin-containing granules (Figure 4). Same products derived in the anaplerosis and cataplerosis processes of TCA cycle can also behave as insulin secretion signals such as NADPH, malonyl-CoA and glutamate [8, 9]. In addition, glucose, through the glycolytic intermediate dihydroxyacetone phosphate (DHAP), can indirectly augment insulin secretion by the metabolic pathway leading to glycerol-3-phosphate (Gly3P) formation. In turn, Gly3P is important to produce factors coupled to lipid metabolism such

as long-chain acyl-CoA and diacylglycerol (DAG), which can increase insulin secretion (Figure 4) [10].
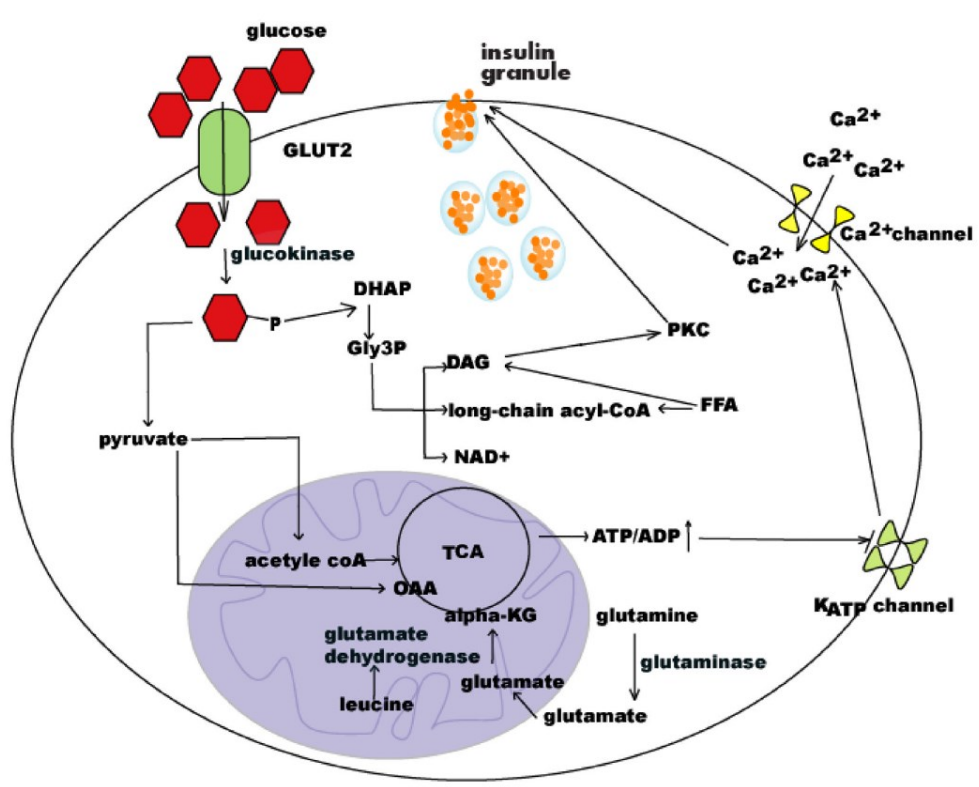
Figure 4. Schematic representation of insulin secretion pathway [11]

1.2.2. Mechanisms of β cell death in type 1 diabetes

The role of inflammatory cytokines in β cell dysfunction and death

In T1DM, pancreatic β cells are the target of an autoimmune attack with a strong inflammatory component called insulitis. Insulitis leads to a progressive reduction of β cell mass in a time that varies according to the aggressiveness of the inflammatory/immune response. Pancreatic islets and even whole pancreatic mass/volume also progressively decrease from the first stage to the advanced stage of the disease [4].

However, a more recent view widely accepted and supported by scientific evidences does not consider β cells as innocent spectators of their destruction by the immune assault but active participants through their responses to the stressful condition and intrinsic signals, which may stimulate and/or reinforce the immune response, such as HLA class 1 antigen

and chemokines overexpression, or neoantigen generation (e.g. mRNA splicing and translation infidelity variants, and novel post-translational modifications) [2; 4; 12]. In insulitic lesions, β cell death favoured by their limited equipment for self-defence against stress is mainly but not exclusively driven by macrophages and T cells direct contact and release of reactive oxygen species (ROS), nitric oxide (NO) and cytokines [13].

Cytokines are a large superfamily of soluble polypeptidic factors, which are produced by many cell types and regulate a wide variety of biological functions. Once secreted they can have effects on adjacent cells functioning as paracrine signals, on distant cells when released into the circulation (hormone-like or endocrine effects), and on the cell of origin itself (autocrine effect). Cytokines are essential mediators for the immune system being important for innate and adaptative response against pathogens. Therefore, they are secreted by immune cells but also produced and released by non-immune cells in response to pathogen infection or any damage compromising their integrity.

Cytokines have been classified into 6 groups: interleukins (ILs), chemokines, interferons (IFNs), tumour necrosis factors (TNFs), colony stimulating factors, and growth factors (transforming growth factor β, TGF-β). They act on target cells by binding and activating specific membrane receptors of diverse structure, which lead to activation of various intracellular signalling pathways. Cytokines with pro-inflammatory activity include several interleukins (IL-1α/β, IL-6, IL-11, IL-18), IFN-γ, and TNF-α/β. The role of proinflammatory cytokines in triggering β cell functional impairment and even death is corroborated by experimental observations. In fact, *in vitro* experiments have shown that β-cell exposure to IL-1β with or without IFN-γ causes reduction of glucose-induced insulin release due to decrease of insulin granule binding and fusion to the cell membrane [14]. Moreover, under the pressure of prolonged treatments with IL-1β plus IFN-γ and/or TNF-α, the functional damage evolves into β cell death [13].
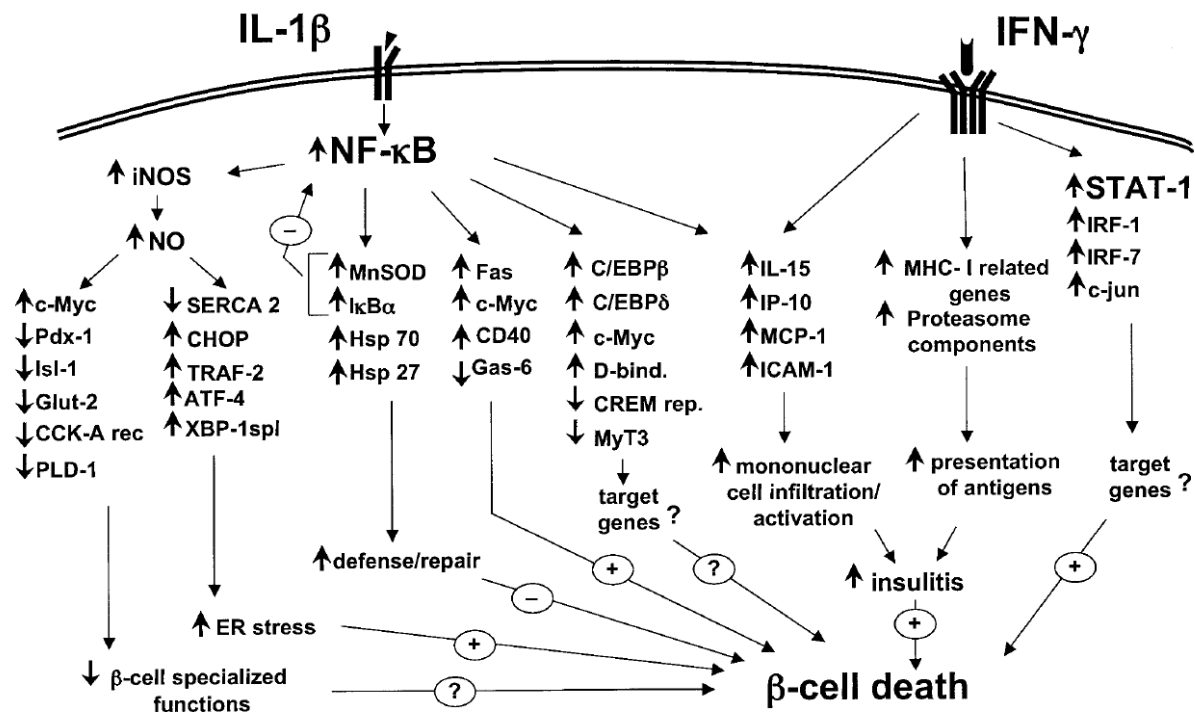
Figure 5. Schematic representation of cytokine effects in β cells during T1DM development. [15]

IL-1β and IFN-γ cause activation of numerous signalling pathways leading to the expression of stress response genes, which are either protective or deleterious for β cell survival (Figure 5). IL-1β but also TNF-α activate a prototypical proinflammatory signaling pathway, the nuclear factor kappa-light-chain-enhancer of activated B cells (NF-κB) pathway, which plays a major role in the expression of proinflammatory genes including cytokines, chemokines, and adhesion molecules. In rat β cells, NF-κB has been found to also induce the expression of stress related genes, downregulate the expression of transcription factors for β cell differentiation and function (e.g., Glut-2, Pancreas/duodenum homeobox protein 1 (PDX-1) and Insulin gene enhancer protein ISL-1, Islet-1 (Isl-1)), and regulates the expression of inducible nitric oxide synthase (iNOS) [16]. Of note, iNOS-mediated NO formation is directly responsible for the expression modification of approximately 50% of cell genes regulated by 8-24 h cytokine treatment [17]. All literature data point out the pivotal role of IL-1β-activated NF-κB in controlling multiple gene regulatory networks that affect β cell differentiated state and endoplasmic reticulum (ER) Ca^{2+} homeostasis, as well

as attract and activate (chemokines and cytokines production and release) of immune cells and contribute to β cell apoptosis (Figure 5).

Whereas IL-1β is sufficient to increase the expression of iNOS and thus the production of NO in rat β cells the simultaneous presence of IL-1β and INF-γ is required to upregulate the enzyme expression in mouse and human β cells [18; 19]. INF-γ causes activation of the signal transducer and activator of transcription 1 (STAT-1), which modulates the expression of a variety of genes with different functions (Figure 5). STAT-1 also mediates the potentiating effect of IFN-γ on IL-1β–induced iNOS expression [16; 19].

The intracellular accumulation of NO can lead to various deleterious effects for cells including inactivation of cytosolic and mitochondrial aconitases by targeting their iron-sulfur centers [20]. The later isoenzyme, which is more susceptible to NO-induced loss of catalytic activity, catalyses the isomerization of citrate to isocitrate in TCA cycle, an essential oxidative pathway for ATP production and therefore for insulin secretion in β cells [21]. Experimental observations have shown that a 36-h treatment of rat β cells or islets with IL-1β induces irreversible inhibition of mitochondrial aconitase activity and insulin secretion while for shorter exposure times this inhibitory effect is reversible [22]. As prove of concept implicating NO production, cotreatment of rat β cells and islets with IL-1β plus an iNOS inhibitor reduces the recovery time and prevents inhibition of protein synthesis, respectively [23]. Concerning the mechanisms involved in rat β cells recovery, the authors have proposed the induction of protective factors by IL-1β [23]. Such factors might be represented by heat shock proteins (HSPs) since Kolb *et al.* have reported that overexpression of human HSP70 in rat β cells confers resistance NO-mediated damage [24]. Moreover, further studies in rat islets have shown that IL-1 stimulates HSP70 expression, which is prevented by treatment with an iNOS inhibitor. This observation indicates that NO endogenous production is required for IL-1-induced HSP70 expression. In human islets, other HSPs or factors seem to be involved in preventing NF-κB activation and iNOS expression induced by IL-1 plus IFN-γ treatment [25].

Prolonged exposure of pancreatic islets to proinflammatory cytokines causes their irreversible degeneration [22]. The functional impairment of β cells further evolves to death [13]. Thus, the fate of β cells following cytokines exposure depends on the duration and intensity of the distress on a complex network of genes through NF-κB and STAT-1 pathway activation as shown in Figure 5.

Mechanisms of cytokine-induced β cell apoptosis

In eukaryotic cells, mitochondria perform the key function of ATP production, but they also trigger cell death by apoptosis. Pancreatic β cells particularly depend by mitochondrial ATP production for the functional activity and survival [26].

Members of the BCL-2 protein family act as crucial regulators of the intrinsic (mitochondrial) apoptotic pathway [27]. The family includes pro-survival proteins, pro-apoptotic multi-BCL-2 homology (-BH) domain proteins (BAK, BAX, BOK), and pro-apoptotic BH3-only proteins (BAD, BID, BIM, BLK, BMF, DP5, NOXA, PUMA) [28]. These proteins interact and the balance between anti- and pro-apoptotic proteins decides the cell fate. The BH3-only proteins can trigger apoptosis by direct activation of BAX/BAK or attaching to pro-survival BCL-2 proteins and thus preventing their inhibition of BAX/BAK [29; 30]. Activated BAX and BAK oligomerize and form pores through the mitochondria outer membrane with the consequent release of cytochrome c, which binds to apoptotic protease-activating factor 1 (Apaf-1) causing apoptosome formation and resulting caspase 9 activation, which in turn activates caspases 3 and 7, the executors of cell death. [31].

Several studies have recognised Bcl-2 interacting mediator (BIM) of cell death as a pivotal factor of cytokine-induced β cell apoptosis. In pancreatic islets, TNF-α and IFN-γ upregulate BIM expression through STAT-1-mediated transcription stimulation thus triggering apoptosis [32]. Moreover, IL-1β in combination with IFN-γ leads to β cell apoptosis via induction of a transcription factor functioning as another activator of BIM expression and the release of BIM mediated by anti-apoptotic proteins (A1, BCL-2, and MCL-1) [33; 34]. Cytokines also trigger ER stress of β cells, which in turn activates the

mitochondrial apoptotic pathway [35; 36]. Pancreatic β-cells with the enormous capacity of insulin synthetise and release have a special need of molecular mechanisms controlling protein folding and preventing of unfolded protein accumulation. Under physiological conditions, elements of the unfolded protein response (UPR) exert a beneficial regulation while they trigger β cell dysfunction and apoptosis under a situation of chronic stress [37]. IL-1β and IFN-γ perturbate ER homeostasis through NO-mediated depletion of ER calcium and inhibition of ER chaperones, respectively, resulting in unfolded protein accumulation and activation of a specific ER stress response or UPR [38; 39]. This stress response, which consists of translational attenuation, upregulation of ER chaperones, and degradation of misfolded proteins, tries to restore ER homeostasis but in the case of a persistent and severe stress the apoptotic program is activated. In β cells, cytokines cause activation of various components of UPR, including activation of inositol-requiring enzyme 1α (IRE-1α) and PKR-like ER kinase (PERK)/activating transcription factor 4 (ATF4), processing of X-box binding protein 1 (Xbp1) mRNA and induction of C/EBP-homologous protein (CHOP) expression [38]. Whereas the ER transmembrane proteins, IRE-1α and PERK, function as sensors of ER stress xbp1 and CHOP are transcription factors connecting sensor activation to nuclear transcription of target genes (Figure 6). Since CHOP is involved in ER stress-induced apoptosis activation of the PERK/ATF4/CHOP pathway represents a pro-apoptotic signaling. On the other hand, numerous observations implicate IRE-1α in both adaptation pro-survival and pro-apoptotic responses [40]. Of note, cytokines do not activate ATF6, another sensor of ER stress, and induce the expression of the endoplasmic reticulum chaperone BiP (GRP78/HSPA5), thus depriving β cells of another important defense against ER stress [38]. An overview of the UPR response is presented in Figure 6.
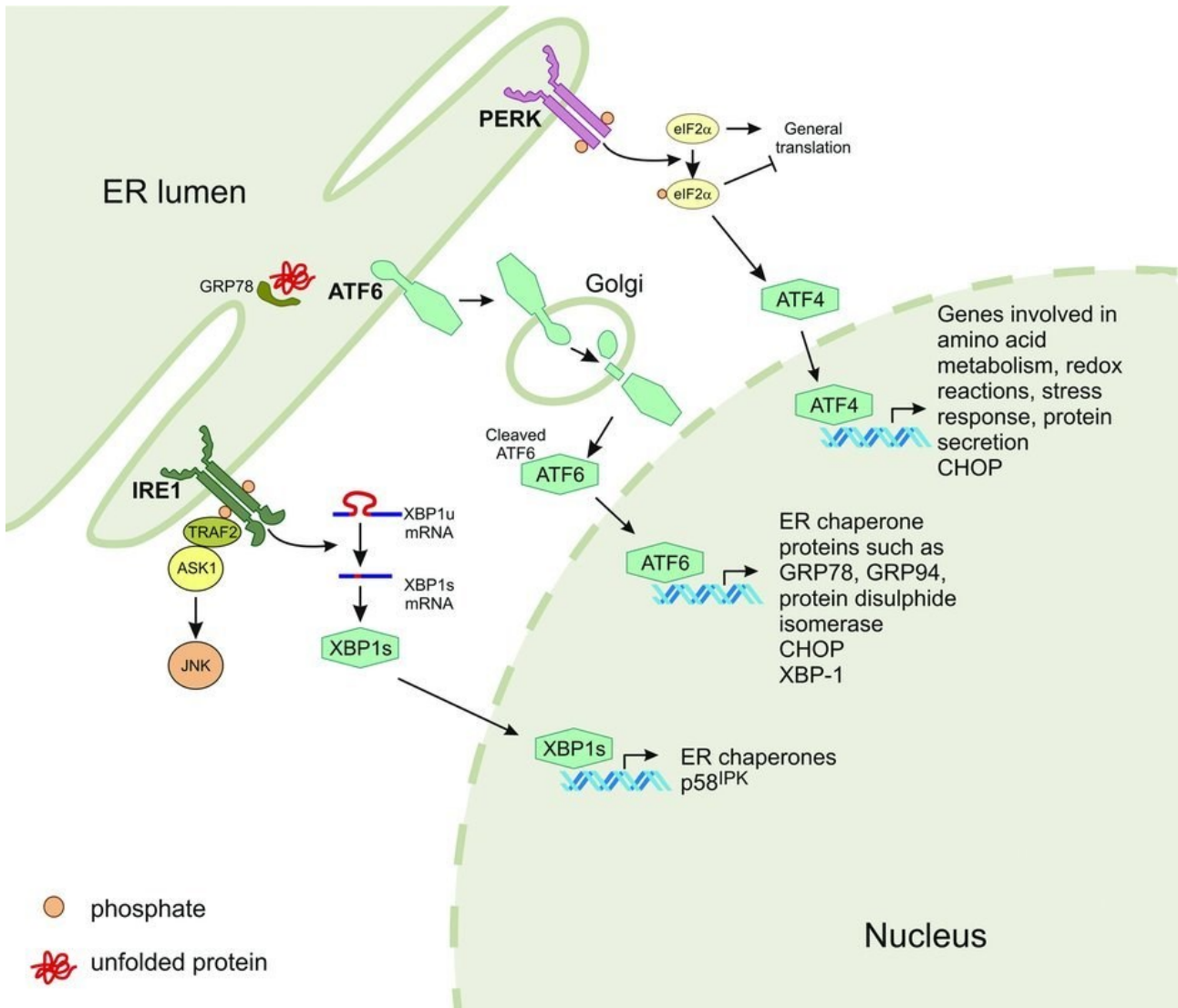
Figure 6. Representation of UPR signalling. Unfolded proteins cause dissociation of BiP/GRP78 from IRE-1, ATF6 and PERK leading to their activation. PERK and IRE1 oligomerise and self-phosphorylate. All three sensors activate distinct pathways, which lead to gene expression [40].

Cytokine-induced β cell death by necrosis

Necrosis is an unregulated type of cell death, which does not need energy or caspase activation as the programmed cell death by apoptosis does. Whereas apoptosis is characterized by an ordered degradation of cellular proteins and organelles with maintenance of plasma membrane integrity necrosis is characterized by the loss of membrane integrity and leakage of cellular contents associated to an inflammatory response. Steer *et al.*, have reported that IL-1 promotes the release of the high mobility group

box 1 (HMGB1), a marker of necrosis, from β cells in a NO-dependent manner [41]. Other studies have been carried out with the aim of clarifying whether cytokines lead to cell death by apoptosis or necrosis, but a clear and unambiguous response has not been identified yet.

1.3.   Proteomics

The suffix "omics" is used to identify a group of biochemical disciplines that aim to study and characterize molecules of biological samples on a large-scale. Each branch studies a specific biochemical aspect of the sample, for example genomics, transcriptomics, metabolomics, and so on, up to proteomics, which aims to study the proteome.

The term proteome refers to the sum of all the proteins in a cell, tissue, or organism. Therefore, proteomics is the science that studies such proteins in relation to their biochemical properties and functional roles, and how their quantities, modifications, and structures change during growth and in response to internal and external stimuli. This science has numerous practical applications such as discovery of disease protein signature and associated pathways, novel drug targets, and diagnostic/prognostic biomarkers. The various branches of the proteomic science allow to obtain different information that combined provide more in-depth knowledge of proteins [42; 43].

1.3.1. Proteomics and post-traslactional modifications (PTMs) of proteins

The study of protein PTMs is one of the most interesting and fascinating field of proteomics. There are more than 400 different types of PTMs and each one is linked to the modulation of protein activity, mobility, and so on, allowing cells to quickly react and adapt to internal and external stimuli. PTMs can occur by direct chemical reactions or be mediated by enzymatic reactions [44]. In addition, they can be irreversible (proteolytic cleavage) or reversible (modifying group additions) but all are covalent processing events. A form of PTM can occur in a single type or multiple amino acids leading to changes in the chemical properties of the modified site. PTMs can affect a wide variety of protein behaviors and properties such as enzyme function and assembly, protein solubility, folding, localization

and lifespan, protein–protein interactions, molecular trafficking, and receptor activation. Hence, these modifications are involved in modulating numerous biological processes including signal transduction, gene expression regulation, gene activation, DNA repair and cell cycle control, and their disruption can consequently lead to diseases. More detailed information on protein PTMs can be found in Ramazi and Zahiri (2021) [45].

The most studied and characterized PTM is phosphorylation, but in recent years other modifications have been deeply investigated, mainly thanks to the improvement of mass spectrometry techniques. The other top PTMs studied include acetylation, ubiquitylation, methylation, N-glycosylation, O-glycosylation, SUMOylation, S-palmitoylation, N-myristoylation, prenylation, and sulfation [45]. The main protein PTMs are phosphorylation, acetylation, and ubiquitination, accounting for more than 90% of all reported PTMs.

Protein acetylation normally occurs in three distinct forms, Nα-acetylation, Nε-acetylation, and O-acetylation, which combined make up the cellular acetylome. Whereas O-acetylation at serine and threonine slightly contributes to the acetylome Nα-acetylation and Nε-acetylation are the major components. The mechanism of protein acetylation involves the transfer of an acetyl group from acetyl-CoA to a residue of the polypeptide chain.

In humans, 80-90% of all proteins become co-translationally acetylated by the addition of an acetyl group to the α-amino group of the N-terminal amino acid [46]. This irreversible modification can be catalysed by different enzymatic complexes, called Nα-acetyltransferases (NATs) (Figure 7), which show distinct subustrate specificity although some redundancy has been described. In humans, a total of 6 different NATs has been reported [47]. Lastly, Nα-acetylation has been also described to occur as a PTM.
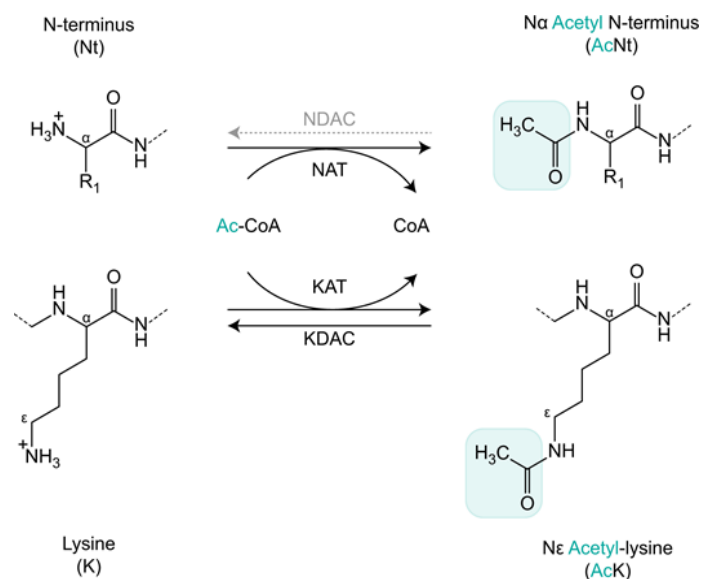
Figure 7. Schematic representation of N-terminal acetylation and ε-lysine acetylation [48].

The other common type of protein acetylation is the Nε-acetylation, in which the acetyl group is added to the ε-amino group of lysine. Acetylated lysine residues were first discovered in histones and thereafter the enzymes catalysing Nε-acetylation and -deacetylation were called histone acetyltransferases (HATs) and histone deacetylases (HDACs), respectively [49]. However, lysine acetylation is not exclusively limited to histones [50] and over the years at least ten of thousands of non-histone proteins have been found Nε-acetylated in various organisms. Therefore, the enzymes have been renamed lysine acetyltransferases (KATs) and lysine deacetylases (KDACs) (Figure 7 and Figure 8). Unlike Nα-acetylation, Nε-acetylation is reversible, tightly regulated, and can also occur through non-enzymatic reactions as happen in mitochondria [51]. Proteomic analysis has lighted upon the widespread Nε-acetylation of proteins in diverse cellular compartments. Acetylation is directly linked to the levels of acetyl-CoA, which is a key metabolite for essential cellular functions. Since acetyl-CoA is membrane impermeable and mitochondrial and non-mitochondrial pools of acetyl-CoA are produced independently, cell compartment-specific levels of the metabolite can locally drive protein Nε-acetylation. In Figure 8b an overview of Acetyl-CoA generation in mitochondria, cytoplasm and nucleus is shown. Fluctuations of acetyl-CoA levels due to dietary variations correlate with changes in protein

Nε-acetylation levels, providing an additional hint that acetyl-CoA acts as a rate-limiting factor for most acetylation events [52].

As mentioned above KATs catalyze the enzymatic Nε-acetylation of proteins while KDACs catalyze the inverse reaction (Figure 7 and Figure 8A). In humans, the number of KATs has not been exactly defined yet, but most of 13 well characterized enzymes are grouped into three families (Figure 8C). The other KATs are rather dissimilar to each other [51]. The human 18 KDACs have been classified into two major categories: Zn^{2+}-dependent HDACs and NAD^+-dependent deacetylases or sirtuins (SIRTs) (Figure 8D). The Zn^{2+}-dependent HDACs, also known as the classical HDACs or classical KDACs, have been further divided into 4 subclasses on the base of sequence similarities and phylogenetic conservation (Figure 8D). Both classical KDACs and sirtuin deacetylases, which are also known as class III KDACs, localize to different cellular compartments, including nucleus (class I and IV KDACs, SIRT1, SIRT6 and SIRT7), cytoplasm (class IIb KDACs and SIRT2), and mitochondria (SIRT3, SIRT4 and SIRT5). In cells, KAT and KDAC enzymatic activities, which are precisely regulated by acetyl-CoA and NAD^+ levels, respectively, are well balanced so to ensure the correct functioning of complex protein networks involved in many cellular processes.
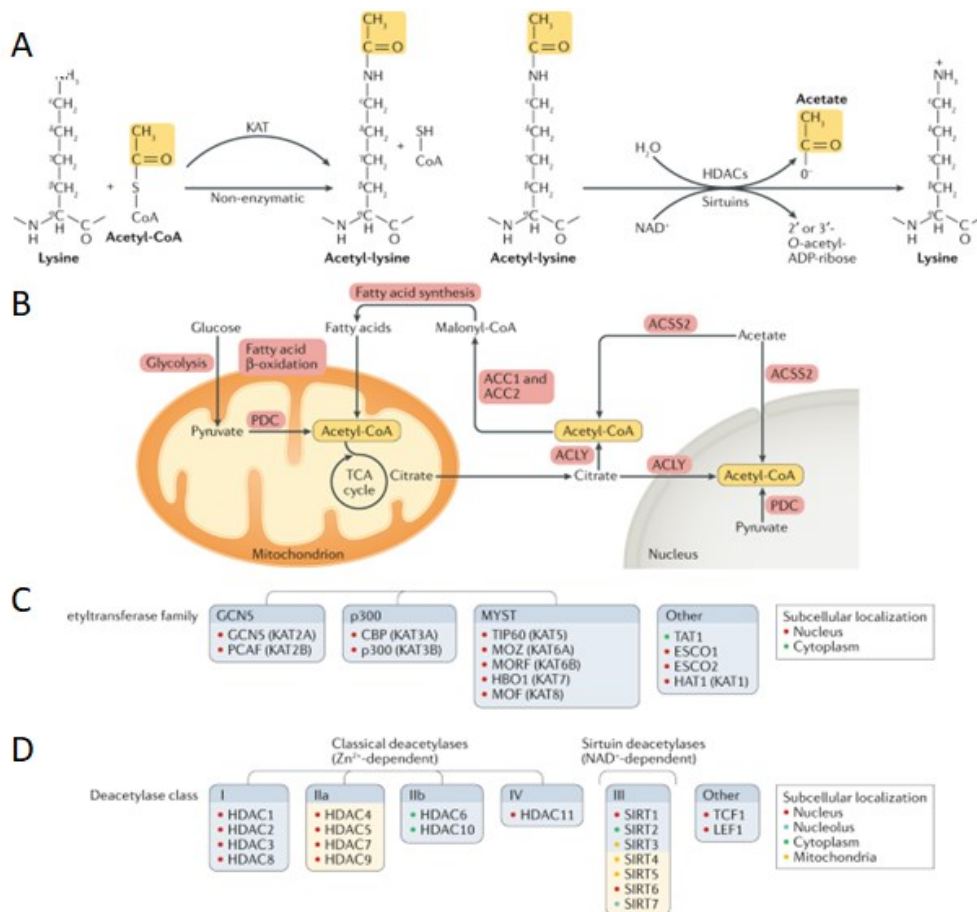
Figure 8. The network of reversible Nε-acetylation. ***a)*** *Reactions of lysine acetylation and deacetylations catalyzed by KATs and classical KDACs or SIRTs, respectively.* ***b)*** *Cellular compartments, in which acetyls-CoA is produced, and the enzymes involved. c) KAT families and subcellular localization of the various KATs.* ***d)*** *KDAC classes and subcellular localization of the various HDACs and SIRTs. The yellow background highlights those KDACs, which lack appreciable deacetylase activity (class IIa) or target other types of acylations. [Adapted from* 51]

1.3.2. Functional role of Nε-acetylation

Nε-acetylation of proteins is significant for the modulation of several cellular pathways, which encompass gene expression, signalling, and metabolism. The importance of this PTM is also exemplified by the fact that its dysregulation is associated with various human diseases, including cancer, neurological, and metabolic diseases. Lysine acetylation is evolutionary conserved from *Escherichia Coli* (*E. Coli*) to humans [53]. The total number of Nε-acetylated proteins and site increases with the complexity of the organism [54; 55].

Protein Nε-acetylation is a major regulator of gene transcription. In fact, most of the canonical KATs localize to the nucleus and function as transcription co-activators. The onco-suppressor p53 has been the first transcription factor described to be acetylated. This PTM

regulates p53 binding to DNA, stability, and interaction with other proteins. Overall, lysine acetylation is involved in regulating more than 100 non-histone nuclear proteins, including transcription factors, transcriptional co-activators, and nuclear receptors [51]. Lysine acetylation also modulates the activity of several proteins involved in cell cycle regulation [e.g. cyclin-dependent kinase 1 (CDK1), CDK2, Aurora kinases A, and B] and DNA damage repair [e.g. kinase ataxia telangiectasia mutated (ATM)]. Among the proteins of the signaling systems, Nε-acetylation of the phosphatase and tensin homolog (PTEN) at two distinct sites positively and negatively regulate its activity while acetylation of the RAC-alpha serine/threonine-protein kinase (AKT) and Pyruvate dehydrogenase acetyl-transferring kinase isozyme 1 (PDK1) in their PH domains prevents their membrane localization and activation. Moreover, lysine acetylation of the mechanistic target of rapamycin complex 2 (mTORC2) subunit rapamycin-insensitive companion of mTOR (RICTOR) increases mTORC2-mediated phosphorylation of AKT promoting cell proliferation [51]. Other major biological processes are modulated by non-histone protein Nε-acetylation, including protein folding, cytoskeleton organization, protein aggregation, autophagy, RNA processing and stability. The role of lysine acetylation in protein aggregation is exemplified by various neurodegenerative diseases characterized by accumulation of protein aggregates. Indeed, some aggregation prone proteins are Nε-acetylated such as Huntingtin (Huntington disease), tau (Alzheimer disease), superoxide dismutase (SOD1), and TAR DNA-binding protein 43 (TDP43) (Atrophic Lateral Sclerosis, ALS). This PTM affects their aggregation (more details in: [51]).

The activities of more than 40 enzymes localized to various cellular compartments are regulated by Nε-acetylation. This PTM has been detected on enzymes of the glycolytic pathway, all enzymes of the TCA cycle, most respiratory chain complex proteins including ATP synthase, and enzymes involved in amino acid and fatty acid metabolism. Many metabolic enzymes are inhibited by lysine acetylation such as acetyl-CoA synthetase 1 (ACSS1), ACSS2, and glucose-6-phosphate dehydrogenase (G6PD). Nε-acetylation inhibits many mitochondrial enzymes. Classic examples are the inhibition of long-chain acyl-CoA

dehydrogenase and pyruvate dehydrogenase complex, although the later by a phosphorylation-mediated mechanism [51; 52]. Some enzymes with various cellular localizations show instead enhancement of their catalytic activity following lysine acetylation [51].

Lysine acetylation also promote or inhibit protein-protein interactions, regulate proteasome-dependent and -independent protein degradation, and protein subcellular localization. Most mammalian proteins are modified by multiple PTMs on the same site (competitive PTMs) or different sites and these diverse modifications can reciprocally influence each other through a crosstalk. Such PTM crosstalk can result in the integration of different signals and thus increase their regulatory potential.

1.3.3. Nε-acetylation in diabetes mellitus

Protein acetylation has been linked to various human diseases including DM, as already mentioned [51]. Many *in vitro* and *in vivo* studies have shown hyperacetylation of diverse protein classes, including histones, transcription factors, and metabolic enzymes, in cells exposed to high glucose concentrations mimicking the diabetic condition or in animal models of DM. Increased histone Nε-acetylation has been found in retinas of diabetic rats and correlated to the expression of pro-inflammatory proteins, which are implicated in the pathogenesis of diabetic retinopathy [56]. In the heart of diabetic rat, lysine acetylation of many important mitochondrial proteins is increased resulting in alteration of metabolic enzyme activity, which can precede the diabetic cardiomyopathy [57]. Significant variations of protein acetylation have been also found in the liver of diabetic mice. Most of acetyl lysine have been detected in mitochondrial proteins involved in energy metabolism, amino acid conversion and urea cycle [58]. Acetylation of liver mitochondrial proteins is also markedly increased in mice challenged with a high-fat diet and likely contributes to fat accumulation in this organ, which plays a central role in controlling metabolic fitness [59]. Recently, a proteome/acetylome study of mouse renal tubular epithelial cells grown under high glucose conditions has revealed 113 hyper- and 374 ipo-acetylated sites within many proteins

associated with oxidative phosphorylation, TCA cycle, and other metabolic pathways [60]. Surely, most of these studies address the issue of acetylation and eventually its functional role in the contest of T2DM and its long-term complications such as diabetic retinopathy, cardiopathy, and nephropathy.

The studies on Nε-acetylation in β cells are less numerous and examine it in the contest of gluco- or lipo-toxicity, which represent *in vitro* models mimicking conditions such as a chronic exposure to a high caloric diet as well as DM and obesity. Proteomic studies have identified hundreds of Nε-acetylated proteins in rat clonal β cells, rat, and human pancreatic islets [61; 62; 63]. These investigations have shown that lysine acetylation in pancreatic β cells and islets occurs on many proteins with functions in a variety of biological processes as found in insulin target tissues including the liver. About 20% of these Nε-acetylated proteins localize to mitochondria while the others are cytosolic, cytoskeletal, and nuclear proteins. Lysine acetylation have been preferentially found in proteins associated with metabolic processes as observed in other tissues. Many mitochondrial enzymes and proteins are Nε-acetylated including all enzymes of the TCA cycle, most respiratory chain complex proteins comprised the ATP synthase, enzymes involved in amino acid and fatty acid metabolism. Additionally, proteins, which facilitate the exchange of metabolites across the inner mitochondrial membrane, and several cytosolic enzymes playing a role in glucose-induced insulin secretion amplification seem to be controlled by lysine acetylation [61; 62]. Therefore, it has been proposed that this PTM can influence the coupling between metabolism and insulin secretion at both trigger and amplification level [59]. Prolonged exposure of β cells to glucose high concentrations or palmitate causes protein hyperacetylation, which may be one of the mechanisms contributing to glucose and palmitate induced β cell dysfunction.

In cells, protein lysine acetylation is precisely regulated by a balance between KAT and KDAC activities. In mitochondria, where the activity of many metabolic enzymes is modulated by lysine acetylation this PTM can also occurs as a result of enzyme-independent reactions. Thus, the enzymatic activity of KDACs represented mainly by SIRT3 is

particularly important to maintain the equilibrium of protein acetylation. SIRT3 is expressed in clonal β cells (INS-1 cells) and pancreatic islets [61; 64]. SIRT3 knockdown in INS-1 cells has been reported to cause decrease of insulin secretion, increased apoptosis and reduced expression of key β cell genes [64]. However, SIRT3 expression manipulation appears to produce differential lysine acetylation of only a subset of quantified acetylated peptides [61].

SIRT3 activity is positively regulated by availability of the cofactor NAD^+ while its expression is modulated by transcription factors, repressors, coactivators and microRNAs [65]. Caton et al. have reported that pro-inflammatory cytokines significantly reduce SIRT3 expression in INS-1 cells [64]. This observation suggest that an unbalance of mitochondrial protein/enzyme acetylation may also occur in β cells exposed to pro-inflammatory cytokines providing a link between cytokine-induced β cell dysfunction and inactivation of key metabolic enzymes and proteins, which are pivotal for coupling energetic metabolism to insulin secretion. Indeed, a deep investigation of β cell proteome and acetylome using modern proteomic approaches could be useful to unveil some molecular aspects underlying T1DM pathogenesis.

1.4. References

[1] Saeedi P, Petersohn I, Salpea P, Malanda B, Karuranga S, Unwin N, Colagiuri S, Guariguata L, Motala AA, Ogurtsova K, Shaw JE, Bright D, Williams R; IDF Diabetes Atlas Committee. Global and regional diabetes prevalence estimates for 2019 and projections for 2030 and 2045: Results from the International Diabetes Federation Diabetes Atlas, 9th edition. *Diabetes Res Clin Pract*. 2019; 157:107843. doi: 10.1016/j.diabres.2019.107843.

[2] Eizirik DL, Pasquali L, Cnop M. Pancreatic β-cells in type 1 and type 2 diabetes mellitus: different pathways to failure. *Nat Rev Endocrinol.* 2020; 16(7):349-362. doi: 10.1038/s41574-020-0355-7.

[3] Grant SFA, Wells AD, Rich SS. Next steps in the identification of gene targets for type 1 diabetes. *Diabetologia.* 2020; 63(11):2260-2269. doi: 10.1007/s00125-020-05248-8.

[4] Powers AC. Type 1 diabetes mellitus: much progress, many opportunities. *J Clin Invest.* 2021; 15;131(8):e142242. doi: 10.1172/JCI142242.

[5] Columbiasurgery.org, Pancreas Functions, Location & Disease. *Columbia Surgery.* [online] Available at: <https://columbiasurgery.org/pancreas/pancreas-and-its-functions>.

[6] Da Silva Xavier G. The Cells of the Islets of Langerhans. *J Clin Med.* 2018; 12;7(3):54. doi: 10.3390/jcm7030054.

[7] Suckale J, Solimena M. Pancreas islets in metabolic signaling--focus on the beta-cell. *Front Biosci.* 2008; 1;13:7156-71. doi: 10.2741/3218.

[8] Maechler P, Wollheim CB. Mitochondrial glutamate acts as a messenger in glucose-induced insulin exocytosis. *Nature.* 1999; 9;402(6762):685-9. doi: 10.1038/45280.

[9] Tan C, Tuch BE, Tu J, Brown SA. Role of NADH shuttles in glucose-induced insulin secretion from fetal beta-cells. *Diabetes.* 2002; 51(10):2989-96. doi: 10.2337/diabetes.51.10.2989. Erratum in: *Diabetes* 2003;52(1):224.

[10] Bender K, Newsholme P, Brennan L, Maechler P. The importance of redox shuttles to pancreatic beta-cell energy metabolism and function. *Biochem Soc Trans.* 2006; 34(Pt 5):811-4. doi: 10.1042/BST0340811.

[11] Fu Z, Gilbert ER, Liu D. Regulation of insulin synthesis and secretion and pancreatic Beta-cell dysfunction in diabetes. *Curr Diabetes Rev.* 2013; 1;9(1):25-53.

[12] Eizirik DL, Szymczak F, Alvelos MI, Martin F. From Pancreatic β-Cell Gene Networks to Novel Therapies for Type 1 Diabetes. *Diabetes.* 2021; 70(9):1915-1925. doi: 10.2337/dbi20-0046.

[13] Eizirik DL, Mandrup-Poulsen T. A choice of death--the signal-transduction of immune-mediated beta-cell apoptosis. *Diabetologia*. 2001; 44(12):2115-33. doi: 10.1007/s001250100021. Erratum in: Diabetologia. 2002 Jun;45(6):936.

[14] Ohara-Imaizumi M, Cardozo AK, Kikuta T, Eizirik DL, Nagamatsu S. The cytokine interleukin-1beta reduces the docking and fusion of insulin granules in pancreatic beta-cells, preferentially decreasing the first phase of exocytosis. *J Biol Chem.* 2004; 1;279(40):41271-4. doi: 10.1074/jbc.C400360200.

[15] Cnop M, Welsh N, Jonas JC, Jörns A, Lenzen S, Eizirik DL. Mechanisms of pancreatic beta-cell death in type 1 and type 2 diabetes: many differences, few similarities. *Diabetes.* 2005; 54 Suppl 2:S97-107. doi: 10.2337/diabetes.54.suppl_2.s97.

[16] Darville MI, Eizirik DL. Regulation by cytokines of the inducible nitric oxide synthase promoter in insulin-producing cells. *Diabetologia.* 1998; 41(9):1101-8. doi: 10.1007/s001250051036.

[17] Kutlu B, Cardozo AK, Darville MI, Kruhøffer M, Magnusson N, Ørntoft T, Eizirik DL. Discovery of gene networks regulating cytokine-induced dysfunction and apoptosis in insulin-producing INS-1 cells. *Diabetes.* 2003; 52(11):2701-19. doi: 10.2337/diabetes.52.11.2701.

[18] Heitmeier MR, Scarim AL, Corbett JA. Prolonged STAT1 activation is associated with interferon-gamma priming for interleukin-1-induced inducible nitric-oxide synthase expression by islets of Langerhans. *J Biol Chem.* 1999; 8;274(41):29266-73. doi: 10.1074/jbc.274.41.29266.

[19] Corbett JA, Sweetland MA, Wang JL, Lancaster JR Jr, McDaniel ML. Nitric oxide mediates cytokine-induced inhibition of insulin secretion by human islets of Langerhans. *Proc Natl Acad Sci U S A.* 1993; 1;90(5):1731-5. doi: 10.1073/pnas.90.5.1731.

[20] Castro LA, Robalinho RL, Cayota A, Meneghini R, Radi R. Nitric oxide and peroxynitrite-dependent aconitase inactivation and iron-regulatory protein-1 activation in mammalian fibroblasts. *Arch Biochem Biophys.* 1998; 15;359(2):215-24. doi: 10.1006/abbi.1998.0898.

[21] Corbett JA, Wang JL, Sweetland MA, Lancaster JR Jr, McDaniel ML. Interleukin 1 beta induces the formation of nitric oxide by beta-cells purified from rodent islets of Langerhans. Evidence for the beta-cell as a source and site of action of nitric oxide. *J Clin Invest.* 1992; 90(6):2384-91. doi: 10.1172/JCI116129.

[22] Scarim AL, Heitmeier MR, Corbett JA. Irreversible inhibition of metabolic function and islet destruction after a 36-hour exposure to interleukin-1beta. *Endocrinology.* 1997; 138(12):5301-7. doi: 10.1210/endo.138.12.5583.

[23] Scarim AL, Heitmeier MR, Corbett JA. Irreversible inhibition of metabolic function and islet destruction after a 36-hour exposure to interleukin-1beta. *Endocrinology.* 1997; 138(12):5301-7. doi: 10.1210/endo.138.12.5583.

[24] Bellmann K, Jäättelä M, Wissing D, Burkart V, Kolb H. Heat shock protein hsp70 overexpression confers resistance against nitric oxide. *FEBS Lett.* 1996; 5;391(1-2):185-8. doi: 10.1016/0014-5793(96)00730-2.

[25] Scarim AL, Heitmeier MR, Corbett JA. Heat shock inhibits cytokine-induced nitric oxide synthase expression by rat and human islets. *Endocrinology.* 1998; 139(12):5050-7. doi: 10.1210/endo.139.12.6366.

[26] Maechler P, Wollheim CB. Mitochondrial function in normal and diabetic beta-cells. *Nature.* 2001; 13;414(6865):807-12. doi: 10.1038/414807a.

[27] Youle RJ, Strasser A. The BCL-2 protein family: opposing activities that mediate cell death. *Nat Rev Mol Cell Biol.* 2008; 9(1):47-59. doi: 10.1038/nrm2308.

[28] Gurzov EN, Eizirik DL. Bcl-2 proteins in diabetes: mitochondrial pathways of β-cell death and dysfunction. *Trends Cell Biol.* 2011; 21(7):424-31. doi: 10.1016/j.tcb.2011.03.001.

[29] Kuwana T, Bouchier-Hayes L, Chipuk JE, Bonzon C, Sullivan BA, Green DR, Newmeyer DD. BH3 domains of BH3-only proteins differentially regulate Bax-mediated mitochondrial membrane permeabilization both directly and indirectly. *Mol Cell.* 2005; 18;17(4):525-35. doi: 10.1016/j.molcel.2005.02.003.

[30] Willis SN, Fletcher JI, Kaufmann T, van Delft MF, Chen L, Czabotar PE, Ierino H, Lee EF, Fairlie WD, Bouillet P, Strasser A, Kluck RM, Adams JM, Huang DC. Apoptosis initiated when BH3 ligands engage multiple Bcl-2 homologs, not Bax or Bak. *Science.* 2007; 9;315(5813):856-9. doi: 10.1126/science.1133289.

[31] Riedl SJ, Salvesen GS. The apoptosome: signalling platform of cell death. *Nat Rev Mol Cell Biol.* 2007; 8(5):405-13. doi: 10.1038/nrm2153.

[32] Barthson J, Germano CM, Moore F, Maida A, Drucker DJ, Marchetti P, Gysemans C, Mathieu C, Nuñez G, Jurisicova A, Eizirik DL, Gurzov EN. Cytokines tumor necrosis factor-α and interferon-γ induce pancreatic β-cell apoptosis through STAT1-mediated Bim protein activation. *J Biol Chem.* 2011; 11;286(45):39632-43. doi: 10.1074/jbc.M111.253591.

[33] Moore F, Santin I, Nogueira TC, Gurzov EN, Marselli L, Marchetti P, Eizirik DL. The transcription factor C/EBP delta has anti-apoptotic and anti-inflammatory roles in pancreatic beta cells. *PLoS One.* 2012; 7(2):e31062. doi: 10.1371/journal.pone.0031062.

[34] Miani M, Barthson J, Colli ML, Brozzi F, Cnop M, Eizirik DL. Endoplasmic reticulum stress sensitizes pancreatic beta cells to interleukin-1β-induced apoptosis via Bim/A1 imbalance. *Cell Death Dis.* 2013; 4;4(7):e701. doi: 10.1038/cddis.2013.236.

[35] Marhfour I, Lopez XM, Lefkaditis D, Salmon I, Allagnat F, Richardson SJ, Morgan NG, Eizirik DL. Expression of endoplasmic reticulum stress markers in the islets of patients with type 1 diabetes. *Diabetologia.* 2012; 55(9):2417-20. doi: 10.1007/s00125-012-2604-3.

[36] Engin F, Yermalovich A, Nguyen T, Hummasti S, Fu W, Eizirik DL, Mathis D, Hotamisligil GS. Restoration of the unfolded protein response in pancreatic β cells protects mice against type 1 diabetes. *Sci Transl Med.* 2013; 13;5(211):211ra156. doi: 10.1126/scitranslmed.3006534. Erratum in: *Sci Transl Med.* 2013; 4;5(214):214er11. Ngyuen, Truc [corrected to Nguyen, Truc].

[37] Eizirik DL, Cardozo AK, Cnop M. The role for endoplasmic reticulum stress in diabetes mellitus. *Endocr Rev.* 2008; 29(1):42-61. doi: 10.1210/er.2007-0015.

[38] Cardozo AK, Ortis F, Storling J, Feng YM, Rasschaert J, Tonnesen M, Van Eylen F, Mandrup-Poulsen T, Herchuelz A, Eizirik DL. Cytokines downregulate the sarcoendoplasmic reticulum pump Ca2+ ATPase 2b and deplete endoplasmic reticulum Ca2+, leading to induction of endoplasmic reticulum stress in pancreatic beta-cells. *Diabetes.* 2005; 54(2):452-61. doi: 10.2337/diabetes.54.2.452.

[39] Schröder M, Kaufman RJ. ER stress and the unfolded protein response. *Mutat Res.* 2005; 6;569(1-2):29-63. doi: 10.1016/j.mrfmmm.2004.06.056.

[40] Jäger R, Bertrand MJ, Gorman AM, Vandenabeele P, Samali A. The unfolded protein response at the crossroads of cellular life and death during endoplasmic reticulum stress. *Biol Cell.* 2012; 104(5):259-70. doi: 10.1111/boc.201100055.

[41] Steer SA, Scarim AL, Chambers KT, Corbett JA. Interleukin-1 stimulates beta-cell necrosis and release of the immunological adjuvant HMGB1. *PLoS Med.* 2006; 3(2):e17. doi: 10.1371/journal.pmed.0030017.

[42] Tyers M, Mann M. From genomics to proteomics. *Nature.* 2003; 13;422(6928):193-7. doi: 10.1038/nature01510.

[43] Aslam B, Basit M, Nisar MA, Khurshid M, Rasool MH. Proteomics: Technologies and Their Applications. *J Chromatogr Sci.* 2017; 55(2):182-196. doi: 10.1093/chromsci/bmw167.

[44] Zhao Y, Jensen ON. Modification-specific proteomics: strategies for characterization of post-translational modifications using enrichment techniques. *Proteomics.* 2009; 9(20):4632-41. doi: 10.1002/pmic.200900398.

[45] Ramazi S, Zahiri J. Posttranslational modifications in proteins: resources, tools and prediction methods. *Database (Oxford).* 2021; 7;2021:baab012. doi: 10.1093/database/baab012.

[46] Brown JL, Roberts WK. Evidence that approximately eighty per cent of the soluble proteins from Ehrlich ascites cells are Nalpha-acetylated. *J Biol Chem.* 1976; 25;251(4):1009-14.

[47] Helbig AO, Gauci S, Raijmakers R, van Breukelen B, Slijper M, Mohammed S, Heck AJ. Profiling of N-acetylated protein termini provides in-depth insights into the N-terminal nature of the proteome. *Mol Cell Proteomics.* 2010; 9(5):928-39. doi: 10.1074/mcp.M900463-MCP200. Epub 2010 Jan 7.

[48] Ree R, Varland S, Arnesen T. Spotlight on protein N-terminal acetylation. *Exp Mol Med.* 2018; 27;50(7):1-13. doi: 10.1038/s12276-018-0116-z.

[49] Allfrey VG, Mirsky AE. Structural Modifications of Histones and their Possible Role in the Regulation of RNA Synthesis. *Science.* 1964; 1;144(3618):559. doi: 10.1126/science.144.3618.559.

[50] Glozak MA, Sengupta N, Zhang X, Seto E. Acetylation and deacetylation of non-histone proteins. *Gene.* 2005; 19;363:15-23. doi: 10.1016/j.gene.2005.09.010.

[51] Narita T, Weinert BT, Choudhary C. Functions and mechanisms of non-histone protein acetylation. *Nat Rev Mol Cell Biol.* 2019; 20(3):156-174. doi: 10.1038/s41580-018-0081-3. Erratum in: *Nat Rev Mol Cell Biol.* 2019; 20(8):508.

[52] Carrico C, Meyer JG, He W, Gibson BW, Verdin E. The Mitochondrial Acylome Emerges: Proteomics, Regulation by Sirtuins, and Metabolic and Disease Implications. *Cell Metab.* 2018; 6;27(3):497-512. doi: 10.1016/j.cmet.2018.01.016.

[53] Zhang J, Sprung R, Pei J, Tan X, Kim S, Zhu H, Liu CF, Grishin NV, Zhao Y. Lysine acetylation is a highly abundant and evolutionarily conserved modification in Escherichia coli. *Mol Cell Proteomics.* 2009; 8(2):215-25. doi: 10.1074/mcp.M800187-MCP200.

[54] Henriksen P, Wagner SA, Weinert BT, Sharma S, Bacinskaja G, Rehman M, Juffer AH, Walther TC, Lisby M, Choudhary C. Proteome-wide analysis of lysine acetylation suggests its broad regulatory scope in Saccharomyces cerevisiae. *Mol Cell Proteomics.* 2012; 11(11):1510-22. doi: 10.1074/mcp.M112.017251.

[55] Lundby A, Lage K, Weinert BT, Bekker-Jensen DB, Secher A, Skovgaard T, Kelstrup CD, Dmytriyev A, Choudhary C, Lundby C, Olsen JV. Proteomic analysis of lysine acetylation sites in rat tissues reveals organ specificity and subcellular patterns. *Cell Rep.* 2012; 30;2(2):419-31. doi: 10.1016/j.celrep.2012.07.006.

[56] Kadiyala CS, Zheng L, Du Y, Yohannes E, Kao HY, Miyagi M, Kern TS. Acetylation of retinal histones in diabetes increases inflammatory proteins: effects of minocycline and manipulation of histone acetyltransferase (HAT) and histone deacetylase (HDAC). *J Biol Chem.* 2012; 27;287(31):25869-80. doi: 10.1074/jbc.M112.375204.

[57] Berthiaume JM, Hsiung CH, Austin AB, McBrayer SP, Depuydt MM, Chandler MP, Miyagi M, Rosca MG. Methylene blue decreases mitochondrial lysine acetylation in the diabetic heart. *Mol Cell Biochem.* 2017; 432(1-2):7-24. doi: 10.1007/s11010-017-2993-1.

[58] Hölper S, Nolte H, Bober E, Braun T, Krüger M. Dissection of metabolic pathways in the Db/Db mouse model by integrative proteome and acetylome analysis. *Mol Biosyst.* 2015; 11(3):908-22. doi: 10.1039/c4mb00490f. Epub 2015 Jan 16. PMID: 25592279.

[59] Santo-Domingo J, Dayon L, Wiederkehr A. Protein Lysine Acetylation: Grease or Sand in the Gears of β-Cell Mitochondria? *J Mol Biol.* 2020; 6;432(5):1446-1460. doi: 10.1016/j.jmb.2019.09.011.

[60] Wan J, Hu M, Jiang Z, Liu D, Pan S, Zhou S, Liu Z. Lysine Acetylation in the Proteome of Renal Tubular Epithelial Cells in Diabetic Nephropathy. *Front Genet.* 2021; 25;12:767135. doi: 10.3389/fgene.2021.767135.

[61] De Marchi U, Galindo AN, Thevenet J, Hermant A, Bermont F, Lassueur S, Domingo JS, Kussmann M, Dayon L, Wiederkehr A. Mitochondrial lysine deacetylation promotes energy metabolism and calcium signaling in insulin-secreting cells. *FASEB J.* 2019; 33(4):4660-4674. doi: 10.1096/fj.201801424R.

[62] Zhang Y, Zhou F, Bai M, Liu Y, Zhang L, Zhu Q, Bi Y, Ning G, Zhou L, Wang X. The pivotal role of protein acetylation in linking glucose and fatty acid metabolism to β-cell function. *Cell Death Dis.* 2019; 10(2):66. doi: 10.1038/s41419-019-1349-z.

[63] Ciregia F, Bugliani M, Ronci M, Giusti L, Boldrini C, Mazzoni MR, Mossuto S, Grano F, Cnop M, Marselli L, Giannaccini G, Urbani A, Lucacchini A, Marchetti P. Palmitate-induced lipotoxicity alters

acetylation of multiple proteins in clonal β cells and human pancreatic islets. *Sci Rep.* 2017; 7(1):13445. doi: 10.1038/s41598-017-13908-w.

[64] Caton PW, Richardson SJ, Kieswich J, Bugliani M, Holland ML, Marchetti P, Morgan NG, Yaqoob MM, Holness MJ, Sugden MC. Sirtuin 3 regulates mouse pancreatic beta cell function and is suppressed in pancreatic islets isolated from human type 2 diabetic patients. *Diabetologia.* 2013; 56(5):1068-77. doi: 10.1007/s00125-013-2851-y.

[65] Zhang J, Xiang H, Liu J, Chen Y, He RR, Liu B. Mitochondrial Sirtuin 3: New emerging biological function and therapeutic target. *Theranostics.* 2020; 10(18):8315-8342. doi: 10.7150/thno.45922.

2. Materials and Methods

2.1. Cell Cultures

INS-1E β cells

INS-1E β cells were grown in RPMI 1640 medium supplemented with 10% heat-inactivated fetal bovine serum (FBS), 1 mM sodium pyruvate, 50 μM 2-mercaptoethanol, 2 mM glutamine, 10 mM HEPES (4-(2-hydroxyethyl)-1-piperazine ethane sulfonic acid), 100 U/ml penicillin, and 100 mg/ml streptomycin (Thermo Fischer Scientific, Whaltam, MA, USA) at 37°C in a CO_2 incubator. For cytokines treatment, cells were incubated for 24 h in the presence of 10 U/ml IL-1β, and 100 U/ml INF-γ (Cyto). The cytokine concentrations and time of treatment were based on previous dose-response experiments [1]. The control (CTRL) was represented by cells incubated for 24 h in complete medium without cytokines.

Human pancreatic islets

Isolated human pancreatic islets were prepared by collagenase digestion and gradient purification from the pancreas of 13 multiorgan donors (age: 68.5 ± 10.4 years; 9F/4M; BMI: 25.5 ± 3.7 kg/m^2) [2; 3], with written consent by next-of-kin (Table 1). Glands, which were not suitable for clinical purposes, were processed [4] with the approval of the local Ethics Committee. Following isolation, islets were cultured in M199 medium (Euroclone SpA, Pero, MI, Italy) containing 5.5 mM glucose, supplemented with 10% FBS, 100 U/mL penicillin, 100 μg/mL streptomycin, 50 μg/mL gentamicin, and 750 ng/mL amphotericin B (all from Sigma-Aldrich, St. Louis, MO, USA) at 37 °C in a CO_2 incubator. Approximately 1,000 islets were incubated with cytokines (50 U/ml IL-1β and 1000 U/ml IFN-γ) for 48 h (Cyto). The cytokine concentrations were based on previous dose-response experiments [5; 6]. The control (CTRL) was represented by islets incubated for 48 h in complete medium without cytokines.

Table 1. Clinical data of subjects

n°	Sex	Age (years)	BMI (Kg/m²)	Cause of death
1	F	77	19.5	CVD
2	F	65	21.5	CVD
3	F	80	24.2	CVD
4	F	52	25.7	CVD
5	F	74	29.3	CVD
6	F	65	23.5	Trauma
7	F	81	31.9	Trauma
8	F	79	23.4	Trauma
9	F	77	31.3	Trauma
10	M	61	23.2	CVD
11	M	64	24.5	CVD
12	M	66	28.4	CVD
13	M	50	24.5	CVD

Body mass index (BMI); cardiovascular disease (CVD).

2.2. Functional assays

2.2.1. Insulin secretion

INS-1E β cells

Studies of insulin secretion in response to acute glucose stimulation were performed as previously described [7]. Briefly, batch of INS-1E cells from CTRL and Cyto were pre-incubated with 2.8 mM of glucose for 45 min, then 3 wells of each group were challenged with 2.8 mM glucose or 16.7 mM glucose in Krebs Ringer HEPES buffer [135 mM NaCl, 3.6 mM KCl, 2 mM $NaHCO_3$, 0.5 mM NaH_2PO_4, 0.5 mM $MgSO_4$, 1.5 mM $CaCl_2$, 10 mM HEPES pH 7.4, and 0.1% bovine serum albumin (BSA)] (Sigma-Alderich). Then, total insulin content of each well was extracted using over-night (O/N) acid-alcohol extraction at 4°C. Insulin was quantified by a radioimmunometric assay (DIAsource ImmunoAssays S.A., Nivelles, Belgium). Insulin release was expressed as percentage of the total insulin content. The student t-test was applied to assess the difference between groups. A p-value < 0.05 was considered statistically significant. Data are expressed as mean ± SEM.

Human pancreatic islets

For insulin secretion after 45 min of pre-incubation in the presence of 3.3 mM glucose, batches of 15 handpicked islets, were challenged acutely (45 min) with 3.3 or 6.7 mM glucose. Then islets were subjected to acid-alcohol extraction for total insulin content measurement, as previously reported [8]. Insulin was quantified by a radioimmunometric assay (DIAsource ImmunoAssays S.A.). Insulin stimulation index was calculated as ratio of insulin release, normalized for total insulin content, at 16.7 mM glucose over release at 3.3 mM glucose.

2.2.2. Caspase 3/7 activity

Human pancreatic islets

Caspase-Glo® 3/7 assay kit (Promega Corporation, Madison, WI, USA) was used to detect caspase activity. Briefly, batch of 10 size-matched islets were seeded in a white solid 96 well plate in a total volume of 100 μl/well. Then 100 μl of caspase 3/7 reagent, a solution containing luciferase and a tetrapeptide substrate linked to aminoluciferin, was added to each well and incubated for 1 h at room temperature. Following caspase cleavage of substrate, aminoluciferin is released and processed by luciferase, resulting in production of light. Luminescence was recorded with a FLUOstar Omega microplate reader (BMG Labtech, Ortenberg, Germany). Data are expressed as mean ± SEM. The student t-test was applied to assess the difference between groups in the insulin content, stimulation index and caspase activation experiments. A p-value < 0.05 was considered statistically significant.

2.3. Proteomic Analysis

2.3.1. Differential expression proteomics using Tandem Mass Tag (TMT) of INS-1E

Batches of INS-1E β cells from 10 biological replicates (5 CTRL and 5 Cyto) were counted with a hemacytometer (Bio-Rad, Hercules, CA, USA) and resuspended for 1 h in Radio-immunoprecipitation assay buffer (RIPA buffer) [50 mM Tris-HCl pH 7.6, 300 mM NaCl, 2% Nonidet P-40 (NP40), 2% Sodium Deoxycholate, 0,2% sodium dodecyl sulphate (SDS)] (Sigma-Alderich) containing protease and phosphatase inhibitors (Thermo Fisher Scientific), 10 mM nicotinamide, and 1 μM tricostatin A. Briefly, cells were lysate with 5 freezing and thawing cycles (-180/+37 °C), and 1 min sonication (3 sec pulse/3 sec pause cycles, 30% amplitude at 4°C). Total protein concentration was measured using the micro-BCA™ protein assay (Thermo Fisher Scientific). Proteins (1 mg of each sample) were reduced using 8 mM dithiothreitol (DTT) (45 min at 55°C) and alkylated with 25 mM of iodoacetamide (IAA) (30 min in the dark). At the end of the incubation time, protein samples were precipitated O/N with cold acetone (-20°C, ratio 1:6 v/v) and resuspended in 20 mM N-(2-Hydroxyethyl)piperazine-N′-(3-propanesulfonic acid) (EPPS) buffer, pH 8.2, containing 8 M urea (Sigma-Alderich). After urea dilution, proteins were firstly digested with endoproteinase Lys -C (1:250 w/w) (Wako, USA) for 4 h at 30°C, and then with trypsin (1:100 w/w) (Promega corporation) O/N at 37°C. Resulting peptides were firstly labelled using the Tandem Mass Tag™ (TMT™) 10-plex reagent (TMT™10, Thermo Fisher Scientific) and then peptides of CTRL and Cyto samples were pooled. Peptide samples were desalted using a Sep-Pak C18 purification column (Water, Milford, MA, USA) and dried with a speed-vac apparatus (Thermo Fisher Scientific). For differential expression analysis, peptides (500 μg) were then fractionated by HPLC at high pH. The remaining peptide sample (~10 mg) was used for acetylome analysis.

2.3.2. Proteome Integral Solubility Alteration (PISA) using Tandem Mass Tag proteomics of INS-1E

Batches of INS-1E β cells of 8 biological replicates (4 CTRL and 4 Cyto) were resuspended in phosphate buffer saline (PBS) (Sigma-Alderich) containing protease and phosphatase inhibitor cocktails (Thermo Fisher Scientific), 10 mM nicotinamide, 1 µM tricostatin A, counted with a hemacytometer (Bio-Rad), and aliquoted. One aliquot of each sample was exposed to a gradient of increasing temperature (43.3°C to 60.6°C) for 3 min and then re-equilibrated at room temperature (RT) for 6 min. Other aliquots were used for expression proteomics to normalize data of proteins thermal stability over protein expression. Thermal treated and untreated cells were then lysed with 5 freezing and thawing cycles (-180/+37 °C) and incubated 1 h at 4°C in the presence of 0.4% NP-40. Thermal treated samples were ultra-centrifugated at 150,000 g for 30 min at 4°C to ensure removal of melted proteins. The total protein concentration of samples was determine using the micro-BCA™ kit (Thermo Fisher Scientific). Aliquots (50 µg of proteins) of each sample were reduced, alkylated, precipitated, and digested as described above (paragraph *"Differential expression proteomics using Tandem Mass Tag (TMT) "*). Resulting peptides were labelled using the the TMTpro™ 16plex Label Reagent (TMT16) (1:4 w/w, 2 h treatment) (Thermo Fisher Scientific). Peptides of thermal treated and untreated CTRL and Cyto samples were pooled together for further analysis. Sample desalting and cleaning was performed using a Sep-Pak C18 column (Waters). [9]

2.3.3. Protein extraction and fractionation for Shotgun analysis of human pancreatic islet

For shotgun analysis [10], triplicate experiments were performed on each islet preparation from three human donors. For each preparation, two different conditions, i.e. CTRL (n = 3) and Cyto (n = 3), were analysed. For each condition, 1,000 human islets were treated as described above and protein extraction was performed as previously described [11]. Briefly, isolated islets were collected and washed twice with PBS (37°C). Cells were suspended in

the rehydration solution [7 M urea, 2 M thiourea, 4% 3-[(3-cholamidopropyl)dimethylammonio]-1-propanesulfonate (CHAPS), 60 mM DTT, 0.002% bromophenol blue] containing 50 mM NaF, 2 mM Na_3VO_4, 1 µM trichostatin A, 10 mM nicotinamide, and 1µL/10^6 cells of a protease inhibitor cocktail] (Sigma-Alderich). After stirring and sonication (4 seconds, 5 times), lysed cells were allowed to rehydrate for 1 h at RT with occasional stirring. Thereafter, the suspension was centrifuged at 17,000 g for 5 min at RT. Protein concentration of the resulting supernatant was determined using the Bio-Rad RC/DC™-protein assay (Bio-Rad). BSA was used as a standard.

Then, proteins were fractionated by SDS polyacrylamide gel electrophoresis (SDS-PAGE). Briefly, 40 µg of proteins were loaded into each well and separation was carried out using a 12% acrylamide resolving gel. After protein staining with Coomassie blue R-250, gel bands (16 paired gel bands for each lane) were excised and washed twice with wash buffer (25 mM NH_4HCO_3 in 50% acetonitrile). Afterwards, proteins were reduced with 10 mM DTT (45 min, 56°C), and alkylated with 55 mM IAA (30 min at RT in the dark). After two washes with washing buffer, protein bands were completely dried in a CentriVap vacuum centrifuge. The dried gel pieces were rehydrated for 30 min at 4°C in a porcine trypsin (Promega Corporation) solution (3 ng/µl in 100 mM NH_4HCO_3) and incubated O/N at 37°C. The reaction was quenched by adding 10% trifluoroacetic acid. The samples were stored at -20 °C before being analysed by LC-MS/MS.

2.5. Acetylome analysis

2.5.1. Immuno-enrichment of acetylated peptides using the PTM-Scan kit

INS-1E β cells

Peptide samples prepared as described in paragraph "Differential expression proteomics using Tandem Mass Tag (TMT)" were resuspended in IAP buffer (50 mM MOPS/NaOH, pH 7.2, 10 mM Na_2HPO_4, and 50 mM NaCl) and immunoprecipitated using anti-ε-acetyl lysine antibodies (PTM-Scan #13416 Cell signalling, Danvers, MA, USA) according to manufacturer's instructions. Briefly, peptides were incubated with the specific anti-ε-acetyl lysine antibodies for 2 h at 4°C. After incubation, Nε-acetylated-peptides were eluted with 0.15% trifluoroacetic acid (TFA), desalted using a Sep-Pak C18 column and fractionated by HPLC at high pH.

Human pancreatic islets

Human pancreatic islets from 3 subjects were used for ε-acetyl lysine peptide immunoprecipitation experiments. Immunoprecipitation was performed essentially according to manufacturer's instructions (PTMScan #13416, Cell signalling). Briefly, each human islet sample was resuspended in a lysis solution (7 M urea, 2 M thiourea, 4% CHAPS, 60 mM DTT, 50 mM NaF, 2 mM Na_3VO_4, 1 μM trichostatin A, 10 mM nicotinamide, and 1 μL/10^6 cells of a protease inhibitor cocktail) (Sigma-Alderich) and sonicated. After reduction and alkylation, proteins were digested with trypsin (Promega Corporation), resulting peptide samples acidified with TFA till a pH < 3 and desalted using a Sep-Pak C18 column (Waters). Peptide samples were then dried using a CentriVap vacuum centrifuge, resuspended in immunoaffinity purification buffer (IAP buffer) (50 mM MOPS/NaOH, pH 7.2, 10 mM Na_2HPO_4, 50 mM NaCl) and incubated with the specific anti-ε-acetyl lysine antibodies (Cell signalling) for 2 h at 4°C. After incubation, Nε-acetylated-peptides were eluted with 0.15% TFA and prepared for mass spectrometry analysis.

2.6. Mass Spectrometry

2.6.1. High pH reverse fractionation for INS-1E

Dried samples of PISA and PTM-Scan ε-acetyl lysine immuno-enrichment were resuspended in 20 mM NH_4OH (1 h at 4°C) and peptides separated by HPLC (Dionex Ultimate 3000 system) on a Xbridge Peptide BEH C18 column (25 cm length; 2.1 mm inner diameter; 3.5 μm particle size; 300 Å pore size) (Waters) at a flow rate of 200 μL/min. Fractionation was carried out using a binary solvent system consisting of 20 mM NH_4OH in H_2O (solvent A) and 20 mM NH_4OH in acetonitrile (solvent B). Peptides were eluted with a gradient of 2-23 % solvent B in 42 min, 23-52% solvent B in 4 min, and 52-63% solvent B in 2 min followed by column washing with 63% solvent B for 5 min. The elution was monitored measuring UV absorbance at 214 nm. A total of 96 fractions of 100 μL each were collected for every assay of PISA, expression, and from PTM-Scan ε-acetyl lysine immuno-enrichment experiments. Fractions of PISA and expression experiments were concatenated into 48 fractions while those of PTM-Scan ε-acetyl lysine immuno-enrichment experiments were gathered into 4 fractions. All 100 fractions were then dried O/N using a speed-vac apparatus.

2.6.2. HPLC-ESI–MS/MS

INS-1E β cells

Each dried fraction was resuspended in 0.1% formic acid and analysed by nano high-performance liquid chromatography−electrospray ionization (HPLC-ESI)−MS/MS, using the Exploris 480 mass spectrometer (Thermo Fisher Scientific) equipped with an EASY Spray Source and connected to an UltiMate 3000 RSLC nanoUPLC system. Injected fractions were preconcentrated and further desalted online using a PepMap C18 nano trap column (2 cm length; 75 μm inner diameter; 3 μm particle size; 100 Å pore size) (Thermo Fisher Scientific) at a flow rate of 3 μL/min for 5 min.

Peptide separation was performed using an EASY-Spray C18 reversed-phase nano LC column (Acclaim PepMap RSLC; 50 cm length; 2 μm inner diameter; 2 μm particle size; 100

Å pore size) (Thermo Fisher Scientific) at 45 °C and a flow rate of 300 nL/min. A binary solvent system consisting of 0.1% formic acid, 2% acetonitrile (solvent A) and 98% acetonitrile, 0.1% formic acid (solvent B) was used and peptide elution was obtained with a gradient of 4–95% solvent B in 90 and 120 min for PISA/proteome and acetylome samples, respectively.

Mass spectra were acquired within a m/z range of 375–1500 with a resolution of 120,000 at m/z. Automatic gain control target was set to 3×10^6 with a maximum injection time of 100 ms. The 20 most abundant peptide ions were selected for higher-energy collision dissociation (HCD) with normalized collision energy value set at 33. The ion abundance threshold was set at 0.1% with charge exclusion of z = 1 ions. The MS/MS spectra were acquired at a resolution of 60,000, with a target value of 2×10^5 ions and a maximum injection time of 120 ms. The fixed first m/z was 100, and the isolation window was 1.6 m/z. The instrument was operated in the positive ion mode for data dependent acquisition of MS/MS spectra with a dynamic exclusion time of previously selected precursor ions of 45s.

Raw data were analysed with Proteome Discoverer, using Mascot and Sequest searching algorithms. Spectra were matched against the SwissProt Rattus Norvegicus database (29,928 entries) and false discovery rate (FDR) was set to 0.1% at the peptide-spectrum matches (PSM) level. The post-translational modification (PTM) profile was set as follows: fixed cysteine carbamidomethylation (ΔMass: 57.02), variable lysine acetylation (ΔMass: 42.01), N-terminal acetylation (ΔMass: 42.01), methionine oxidation (ΔMass: 15.99) and glutamine and asparagine deamidation (ΔMass: 0.98). Non-specific cleavage was allowed to one end of the peptides, with a maximum of 2 missed cleavages and trypsin enzyme specificity. The highest error mass tolerances for precursors and fragments were set at 10 ppm and 0.05 Da, respectively.

The quantitative analysis of identified peptides was performed through TMT™16 and TMT™10 reporter ions for PISA, and proteome or acetylome experiments, respectively. The abundance of Nε- or Nα-acetylated peptides was firstly normalised for the total abundance of TMT™10 for every channel used, and subsequently normalised for protein expression.

In the analysis of differentially acetylated peptides, only peptides with p-value < 0.05 and fold change > 1.5 were considered. The abundance of peptides from PISA experiment was firstly normalised for the total abundance of TMT™16 for every channel used, and then normalised for protein expression.

Human pancreatic islets

Proxeon EASY-nLCII (Thermo Fisher Scientific) chromatographic system coupled to a Maxis HD UHR-TOF (Bruker Daltonics GmbH, Bremen, Germany) mass spectrometer equipped with a nanoESI spray source was used to perform, in technical triplicates, shotgun (32 samples for each subject: 16 CTRL and 16 Cyto, grouped by band) and acetylome analyses (6 samples from 3 subjects: 3 CTRL and 3 Cyto) of tryptic peptides.

Peptides were loaded on the EASY-Column C18 trapping column (2 cm length; 100 μm inner diameter; 5 μm particle size) (Thermo Fisher Scientific), and subsequently separated on an Acclaim PepMap100 C18 (25 cm length; 75 μm inner diameter; 5 μm particle size) (Thermo Fisher Scientific) nano scale chromatographic column. The flow rate was set to 300 nL/min and the gradient (mobile phase A: 0.1% formic acid in H_2O) was from 3 to 35% of mobile phase B (1% formic acid in acetonitrile) in 80 min followed by 35 to 45% in 10 min and from 45 to 90% in 11 min. The mass spectrometer was operated in positive ion polarity and Auto MS/MS mode (Data Dependent Acquisition - DDA), using N_2 as collision gas for CID fragmentation. Precursors in the range of 350 to 2,200 m/z (excluding 1,220.0–1,224.5 m/z) with a preferred charge state +2 to +5 (excluding singly charged ions) and absolute intensity above 4,706 counts were selected for fragmentation in a maximum cycle time of 3 seconds. After acquiring one MS/MS spectrum, the precursors were actively excluded from selection for 30 seconds. Isolation width and collision energy for MS/MS fragmentation were set according to the mass and charge state of the precursor ions (from 3 to 9 Da and from 21 eV to 55 eV). In-source reference lock mass (1,221.9906 m/z) was acquired online throughout the runs. Altogether, 288 and 18 instrumental runs were performed for expression and

acetylome experiments, respectively. Each raw data file was converted to mzXML format and submitted to the label free quantification (LFQ) processing.

Raw mass spectrometry data were analysed using the PEAKS Studio 7.5 software using the 'correct precursor only' option. Spectra were matched against the neXtProt database (including isoforms as of June 2017; 42,151 entries) and false discovery rate (FDR) was set to 0.1% at the peptide-spectrum matches (PSM) level. The PTM profile was set as follows: fixed cysteine carbamidomethylation (ΔMass: 57.02), variable methionine oxidation (ΔMass: 15.99) and glutamine and asparagine deamidation (ΔMass: 0.98). Variable lysine acetylation (ΔMass: 42.01) and N-terminal acetylation (ΔMass: 42.01) were added for acetylome analysis. Non-specific cleavage was allowed to one end of the peptides, with a maximum of 2 missed cleavages and trypsin enzyme specificity. The highest error mass tolerances for precursors and fragments were set at 10 ppm and 0.05 Da, respectively. Parameters for LFQ were set as follows: quantification type as label free quantification; mass error tolerance, 10.0 ppm; retention time shift tolerance, 2.0 min; FDR threshold, 0.5%.

The six shotgun samples for each of the sixteen slices were allotted in 2 groups corresponding to CTRL and Cyto. For quantitative analysis, the significance threshold at the protein level was set to ≥ 20 -10log p-Value with fold change ≥ 2.0. Sixteen lists of differentially expressed proteins were obtained for each subject.

The six acetylome samples were allotted in 2 groups corresponding to CTRL and Cyto. Eighteen lists of acetylated peptides were generated (9 CTRL and 9 Cyto). These lists were then grouped for technical replicates choosing only peptides identified in at least 2 runs of the same sample, obtaining 6 list (3 CTRL and 3 Cyto). The final comparison was set for pair data of the obtained lists. Only peptides identified in at least 2 patients and with a fold change of acetylation > 1.5 were chosen.

2.7. Western blot analysis of human pancreatic islets

Western blot (WB) was performed to validate the differential expression of endoplasmic reticulum aminopeptidase 2 (ERAP2) and γ-interferon-inducible lysosomal thiol reductase (IFI30) observed in shotgun proteomic analysis of cytokine treated and untreated human islets. Aliquots of protein samples (20 μg and 50 μg for IFI30 and ERAP2, respectively) from 4 different patient were mixed with Laemmli sample buffer, run in 8-16% polyacrylamide gels (Mini-PROTEAN® Precast Gels, Bio-Rad) using a mini-Protean Tetracell (Bio-Rad) and transferred onto nitrocellulose membranes (0.2 μm) using a Trans-Blot Turbo transfer system (Bio-Rad), as described [11]. The mouse anti-ERAP2 monoclonal antibody (R&D Systems, Minneapolis, MN, USA) was used at 1:1,000 dilution whereas the mouse anti-IFI30 monoclonal antibody (Santa-Cruz Biotechnology, Dallas, TX, USA) was diluted 1:500. A mouse anti-β-actin monoclonal antibody (1:5,000 dilution) (Millipore, Burlington, MA, USA), was used for internal normalization. The HRP-goat anti-mouse secondary antibody was used at 1:10,000 dilution (Perkin Elmer, Waltham, MA, USA). Immunoblots were developed using the enhanced chemiluminescence detection system, ECL-Pro (Perkin Elmer). The chemiluminescent images were acquired using LAS4010 (GE Health Care, Chicago, IL, USA). The immunoreactive specific bands were quantified using Image Quant-TL software (GE Health Care). Data are expressed as mean ± SEM. The student t-test was used to assess the difference between groups; a p-value < 0.05 was considered statistically significant.

2.8. Bioinformatic analysis

2.8.1. Pathway analysis

Pathway analysis of differentially expressed proteins was performed by Medscape (http://metascape.org/) and Ingenuity Pathway Analysis (IPA, QIAGEN Redwood City, www.qiagen.com/ingenuity, Build version: 321501 M, Content version: 21249400).

Pathway and process enrichment analyses of each given gene list were carried out by Metascape using the following ontology sources: KEGG Pathway, GO Biological Processes

and Reactome. All genome genes were used as the enrichment background. Terms with a p-value < 0.01, a minimum count of 3, and an enrichment factor > 1.5 were collected and grouped into clusters based on their membership similarities. More specifically, the bioinformatic application calculates p-values based on the accumulative hypergeometric distribution and q-values using the Banjamini-Hochberg procedure to account for multiple testing. Kappa scores were used as the similarity metric when performing hierarchical clustering on the enriched terms, and sub-trees with a similarity of > 0.3 were considered a cluster. The most statistically significant term within a cluster was chosen to represent the cluster. To further capture the relationships between the terms, a subset of enriched terms was selected and rendered as a network plot. In the network plot, terms with a similarity > 0.3 are connected by edges. The network is visualized using Cytoscape, where each node represents an enriched term and is coloured by its cluster ID. [12]

The IPA core analysis does not only provide gene functional annotation, canonical pathways, and network discovery but it also estimates the status of upstream regulators and downstream effects associated with canonical pathways, diseases, and functions. The upstream regulator analysis highlights the expected effects between transcriptional regulators and their target genes. The predicted activation or inhibition of each transcriptional regulator is inferred by the z score, which in turn derives the protein ratios in the dataset. Thus, z scores > 2.0 indicate that a molecule is predicted activated, whereas z scores < −2.0 indicate the probable inhibition of target molecules. Swiss-Prot accession numbers with corresponding ratios were imported into the software; analysis was performed selecting only direct relationships among genes and molecules in all species, and confidence setting was set to high predicted or experimental observed. The resulting networks highlight the functional relationships among proteins based on known associations in the literature. IPA comparison analysis between the results of the different sections for every condition was also performed.

2.8.2. Motif enrichment analysis

Motif-R (omicsolution.org/wukong/motifeR/) was used to analyse models of sequences with amino acids in specific positions of modify-21-mers (10 amino acids upstream and downstream of the site) for all protein sequences. Swiss-Prot protein sequence databases were used as background-database parameters (Human and Rattus norvegicus). The set of acetylated peptides from our dataset were pre-aligned, the acetylated lysine was taken in position 11 in a total of 21 amino acids for each site, and matched with background databases. All motifs with $p < 0.05$, a frequency ≥ 10 were enriched, and a table composed of enriched results was generated. A plot of enriched results was then generated and inserted in the table [13]. The percentage of variation of amino acids divided by groups, positively charged (K, R and H), negatively charged (D and E), neutral polar (S, T, C, N and Q), neutral apolar (G, A, P, V, L, I, M) and aromatic residues (W, F and Y), was analysed in -5 to +5 positions surrounding the Nε-acetylated site.

2.9. References

[1] Brozzi F, Nardelli TR, Lopes M, Millard I, Barthson J, Igoillo-Esteve M, Grieco FA, Villate O, Oliveira JM, Casimir M, Bugliani M, Engin F, Hotamisligil GS, Marchetti P, Eizirik DL. Cytokines induce endoplasmic reticulum stress in human, rat and mouse beta cells via different mechanisms. *Diabetologia.* 2015; 58(10):2307-16. doi: 10.1007/s00125-015-3669-6.

[2] Marchetti P, Suleiman M, De Luca C, Baronti W, Bosi E, Tesi M, Marselli L. A direct look at the dysfunction and pathology of the β cells in human type 2 diabetes. *Semin Cell Dev Biol.* 2020; 103:83-93. doi: 10.1016/j.semcdb.2020.04.005.

[3] Marselli L, Piron A, Suleiman M, Colli ML, Yi X, Khamis A, Carrat GR, Rutter GA, Bugliani M, Giusti L, Ronci M, Ibberson M, Turatsinze JV, Boggi U, De Simone P, De Tata V, Lopes M, Nasteska D, De Luca C, Tesi M, Bosi E, Singh P, Campani D, Schulte AM, Solimena M, Hecht P, Rady B, Bakaj I, Pocai A, Norquay L, Thorens B, Canouil M, Froguel P, Eizirik DL, Cnop M, Marchetti P. Persistent or Transient Human β Cell Dysfunction Induced by Metabolic Stress: Specific Signatures and Shared Gene Expression with Type 2 Diabetes. *Cell Rep.* 2020; 1;33(9):108466. doi: 10.1016/j.celrep.2020.108466.

[4] Marchetti P, Suleiman M, Marselli L. Organ donor pancreases for the study of human islet cell histology and pathophysiology: a precious and valuable resource. *Diabetologia.* 2018; 61(4):770-774. doi: 10.1007/s00125-018-4546-x.

[5] Ramos-Rodríguez M, Raurell-Vila H, Colli ML, Alvelos MI, Subirana-Granés M, Juan-Mateu J, Norris R, Turatsinze JV, Nakayasu ES, Webb-Robertson BM, Inshaw JRJ, Marchetti P, Piemonti L, Esteller M, Todd JA, Metz TO, Eizirik DL, Pasquali L. The impact of proinflammatory cytokines on the β-cell regulatory landscape provides insights into the genetics of type 1 diabetes. *Nat Genet.* 2019; 51(11):1588-1595. doi: 10.1038/s41588-019-0524-6.

[6] Bugliani M, Syed F, Paula FMM, Omar BA, Suleiman M, Mossuto S, Grano F, Cardarelli F, Boggi U, Vistoli F, Filipponi F, De Simone P, Marselli L, De Tata V, Ahren B, Eizirik DL, Marchetti P. DPP-4 is expressed in human pancreatic beta cells and its direct inhibition improves beta cell function and survival in type 2 diabetes. *Mol Cell Endocrinol.* 2018; 15;473:186-193. doi: 10.1016/j.mce.2018.01.019.

[7] Ferri G, Tesi M, Massarelli F, Marselli L, Marchetti P, Cardarelli F. Metabolic response of Insulinoma 1E cells to glucose stimulation studied by fluorescence lifetime imaging. *FASEB Bioadv.* 2020; 19;2(7):409-418. doi: 10.1096/fba.2020-00014.

[8] Del Guerra S, Lupi R, Marselli L, Masini M, Bugliani M, Sbrana S, Torri S, Pollera M, Boggi U, Mosca F, Del Prato S, Marchetti P. Functional and molecular defects of pancreatic islets in human type 2 diabetes. *Diabetes.* 2005; 54(3):727-35. doi: 10.2337/diabetes.54.3.727.

[9] Gaetani M, Sabatier P, Saei AA, Beusch CM, Yang Z, Lundström SL, Zubarev RA. Proteome Integral Solubility Alteration: A High-Throughput Proteomics Assay for Target Deconvolution. *J Proteome Res.* 2019; 1;18(11):4027-4037. doi: 10.1021/acs.jproteome.9b00500.

[10] Ciregia F, Giusti L, Ronci M, Bugliani M, Piga I, Pieroni L, Rossi C, Marchetti P, Urbani A, Lucacchini A. Glucagon-like peptide 1 protects INS-1E mitochondria against palmitate-mediated beta-cell dysfunction: a proteomic study. *Mol Biosyst.* 2015; 11(6):1696-707. doi: 10.1039/c5mb00022j.

[11] Ciregia F, Bugliani M, Ronci M, Giusti L, Boldrini C, Mazzoni MR, Mossuto S, Grano F, Cnop M, Marselli L, Giannaccini G, Urbani A, Lucacchini A, Marchetti P. Palmitate-induced lipotoxicity alters acetylation of multiple proteins in clonal β cells and human pancreatic islets. *Sci Rep.* 2017; 18;7(1):13445. doi: 10.1038/s41598-017-13908-w.

[12] Zhou Y, Zhou B, Pache L, Chang M, Khodabakhshi AH, Tanaseichuk O, Benner C, Chanda SK. Metascape provides a biologist-oriented resource for the analysis of systems-level datasets. *Nat Commun.* 2019; 3;10(1):1523. doi: 10.1038/s41467-019-09234-6.

[13] Wang S, Cai Y, Cheng J, Li W, Liu Y, Yang H. motifeR: An Integrated Web Software for Identification and Visualization of Protein Posttranslational Modification Motifs. *Proteomics.* 2019; 19(23):e1900245. doi: 10.1002/pmic.201900245.

3. Results

3.1. Proteome and acetylome analysis of human pancreatic islets

3.1.1. Effect of cytokine-induced damage

To ensure that cytokines (50 U/ml IL-1β, and 1000 U/ml IFN-γ for 48 h) affect both function and vitality of human islet β cells, insulin content, insulin secretion, and caspase 3/7 activity were measured. As expected, insulin content and insulin stimulation index in response to glucose were significantly reduced after cytokine-treatment (Figure9A, 9B) while the activity of caspase 3/7 was significantly increased (Figure 9C).
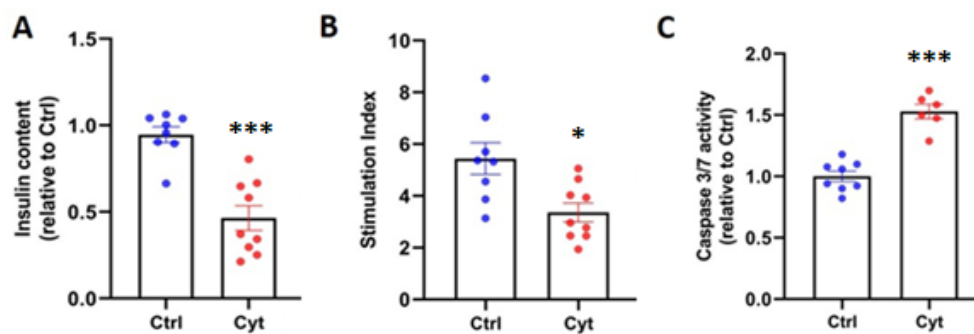
Figure 9. A) Insulin content, reduced after cytokine-treatment. B) Insulin stimulation index was reduced after 48 h treatment with cytokines. C) Cytokines induced a significant activation of caspase 3/7. One to three replicates from three to four independent islet preparations were studied. The different groups were compared by one-way ANOVA followed by Tukey correction. ****p<0.0001, **p<0.01, *p<0.05

3.1.2. Protein expression analysis by multidimensional shotgun proteomics

Isotope free shotgun proteomic analysis, performed after 1D-PAGE separation, was carried out to identify differentially expressed proteins in human pancreatic islets from 3 donors (biological replicates) treated with and without cytokines.

In Figure 10A, the 16 extracted protein bands are highlighted and paired to the corresponding average mass of the proteins identified in each band. Approximately 2,500 proteins were identified by merge-processing in the 16 bands of CTRL and Cyto samples from subject 2 and 3 while around 2,000 proteins were identified in samples from subject 1. Approximately half the proteins are common among subjects as shown in the Venny

diagram (Figure 10 C). The false FDR was set to 0.1% at the PSM level, resulting in an average protein FDR lower than 1.0%. Expression analysis for relative abundance of identified proteins was performed at the band-slice level by the label-free quantification module PEAKS-Q, part of PEAKS Studio v. 7.5. This quantification method is based on the MS1 ion peak intensity of the extracted chromatograms of peptides detected in multiple samples and applies the expectation-maximization algorithm to detect and resolve overlapping features. A high-performance retention time alignment algorithm is also used to align features of the same peptide from multiple samples. An example of a single band LFQ analysis is displayed in Figure 10 B, in which the heatmap showing the ratio of differential protein expression in band 8 of subject 1 is reported. The differentially expressed proteins were calculated for each band using 0.5% FDR and the resulting ID lists were filtered considering only peptides confidently identified in at least 1 sample with significance ≥ 20 (-10lgP), quality factor ≥ 0.5, and by considering only proteins identified with significance ≥ 20 and fold change ≥ 2. The lists of resulting deregulated proteins of each band-slice were merged and manually curated to remove proteins identified in multiple adjacent bands, non-distinguishable isoforms, and keratins.

Two thousand two hundred and seventy-one (2271) and 2362 proteins were identified in CTRL and Cyto groups (n=3), respectively, with at least 2 unique peptides in 2 or 3 patients. Four hundred ninety-two (492), 841, and 1073 differentially expressed proteins were obtained by the paired comparison. To increase analysis confidence, proteins, which were present in at least 2 out of 3 subjects and featuring a consistent modulation, were selected for further processing and pathway analysis. Therefore, 245 differentially expressed proteins were found by comparing Cyto to CTRL. Table 2 shows the top 25 over- and the top 25 under- expressed proteins based on the ratio (Cyto/CTRL) value.
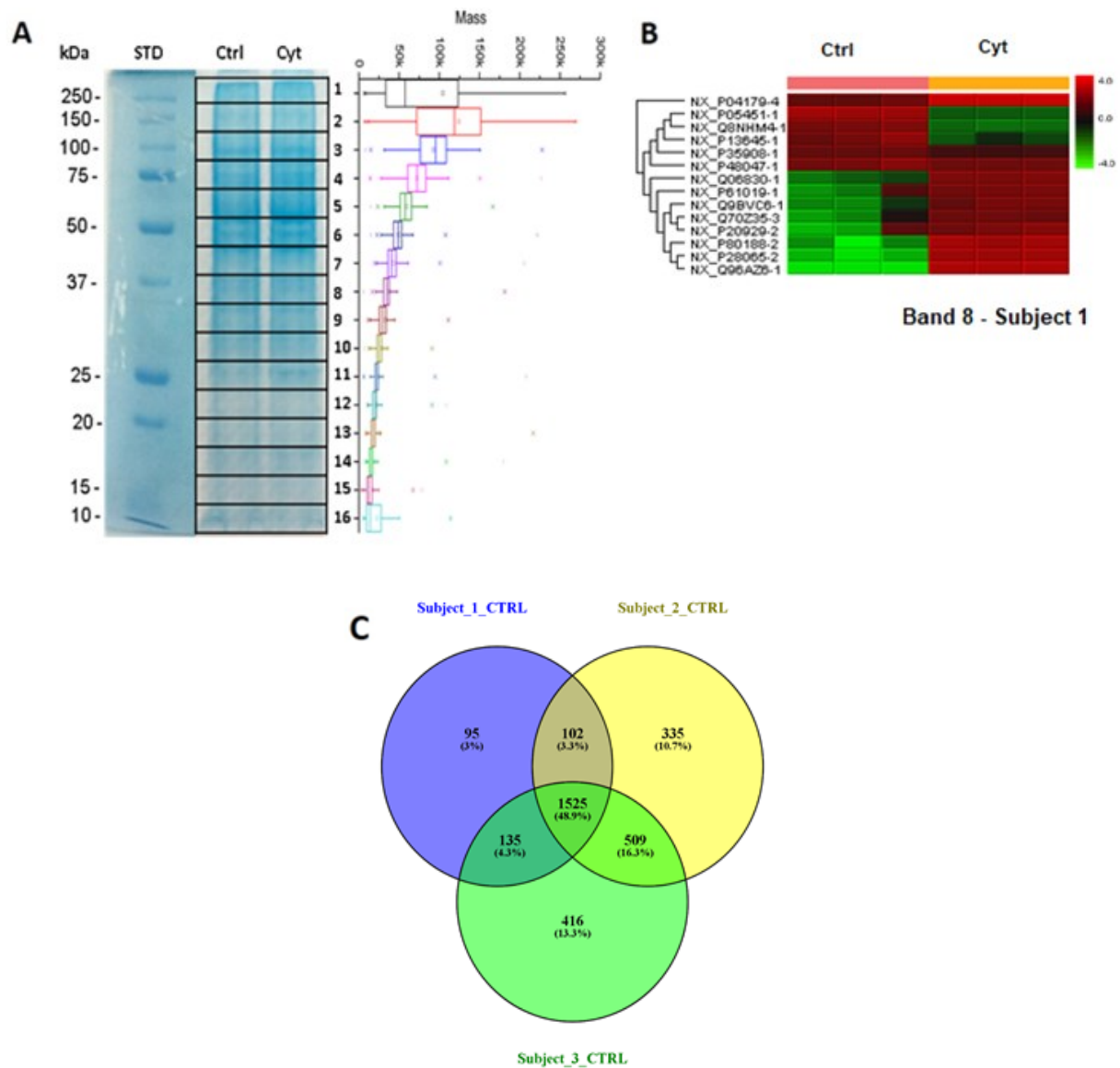
Figure 10. Global view of the shotgun proteomic analysis of human pancreatic islets treated (Cyto) and untreated (CTRL) with cytokines. A) A representative 1D gel, in which the 16 extracted bands are highlighted and paired to the corresponding average mass of the proteins identified in each band. B) Heatmap of the LFQ result summary of the proteins extracted from band 8 of subject 1 islets (Cyto vs CTRL). C) Venn diagram showing the number of proteins found in the islets of each subject in basal conditions (CTRL) and the overlaps.

The curated list of 245 proteins consistently deregulated was submitted to Metascape analysis. The pathway enrichment analysis is shown in Figure 11. The most significant enriched pathway included 54 proteins annotated as "Cytokine Signaling in Immune system" with a score enrichment -$\log_{10}$ p-value of 35,97. Regulator enrichment analysis

highlighted the involvement of regulators such as the transcription factor p65 (RELA), NF-κB, STAT1, and interferon regulatory factor 1 (IRF1), which included 23, 23, 11, and 9 proteins with 14, 14, 12 and 7.10 -Log$_{10}$ p-values, respectively.
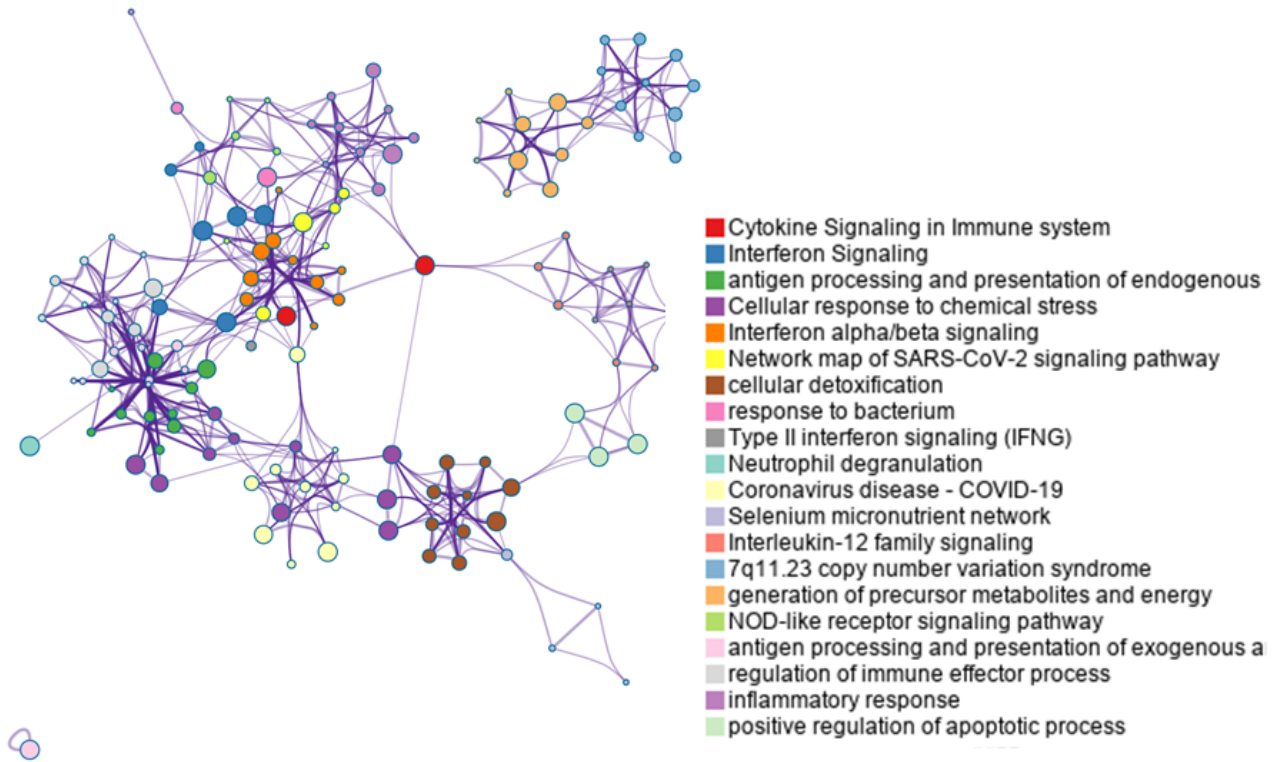
Figure 11. Metascape enrichment analysis. Network of enriched terms coloured by cluster ID. Nodes that share the same cluster ID are typically close to each other. The most significant enriched pathway includes 54 proteins annotated as "Cytokine Signalling in immune system".

Table 2. List of top 50 differentially expressed proteins in human islets exposed to cytokines.

ID	Gene	Name	-10lgP	Cov.	Pept.	Uniq.	Length	Log₂ Ratio
P20591	MX1	Interferon-induced GTP-binding protein Mx1	231.14	40	33	29	662	5.31
P13284	IFI30	Gamma-interferon-inducible lysosomal thiol reductase	69.56	15	3	3	250	5.25
P10321	HLA-C	HLA class I histocompatibility antigen, C alpha chain	233.59	53	20	2	366	5.22
P14174	MIF	Macrophage migration inhibitory factor	127.8	45	12	10	115	5.13
P0C0S5	H2AZ1	Histone H2A.Z	111.31	38	7	3	128	5.09
P00751	CFB	Complement factor B	199.19	22	17	16	764	5.04
Q13113	PDZK1IP1	PDZK1-interacting protein 1	77.85	39	5	4	114	4.76
P05362	ICAM1	Intercellular adhesion molecule 1	235.35	40	23	22	532	4.63
P55769	SNU13	NHP2-like protein 1	108.56	52	6	6	128	4.54
P69905	HBA1;	Hemoglobin subunit alpha	118.82	35	5	5	142	4.54
P00450	CP	Ceruloplasmin	173.93	20	19	19	1065	4.45
P23381	WARS1	Tryptophan--tRNA ligase, cytoplasmic	340.9	85	65	62	471	4.19
P10145	CXCL8	Interleukin-8	99.08	38	4	4	99	4.14
P01911	HLA-DRB1	HLA class II histocompatibility antigen, DRB1 beta chain	56.34	8	2	2	266	3.89
Q03519	TAP2	C-X-C motif chemokine 8	104.97	15	10	10	686	3.80
O14933	UBE2L6	Ubiquitin/ISG15-conjugating enzyme E2 L6	43.31	10	2	2	153	3.54
P09341	CXCL1	Growth-regulated alpha protein	176.27	54	9	6	107	3.49
O95786	DDX58	Antiviral innate immune response receptor RIG-I	135.75	12	11	10	925	3.49
P40306	PSMB10	Proteasome subunit beta type-10	62.22	12	4	3	273	3.42
Q03518	TAP1	Antigen peptide transporter 1	171.55	21	13	10	808	3.40
Q63HN8	RNF213	E3 ubiquitin-protein ligase RNF213	321.06	25	123	109	5207	3.37
P02778	CXCL10	C-X-C motif chemokine 10	123.49	36	5	4	98	3.32
P14902	IDO1	Indoleamine 2,3-dioxygenase 1	174.5	37	16	16	403	3.32
Q96AZ6	ISG20	Interferon-stimulated gene 20 kDa protein	133.1	40	7	5	181	3.32
P68133	ACTA1	Actin, alpha skeletal muscle	283.44	45	48	3	377	3.32
Q8WY91	THAP4	Peroxynitrite isomerase THAP4	49.4	2	2	2	577	-2.56
P02753	RBP4	Retinol-binding protein 4	132.96	17	6	6	201	-2.74
P04439	HLA-A	HLA class I histocompatibility antigen, A alpha chain	272.93	59	28	4	365	-3.32
P34059	GALNS	N-acetylgalactosamine-6-sulfatase	35.88	2	2	2	522	-3.32
Q96JB6	LOXL4	Lysyl oxidase homolog 4	80.01	7	4	4	756	-3.32
Q9ULP0	NDRG4	Protein NDRG4	29.03	3	2	2	352	-3.32
P51580	TPMT	Thiopurine S-methyltransferase	67.67	11	3	3	245	-3.32
Q5BJF2	TMEM97	Sigma intracellular receptor 2	71.57	10	2	2	176	-3.32
Q9BYX7	POTEKP	Putative beta-actin-like protein 3	244.98	29	27	2	375	-3.32
P13637	ATP1A3	Sodium/potassium-transporting ATPase subunit alpha-3	231.16	17	17	2	1013	-3.32
P02751	FN1	Fibronectin	158.5	12	22	21	2477	-3.32
Q6KB66	KRT80	Keratin, type II cytoskeletal 80	89.23	9	4	3	452	-3.32
P43246	MSH2	DNA mismatch repair protein Msh2	72.08	6	7	3	934	-3.32
Q14966	ZNF638	Zinc finger protein 638	71.38	3	7	2	1978	-3.32
Q32P28	P3H1	Prolyl 3-hydroxylase 1	74.53	6	6	3	736	-3.32
O95140	MFN2	Mitofusin-2	55.62	4	4	2	757	-3.32

Q12860	CNTN1	Contactin-1	61.85	4	4	3	1018	-3.32
Q9BZH6	WDR11	WD repeat-containing protein 11	49.08	2	2	2	1224	-3.32
Q9NRH3	TUBG2	Tubulin gamma-2 chain	48.73	4	2	2	451	-3.32
Q9NR30	DDX21	Nucleolar RNA helicase 2	39.59	4	2	2	783	-3.32
P52815	MRPL12	39S ribosomal protein L12, mitochondrial	80.07	14	3	2	198	-3.32
Q13123	IK	Protein Red	32.21	2	2	2	557	-3.32
Q99442	SEC62	Translocation protein SEC62	34.7	5	2	2	399	-3.32
P61204	ARF3	ADP-ribosylation factor 3	167.83	47	13	7	181	-3.32
Q01995	TAGLN	Transgelin	130.88	50	11	10	201	-3.47

ID, protein accession number; Cov., coverage; Pep., number of identified peptides; Uniq., unique peptides; Length, protein length; Cyto/CTRL, Cyto/CTRL ratio value.

3.1.3. Ingenuity Pathway Analysis (IPA) of differentially expressed proteins

The effects of cytokines on human islets are well documented [1; 2; 3] but an extensive analysis of protein expression variations has not been performed yet. Therefore, IPA was used to confirm the strength of our results achieved by the shotgun proteomic approach. Two hundred forty-five proteins differentially expressed in Cyto respect to CTRL samples were included in IPA analysis to obtain related molecular functions and canonical pathways. The IPA canonical pathways indicated that the highest p-values were linked to the "Antigen Presentation Pathway", "Phagosome Maturation", "Acute Phase Response Signaling", and "Interferon Signaling". Interestingly, we also found other inflammation-related pathways, such as the "IL-17 Signaling" and "Neuroinflammation Signaling", and some stress-related pathways, such as the "NRF2-mediated Oxidative Stress Response", "Mitochondrial Disfunction", and, of course, the "Type 1 Diabetes Mellitus Signaling" (data not show). The Upstream Regulators resulting from IPA confirmed the activation of some transcription factors such as STAT1, IRF1, RELA, and IRF7 with high positive values of the z-score. The top 25 upstream regulators ordered by p-value are listed in Table 3.

Table 3. List of top 25 upstream regulators ordered by p-value.

Upstream Regulator	Predicted Activation State	Activation z-score	-Log$_{10}$ p-value
IFNG	Activated	6.443	26,90
IRF1	Activated	3.646	25,84
STAT1	Activated	5.441	25,50
TNF	Activated	5.978	23,84
OSM	Activated	4.303	22,88
IFNA2	Activated	4.873	22,40
PML	Activated	2.915	22,14
IL1B	Activated	5.231	21,55
IFNL1	Activated	4.385	20,74
IFN-α	Activated	5.445	20,18
CD40LG	Activated	3.216	20,07
RELA	Activated	2.433	19,75
IRF7	Activated	4.779	19,30
APP	Activated	3.58	18,79
IFNAR	Activated	4.293	18,47
MYC	-	-0.832	17,29
TP53	-	0.986	17,06
STAT3	-	1.018	16,89
IFNAR2	Activated	3	16,48
HRAS	-	1.445	15,72
MAPK1	Inhibited	-4.861	15,66
IL6	Activated	2.55	15,60
IRF3	Activated	3.717	15,37
PRL	Activated	2.315	15,19
IRF2	-	0.928	14,59
MAP3K7	-	1.195	14,26

3.1.4. WB analysis of ERAP2 and IFI30 expression in human islets treated and untreated with cytokines

To validate shotgun proteomic results, two proteins were selected and their difference of expression in human islets treated and untreated with cytokine was evaluated using WB analysis. Specifically, based on availability of specific antibody and value of fold variation observed, ERAP2 and IFI30 were selected. Four mains specific immunoreactive bands with apparent molecular weight (MW) of 110, 105, 70, and 45 kDa, were detected for ERAP2

corresponding to different protein isoforms (Q6P179-1 corresponding to 110kDa, Q6P179-2 60kDa, Q6P179-3 105kDa and Q6P179-4 40kDa,). In our shotgun experiments, ERAP2 was identified in band 3 of 1DE gel corresponding to higher molecular weight isoforms 1 and 3 of 110 and 105 KDa, respectively. A significant different expression of 110 KDa but not 105 KDa band was observed suggesting the involvement of isoform 1 in the cytokine response. A specific 28 kDa immunoreactive band was detected for IFI30. For each tested protein, the optical density of the specific immunoreactive band was normalized by β-actin optical density; the resulting mean values ± SEM were then compared. Bar graphs obtained for the validated proteins are shown in Figure 12. In agreement with the shotgun proteomic analysis, ERAP2 and IFI30 expression was affected by cytokines treatment.
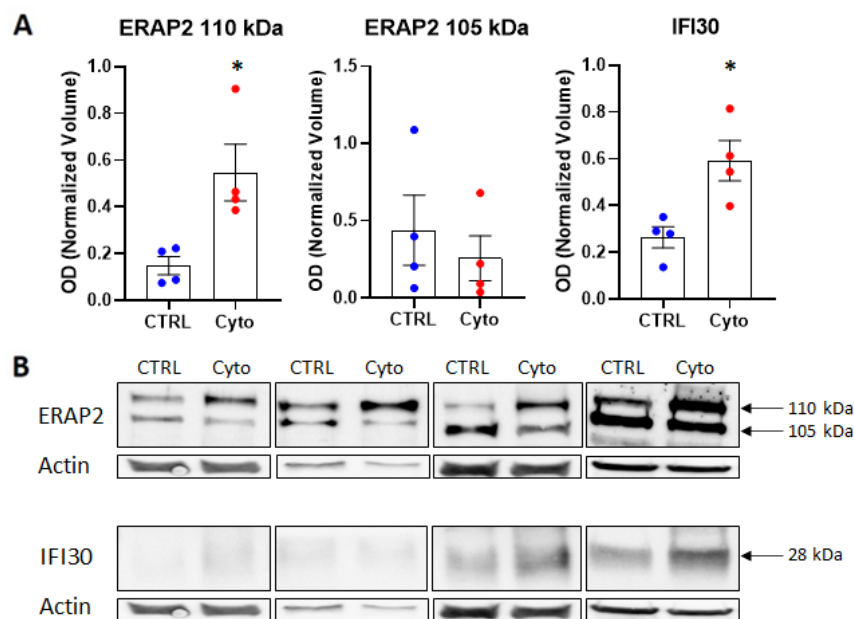
Figure 12. Validation of two differentially expressed proteins, ERAP2 and IFI30, in cytokines treated (Cyto) and untreated (CTRL) human islets using WB analysis. A) Bar graph of the normalized optical density (OD) of ERAP2 and IFI30 bands. B) The immunoreactive bands of ERAP2 (110 and 105 kDa) and IFI30 (28 kDa) observed in four independent islet preparations treated (Cyto) and untreated (CTRL) with cytokines are shown. Each islet preparation was analyzed in duplicate. Statistical analysis was performed using a parametric paired t test. *, p<0.05.

3.1.5. Acetylome analysis of human pancreatic islets

Immuno-enrichment of ε-acetyl lysines, was carried out to identify differentially acetylated proteins in 3 human donor pancreatic islets treated and untreated with cytokines. Only peptides identified with significance ≥ 20 and fold change ≥ 1,5 were consider for differentially acetylated peptides analysis. In total, 785 and 665 acetylated peptides were identified in CTRL and Cyto samples, respectively. The paired comparison revealed 144 differentially acetylated sites in Cyto, among which 31 and 113 sites showed increased and decreased acetylation, respectively (Table 4).

Table 4. List of differentially Nε-acetylated proteins in human islets treated (Cyto) and untreated (CTRL) with cytokines.

ID	Gene	Name	# Lysine	Log$_2$ Ratio
P56381	ATP5E	ATP synthase subunit epsilon, mitochondrial	K21	2.95
P50440	GATM	Glycine amidinotransferase, mitochondrial	K385	0.77
Q99880	H2BC13	Histone H2B type 1-L	K21-24, K21-25, K121, K17-21	3.32; 3.322; 3.322; 3.322
P01889	HLA-B	HLA class I histocompatibility antigen, B alpha chain	K267	12.36
P60842	EIF4A1	Eukaryotic initiation factor 4A-I	K54, K54	2.33; 2.34
Q13423	NNT	NAD(P) transhydrogenase, mitochondrial	K70	1.77
P07237	P4HB	Protein disulfide-isomerase	K502, K200	3.32; 2.34
Q99623	PHB2	Prohibitin-2	K147, K142	0.86; 1.20
P04179	SOD2	Superoxide dismutase [Mn], mitochondrial	K122, K130, K221, K222	1.06; 1.48; 2.34; 3.32
Q03518	TAP1	Antigen peptide transporter 1	K449	3.32
Q8WZ42	TTN	Titin	K19841, K19842, 32825, K11527	2.74; 2.32; 1.75; 2.34
P29401	TKT	Transketolase	K314	2.75
P45880	VDAC2	Voltage-dependent anion-selective channel protein 2	K74	0.43
Q9Y277	VDAC3	Voltage-dependent anion-selective channel protein 3	K12	1.34
P00338	LDHA	L-lactate dehydrogenase A chain	K118, K118, K126	2.77; 2.34; -3.32
P00505	GOT2	Aspartate aminotransferase, mitochondrial	K363	-0.81
P60709	ACTB	Actin, cytoplasmic 1	K314, K316	-0.89; -1.69
P68032	ACTC	Actin, alpha cardiac muscle 1	K328, K330	-0.45; -0.67
P63261	ACTG	Actin, cytoplasmic 2	K328	-0.62
P68133	ACTA	Actin, alpha skeletal muscle	K328, K330	-0.45; -0.67
P05141	SLC25A5	ADP/ATP translocase 2	K92	-1.32
P12236	SLC25A6	ADP/ATP translocase 3	K23, K92	-1.22; -1.32
P00352	ALDH1A1	Retinal dehydrogenase 1	K412, K410, K412	-3.47; -1.12; -1.00
Q13825	AUH	Methylglutaconyl-CoA hydratase, mitochondrial	K211	-0.67
P13987	CD59	CD59 glycoprotein	K66	-1.18
P61604	HSPE1	10 kDa heat shock protein, mitochondrial	K40	-3.32
P10809	HSPD1	60 kDa heat shock protein, mitochondrial	K473	-1
Q96KP4	CNDP2	Cytosolic non-specific dipeptidase	K37	-1.4
P17538	CTRB1	Chymotrypsinogen B	K111	-3.32
Q6GPI1	CTRB2	Chymotrypsinogen B2	K111, K108, K111	-3.32; -3.32; -3.32
P09622	DLD	Dihydrolipoyl dehydrogenase, mitochondrial	K143, K146, K267	-0.67; -2.32; -0.54
P40939	HADHA	Trifunctional enzyme subunit alpha, mitochondrial	K534, K289, K326, K406	-2.25; -0.84; -0.56; -0.89

P68104	EEF1A1	Elongation factor 1-alpha 1	K179	-2.12
Q5VTE0	EEF1A1P5	Putative elongation factor 1-alpha-like 3	K179	-2.12
P26641	EEF1G	Elongation factor 1-gamma	K434	-2.64
P06733	ENO1	Alpha-enolase	K228, K80, K193	-0.97; -1.32; -1.47
P07954	FH	Fumarate hydratase, mitochondrial	K80	-1
P04406	GAPDH	Glyceraldehyde-3-phosphate dehydrogenase	K84, K194, K254, K259, K260	-1.36; -0.54; -3.32; -3.32
Q9BTM1	H2AJ	Histone H2A.J	K10, K6-10	-1.18; -1.89
P62807	H2BC4	Histone H2B type 1-C/E/F/G/I	K21-24, K121, K21, K6	-1.40; -0.84; -0.92; -1.89
Q16778	H2BC21	Histone H2B type 2-E	K21-24, K121, K21, K6, K109	-0.94; -0.79; -1; -1.69; -3.18
Q5QNW6	H2BC18	Histone H2B type 2-F	K21, K121, K17-21, K17-24, K109	-2.18; -2.18; -1.94; -3.32; -2.94
P68431	H3C1	Histone H3.1	K80, K19-24, K10-15, K24, K15	-0.51; -1.09; -0.71; -1.47
Q71DI3	H3C15	Histone H3.2	K80, K19-24, K10-15, K24, K15	-0.51; -1.09; -0.71; -1.47
P84243	H3-3A	Histone H3.3	K80, K19-24, K10-15, K24, K15	-0.51; -1.09; -0.71; -1.47
P62805	H4C1	Histone H4	K13, K13-17	-0.79; -0.62
Q16836	HADH	Hydroxyacyl-coenzyme A dehydrogenase, mitochondrial	K179	-3.32
Q9BSH5	HDHD3	Haloacid dehalogenase-like hydrolase domain-containing protein 3	K15	-0.92
O60812	HNRNPCL1	Heterogeneous nuclear ribonucleoprotein C-like 1	K29	-3.32
B2RXH8	HNRNPCL2	Heterogeneous nuclear ribonucleoprotein C-like 2	K29	-3.32
B7ZW38	HNRNPCL3	Heterogeneous nuclear ribonucleoprotein C-like 3	K29	-3.32
P0DMR1	HNRNPCL4	Heterogeneous nuclear ribonucleoprotein C-like 4	K29	-3.32
P07910	HNRNPC	Heterogeneous nuclear ribonucleoproteins C1/C2	K29	-3.32
P61978	HNRNPK	Heterogeneous nuclear ribonucleoprotein K	K34, K163	-1.03; -1.18
P08238	HSP90AB1	Heat shock protein HSP 90-beta	K438	-1.32
P30740	SERPINB1	Leukocyte elastase inhibitor	K87	-1.22
P14174	MIF	Macrophage migration inhibitory factor	K78	-0.56
P06748	NPM1	Nucleophosmin	K267	-0.58
P36957	DLST	Dihydrolipoyllysine-residue succinyltransferase component of 2-oxoglutarate dehydrogenase complex, mitochondrial	K273	-0.97
A6NHN0	OTOL1	Otolin-1	K190-K193	-1.74
Q8WUM4	PDCD6IP	Programmed cell death 6-interacting protein	K350	-0.71
Q96JY6	PDLIM2	PDZ and LIM domain protein 2	K282	-3.32
P00558	PGK1	Phosphoglycerate kinase 1	K48	-0.51
P62937	PPIA	Peptidyl-prolyl cis-trans isomerase A	K28	-3.32
P06454	PTMA	Prothymosin alpha	K15	-1.12
P62826	RAN	GTP-binding nuclear protein Ran	K60	-0.89
P43487	RANBP1	Ran-specific GTPase-activating protein	K150	-4.64
P05451	REG1A	Lithostathine-1-alpha	K165, K148	-1.22; -1.43
P48304	REG1B	Lithostathine-1-beta	K148	-2.56
P62861	FAU	40S ribosomal protein S30	K51	-1.36
P08865	RPSA	40S ribosomal protein SA	K52	-0.58
P31040	SDHA	Succinate dehydrogenase [ubiquinone] flavoprotein subunit, mitochondrial	K547	-1.69
Q9UHD8	SEPTIN9	Septin-9	K62	-3.32
P17987	TCP1	T-complex protein 1 subunit alpha	K484	-0.94
P24752	ACAT1	Acetyl-CoA acetyltransferase, mitochondrial	K174	-1
P42765	ACAA2	3-ketoacyl-CoA thiolase, mitochondrial	K13	-0.79
Q8IYQ7	THNSL1	Threonine synthase-like 1	K281	-1.09
P12270	TPR	Nucleoprotein TPR	K748	-0.86
P21796	VDAC1	Voltage-dependent anion-selective channel protein 1	K224	-0.81
P04075	ALDOA	Fructose-bisphosphate aldolase A	K200, K147	-1.79; 3.32

ID	Gene	Protein	#Lys	Log₂
P25705	ATP5F1A	ATP synthase subunit alpha, mitochondrial	K539, K541, K506	-0.76; 2.34; -0.81
P14625	GRP94	Endoplasmin	K75	3.32
P40926	MDH2	Malate dehydrogenase, mitochondrial	K324, K296	0.61; -1.18

ID, protein accession number; gene, gene name; protein, protein name; #Lys, lysine position in the polypeptide chain; Log₂,

Log₂ Cyto/CTRL ratio value.

IPA analysis of differentially acetylated proteins highlighted 93 significant canonical pathways. In Table 5, the top 10 canonical pathways ordered according to $-\text{Log}_{10}$ (p-value) are shown. The analysis also showed up other canonical pathways, which are important in the contest of this research, such as cytokine-induced β cell death, nuclear factor erythroid 2-related factor 2 (NRF2) mediated oxidative stress response, protein ubiquitination pathway, Peroxisome proliferator-activated receptor alpha (PPARα) / Retinoic acid receptor RXR-alpha (RXRα) activation, mTOR Signalling, unfolded protein response, and NO signalling.

Table 5. List of top 10 canonical pathways highlighted by IPA analysis of differentially acetylated proteins.

Canonical Pathways	$-\text{Log}_{10}$ p-value
Sirtuin Signalling Pathway	10.1
Isoleucine Degradation I	8.74
TCA Cycle II (Eukaryotic)	8.15
Gluconeogenesis I	7.86
Mechanisms of Viral Exit from Host Cells	6.82
Glutaryl-CoA Degradation	6.35
Mitochondrial Dysfunction	6.06
Glycolysis I	5.89
Tryptophan Degradation III (Eukaryotic)	5.83
RHOA Signalling	5.68

3.1.6. Motif enrichment analysis

To characterize the possible specific sequence motifs surrounding acetylated lysine residues of proteins, a motif analysis was generated to evaluate the likelihood of amino acids being over- or under-represented at positions surrounding the acetyl lysine sites (Table 6). Five motifs were significantly enriched in all ε-acetyl lysine sites, including ....KF........., ...A......K.........., ...K....T....., ...K....K..... and ..K.......K.......... . The amino acid frequencies of sequences flanking acetylated sites were assessed to confirm whether there were position-specific amino acids adjacent to Nε-acetyl sites by motif model.

Phenylalanine (F), alanine (A), threonine (T), and lysine (K) were overrepresented surrounding Nε-acetyl sites. Phenylalanine was often found in +1 position while alanine, threonine, and lysine were frequently present in more distant positions as shown in Table 6.

Table 6. Motif enriched analysis of human islet acetylome. Schematic representation and plot of motifs are shown; a dot stands for a generic amino acid. The motif score was calculated by taking the sum of the -Log₁₀ p-value used to fix each position of the motif. Higher motif scores typically correspond to motifs that are statistically more significant as well as more specific. Match represents the sequence frequency matching with this motif in the dataset. Fold is an indicator of the enrichment level of the extracted motifs. It was calculated by using the following mathematical ratio, (Dataset matches/Dataset size)/(Background matches/Background size).

Motif	Plot	Score	Match	Size	Fold
.........KF.........		7,03	16	106	5,14
...A......K..........		2,83	14	90	2,49
.........K....T.....		2,32	10	76	2,64
.........K....K.....		2,52	13	66	2,38

| ..K.......K.......... | | 2,84 | 11 | 53 | 2,86 |

To complete the motif analysis, the percentage of variation of grouped amino acids from -5 to +5 positions was calculated. Amino acids were grouped based on their chemical propriety in positively and negatively charged at physiologic pH, aromatic, polar and non-polar residues. The percentage of variation was calculated as percentage of amino acids in a specific position minus medium percentage in previous (for negative position) or following (for positive positions) amino acids divided by the medium percentage in previous or following amino acids multiplied by 100. This type of analysis suggested an increased frequency of aromatic amino acids in +1 (281,82%) and -1 (68.00%) positions (Table 7). Positively charged amino acids showed a 18.87% increase in position +1, and 53.55% and 56.46% decreases in -1 and -2 positions, respectively. On the contrary, the negatively charged amino acids showed variation percentage decreases in + 1 (47.93%) and +2 (35.71%) positions (Table 7).

Table 7. Percentage of amino acid variation in -5 to +5 positions around Nε-acetylated sites. Green and red colours indicate decreased (-) and increased (+) % of variation, respectively while colour intensity correlates to the % value.

	-5	-4	-3	-2	-1	K	+1	+2	+3	+4	+5
AA +	-29.35	31.43	3.91	-56.46	-53.55	/	18.87	-21.24	-0.59	14.08	-13.22
AA -	13.21	1.54	19.74	7.87	-1.98	/	-47.93	-35.71	43.01	-11.11	32.81
AA +/- polar	0.00	34.62	-1.05	10.09	-2.02	/	-45.33	35.52	-28.31	-27.03	43.48
AA +/- apolar	-0.34	-32.95	-2.58	6.79	7.78	/	-7.19	24.10	12.54	17.69	-11.76
AA Aromatics	61.76	60.00	-14.04	37.50	68.00	/	281.82	-75.00	-14.04	-2.04	-30.23

Amino acid (AA), positively charged (+), negatively charged (-), neutral (+/-).

3.2. Proteome, Acetylome and Thermal stability analysis of INS-1E β cells

3.2.1. Effect of cytokine-induced damage

To ensure that cytokines (10 U/ml IL-1β and 50 U/ml IFN-γ for 24 h) affects INS-1E cell vitality and functional activity, morphological modifications, growth ratio, insulin content and insulin release were evaluated. After cytokine exposure, cells showed a spherical or needle shape and tended to detach themselves from each other, suggesting a damage and possible progression to apoptosis (Figure 13A). The growth ratio, which was calculated dividing the cell number after 24 h cytokine treatment by the number of cells seeded, showed a significant reduction of cell proliferation (Figure 13B). The insulin content was significantly lower in cells treated (Cyto) than those untreated (CTRL) (Figure 13C). The insulin stimulated release (16.7 mM glucose) did not significantly increase in Cyto cells while CTRL cells showed a significant release increase upon stimulation (Figure 13D).
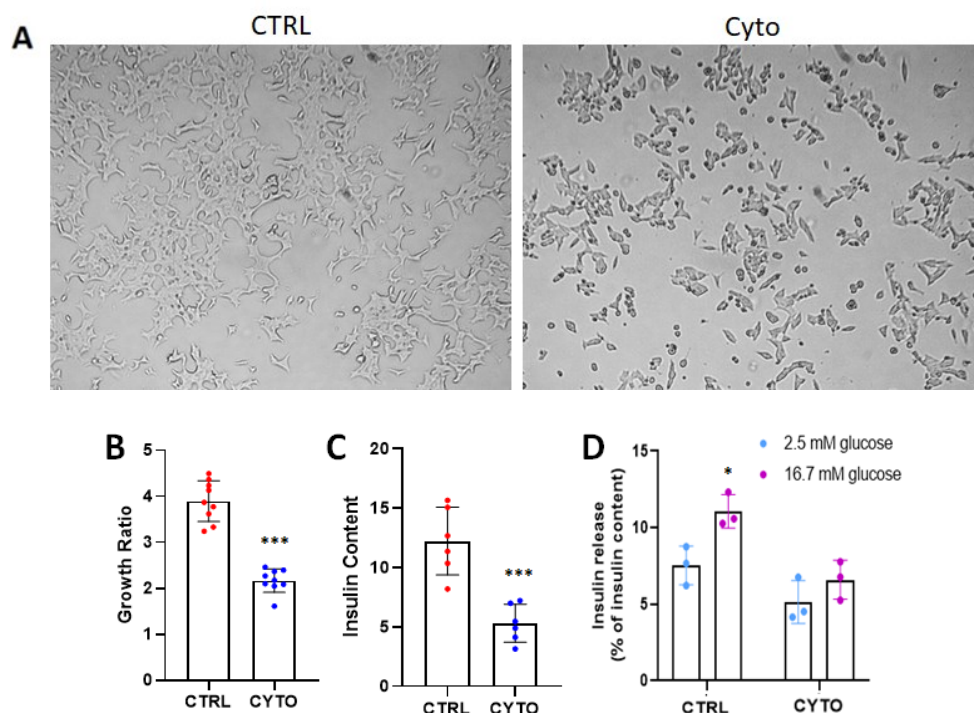
Figure 13. A) Morphological change of INS-1E β cells after cytokine treatment. B) Growth ratio calculated as number of cells after treatment with (Cyto) or without (CTRL) cytokines/number of cells seeded. C) Total insulin content in treated (Cyto) and untreated (CTRL) cells. D) Insulin release after 19.7 mM glucose stimulation of Cyto and CTRL cells. Cyto and CTRL data were compared by parametric t test. *, p<0.05; ***, p<0.001.

3.2.2. Protein expression analysis by Tandem Mass Tag (TMT) proteomics

Nine thousand seven hundred fifty-two (9752) proteins were identified with at least 2 unique peptides and quantified through TMT™10 in all INS-1E cell samples. Protein amount was normalized by the total amount of TMT™10 for each channel used.

Six thousand six hundred five (6605) proteins were found differentially expressed in cytokine treated cells (Cyto cells). To increase the confidence of the analysis, only proteins with a fold change greater than 1.5 were taken into account, thus reducing the list of proteins that showed a statistically significant variation to 637 proteins, of these 460 reduced and 177 increased in Cyto cells. (Figure 14, Table 8).
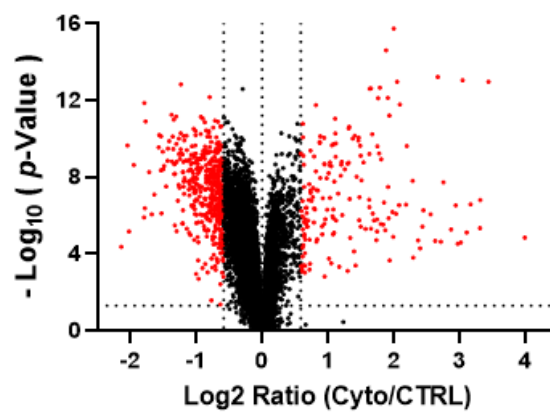
Figure 14. Volcano plot of differentially expressed proteins with a cut-off of 1.3 for -$\log_{10}$ p-values and ± 0.584 for $\log_2$ Cyto/CTRL ratio values. The red dots represent the curated list of proteins showing significant changes.

Table 8. List of top 50 differentially expressed proteins (25 up-regulated and 25 down-regulated) ordered by $\log_2$ Cyto/CTRL ratio values.

ID	Gene	Name	Cov.	Pept.	Uniq.	MW [kDa]	$\log_2$ Ratio	-$\log_{10}$ p-Value
Q7TNL0	Cxcl11	C-X-C motif chemokine	28	3	3	11.1	3.99	4.85
Q4FZX6	Rt1-ce10	RT1 class I, locus CE10	38	11	5	41.5	3.44	12.97
M0RDG2	Nos2	Nitric oxide synthase	73	66	87	130.5	3.31	6.81
F1LPS6	Ifit1	Interferon-induced protein with tetratricopeptide repeats 1	43	20	19	53.4	3.31	5.34
F1M9F6	Gbp5	Guanylate-binding protein 5	35	20	20	66.9	3.16	6.58
P18589	Mx2	Interferon-induced GTP-binding protein Mx2	75	44	41	75	3.11	5.11
Q63663	Gbp2	Guanylate-binding protein 1	46	24	24	67.1	3.04	13.05
Q499S4	Mx1	Interferon-induced GTP-binding protein Mx1	50	23	16	74.5	3.01	4.59
Q00238	Icam1	Intercellular adhesion molecule 1	24	13	13	60.1	2.97	4.53
A0A0H2UHF4	Rsad2	RCG62278	55	17	17	41.4	2.94	6.53

66

ID	gene	protein	Cov.	Pept.	Uniq.	MW	Log$_2$	-Log$_{10}$
Q4V797	RGD1309362	Interferon-gamma-inducible GTPase Ifgga1 protein	52	18	18	48.2	2.87	5.27
F1M512	Apol11a	Uncharacterized protein	18	4	4	34.9	2.75	7.72
Q8K4B1	Cxcl9	C-X-C motif chemokine	36	4	4	14.3	2.71	4.63
F7F469	Igtp	Interferon gamma-induced GTPase	24	23	26	157	2.66	13.22
A0A0G2JXY3		Uncharacterized protein	10	4	4	34.6	2.63	4.67
P48973	Cxcl10	C-X-C motif chemokine 10	45	3	3	10.7	2.56	6.05
F1LQF2	Rt1-s3	RT1 class Ib, locus S3	36	11	10	41.3	2.45	6.28
D4A2T4	RGD1305184	Interferon-gamma-inducible GTPase Ifgga4 protein	49	17	15	47.5	2.43	5.42
Q811A2	Bst2	Bone marrow stromal antigen 2	20	3	3	19.7	2.40	4.29
P30348	Cxcl2	C-X-C motif chemokine 2	49	3	3	10.8	2.37	4.70
M0RBH3		Takusan domain-containing protein	32	5	5	20	2.29	3.81
Q6DGG4	Irf1	Interferon regulatory factor	36	7	7	37.1	2.29	7.81
Q5M851	Cd69	CD69	20	4	4	22.3	2.20	9.62
P07151	B2m	Beta-2-microglobulin	63	5	5	13.7	2.18	6.57
P14095	Cxcl1	Growth-regulated alpha protein	46	3	3	10.2	2.09	11.78
P01322	Ins1	Insulin-1	72	7	5	12.4	-1.33	5.48
A0JPM2	Btg3	B-cell translocation gene 3, isoform CRA_b	23	5	5	28.9	-1.37	8.81
Q9JKA9	Hcn2	Potassium/sodium hyperpolarization-activated cyclic nucleotide-gated channel 2	8	7	2	94.9	-1.41	9.87
Q925B5	Syt13	Synaptotagmin-13	35	11	11	46.9	-1.43	9.49
D3ZNT6	Mafa	Transcription factor MafA	18	6	6	37.8	-1.43	8.85
P35739	Ntrk1	High affinity nerve growth factor receptor	17	10	9	87.8	-1.46	7.51
Q4G052	Wnt4	Protein Wnt	40	12	12	39	-1.49	8.58
Q5BJX4	Snx10	Sorting nexin 10	13	3	3	23.6	-1.50	8.41
D4ABF5	Zfp703	RCG43251	15	7	7	58.5	-1.51	9.33
P17425	Hmgcs1	Hydroxymethylglutaryl-CoA synthase, cytoplasmic	48	18	18	57.4	-1.53	6.11
P62024	Phactr1	Phosphatase and actin regulator 1	35	16	15	66.2	-1.54	10.13
Q6P7B9	Scd2	Stearoyl-CoA desaturase 2	30	9	9	41	-1.54	8.35
Q4KLN6	Rrm2	Ribonucleoside-diphosphate reductase subunit M2	49	17	17	45	-1.56	10.19
P0CD96	Occ1	Overexpressed in colon carcinoma 1 protein homolog	54	2	2	6.4	-1.57	9.55
P24464	Cyp4a12	Cytochrome P450 4A12	8	3	2	58.5	-1.64	7.08
D3ZGZ4	Rai2	RCG49718	28	11	11	57.1	-1.68	6.06
A0A096MIT8	LOC100912195	Protein BEX1-like	34	6	6	15.1	-1.72	8.26
Q64654	Cyp51a1	Lanosterol 14-alpha demethylase	42	17	17	56.7	-1.77	10.91
M0RA54	Smim24	RCG29408	9	2	2	13.4	-1.78	6.38
B2RYH5	Irak1	Interleukin-1 receptor-associated kinase 1	24	11	11	77.8	-1.79	11.86
Q923S2	Pdzk1ip1	PDZK1-interacting protein 1	28	3	3	12.2	-1.79	5.90
P05943	S100a10	Protein S100-A10	18	2	2	11.1	-1.95	8.63
P97563	Tmsb15b2	Thymosin beta	67	5	5	5.3	-2.02	5.17
B5DEN8	Hepacam2	HEPACAM family member 2	13	4	4	51.2	-2.05	9.64
Q3MKQ2	Bex1	Protein BEX1	30	5	2	15.2	-2.14	4.37

ID, protein accession number; gene, gene name; protein, protein name; Cov., coverage; Pept., number of identified peptides;

Uniq., unique peptides; MW, molecular weight; Log$_2$, Log$_2$ Cyto/CTRL ratio value; - Log$_{10}$, -Log$_{10}$ p-value.

The list of 637 proteins consistently deregulated were submitted to Metascape analysis. The pathway enrichment analysis is shown in Figure 15. Important pathways involved in cytokine signalling and inflammatory responses emerged such as "Type II Interferon Signalling", "Cytokine-mediated Signalling Pathway", "Positive Regulation of Cytokine Production", "TNF Signalling Pathway", and "NF-κB Signalling Pathway" with a -log10 p-value of 6.11, 5.95, 5.00, 6.64, and 6.54, respectively.
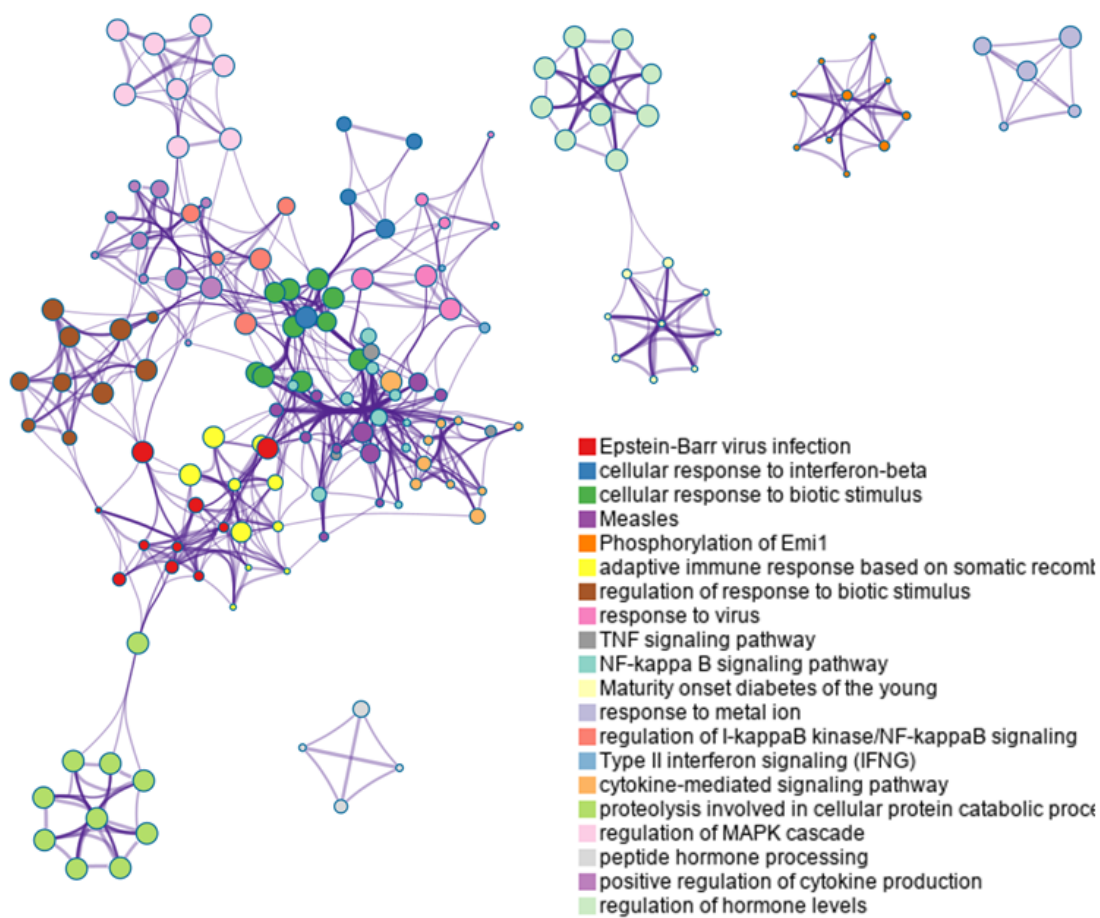

Figure 15. Metascape enrichment analysis. Network of enriched terms are coloured by cluster ID. Nodes that share the same cluster ID are typically close to each other.

3.2.3. Acetylome analysis of INS-1E cells

Three thousand six hundred thirteen (3613) acetylated peptides were overall identified in pooled samples (Cyto e CTRL), of which 477 were Nα-acetylated sites and 3136 were Nε-acetylated sites. By comparing Cyto to CTRL, a total of 334 differentially acetylated sites were found, of which 331 were Nε-acetylated sites (Table 9)

Table 9. List of top 50 differentially Nε- acetylated proteins in cytokine treated INS-1E cells.

ID	Gene	Protein	#Lysine	Log$_2$ Ratio
Q5XI78	Ogdhl	2-oxoglutarate dehydrogenase, mitochondrial	K276	2.71
Q03344	Atp5if1	ATPase inhibitor, mitochondrial	K52; K71	2.26
A0A0G2K4G0	Rai1	Retinoic acid-induced 1	K1074; K1077	2.22
G3V7J0	Aldh6a1	Aldehyde dehydrogenase family 6, subfamily A1, isoform CRA_b	K129	2.09
P97563	Tmsb15b2	Thymosin beta	K39; K4; K	2.06; 1.17; 1.00
G3V9U2	Acaa2	3-ketoacyl-CoA thiolase, mitochondrial	K158; K137	1.96; 1.10
A0A0G2KAN7	Gls	Glutaminase	K168; K201; K315	1.90; 0.64; 0.92
P13264	Gls	Glutaminase kidney isoform, mitochondrial	K169; K202; K316	1.90; 0.64; 0.92
P12785	Fasn	Fatty acid synthase	K1234; K1746; K673; K993; K1698	1.76; 0.76; 1.12; 0.85; 0.95
G3V7I0	Prdx3	Peroxiredoxin 3	K84	1.73
F1M9G7	Crebbp	Histone acetyltransferase	K1745	1.73
Q9JLH6	Cdk5rap1	Mitochondrial tRNA methylthiotransferase CDK5RAP1	K529	1.70
D3ZAI6	Nt5dc3	5'-nucleotidase domain-containing 3	K246; K136	1.69; 0.61
P62856	Rps26	40S ribosomal protein S26	K66	1.65
F1M5N4	Me3	Malic enzyme	K119	1.58
D3ZJH9	Me2	Malic enzyme	K94; K74; K197; K578	1.58; 0.91; 1.86; 0.89
D3ZT98	Bola3	BolA family member 3	K76	1.54
P05065	Aldoa	Fructose-bisphosphate aldolase A	K153	1.50
P10860	Glud1	Glutamate dehydrogenase 1, mitochondrial	K90; K548; K84; K503	1.47; 0.87; 0.90; 1.20
A0A0G2K3F1	RGD1565059	Similar to hypothetical protein E130311K13	K117	1.46
F1M953	Hspa9	75 kDa glucose-regulated protein	K675; K612; K600; K567; K143; K314; K234	1.44; 0.60; 0.73; 0.74; 1.11; 0.86; 1.08
Q6P9Y4	Slc25a4	ADP/ATP translocase	K272; K166	1.43; 0.60
D3ZVE5	RGD1561662	Similar to AI661453 protein	K748	1.42
P29418	Atp5f1e	ATP synthase subunit epsilon, mitochondrial	K44	1.41
Q5U300	Uba1	Ubiquitin-like modifier-activating enzyme 1	K657	1.39; 1.47
D4A1B9	Smc3	Structural maintenance of chromosomes protein	K105	-0.72
Q8CJB9	Rnf40	E3 ubiquitin-protein ligase BRE1B	K20	-0.72
G3V8B3	Hist1h2bq	Histone H2B	K21; K21, K24; K6	-0.72; -0.60; -0.45
D4A411	Brpf1	Bromodomain and PHD finger-containing, 1	K894	-0.73
D3ZSX2	Aff4	AF4/FMR2 family, member 4	K850	-0.75
P11232	Txn	Thioredoxin	K	-0.75
Q6AXQ0	Sae1	SUMO-activating enzyme subunit 1	K198	-0.76

ID	Gene	Protein	#Lys	Log2
G3V781	Mre11a	Double-strand break repair protein	K671	-0.77
Q9ERU2	Znf22	Zinc finger protein 22	K18	-0.80
A0A0G2JXW4	Hnrnpc	Heterogeneous nuclear ribonucleoprotein C, isoform CRA_a	K157	-0.80
A0A0G2K7B3	Hnrnpc	Heterogeneous nuclear ribonucleoproteins C1/C2-like	K144	-0.80
F1MAC0	Ifi47	Interferon gamma-inducible protein 47		-0.84
P52631	Stat3	Signal transducer and activator of transcription 3	K531	-0.92
Q62785	Pdap1	28 kDa heat- and acid-stable phosphoprotein	K172	-0.97
A0A0G2JVW6	Samd9	Sterile alpha motif domain-containing 9	K1552	-1.11
D3ZC87	Maff	MAF bZIP transcription factor F	K9	-1.16
G3V783	Ripk2	Receptor-interacting serine/threonine-protein kinase 2		-1.54
D3ZJ08	Hist2h3c2	Histone H3	K28; K28	-1.55; -1.35
G3V6P2	Dlst	Dihydrolipoyllysine-residue succinyltransferase component of 2-oxoglutarate dehydrogenase complex, mitochondrial	K273; K354	-1.64; 0.76
Q63663	Gbp2	Guanylate-binding protein 1	K395	-1.64
F1M7J7	Cep250	Centrosomal protein 250	K902; K908	-1.81
A0A0G2K4X1	RT1-A1	RT1 class Ia, locus A1	K79	-1.84
M0RBH3		Takusan domain-containing protein	K143	-2,14
F1LPS6	Ifit1	Interferon-induced protein with tetratricopeptide repeats 1	K88	-3.17
A0A096MJ38	Ifit1bl	Interferon-induced protein with tetratricopeptide repeats 1B-like	K97	-3.17

ID, protein accession number; Gene, gene name; Protein, protein name; #Lys, lysine position in the polypeptide chain;

Log2, Log2 of Cyto/CTRL ratio;.

IPA analysis indicated that the differentially acetylated proteins of cytokine treated cells were significantly involved in 99 canonical pathways. In Table 10, the top 10 canonical pathways ordered by p-value are shown. Many of these pathways are related to cellular metabolism, such as fatty acid β-oxidation I, gluconeogenesis I, TCA cycle II, and oxidative phosphorylation while others are linked to Sirt signalling, mitochondrial dysfunction and insulin secretion. Moreover, other canonical pathways, which play a role in the contest of β cell stress responses, were also revealed by the analysis such as the protein ubiquitination pathway, PPARα/RXRα activation, sumoylation pathway, unfolded protein response, and necroptosis signalling pathway.

Table 10. Top 10 ingenuity canonical pathway of INS-1E acetylated proteins.

Ingenuity Canonical Pathways	-Log$_{10}$ p-value
Sirtuin Signalling Pathway	13.8
Mitochondrial Dysfunction	12.7
Fatty Acid β-oxidation I	12.3
Oxidative Phosphorylation	12
TCA Cycle II (Eukaryotic)	10.9
Gluconeogenesis I	8.68
Ketogenesis	7.66
Folate Transformations I	6.15
Valine Degradation I	6.04
Insulin Secretion Signalling Pathway	5.25

3.2.4. Motif enrichment analysis

To characterize the possible specific sequence motifs surrounding acetylated lysine residues of proteins, a motif analysis was generated to indicate the likelihood of amino acids being over- or under-represented at the positions surrounding the Nε-acetylated sites (Table 12). Ten significantly enriched motifs were inferred analysing all identified acetyl lysine sites, including ....KY........., ...GK.........., ...DK.........., ...KF........., ...L.K.........., ...K..K......., D.........K.........., ...FK.........., .T........K.........., ...Q.EK........... The amino acid frequencies of the sequences flanking Nε-acetylated sites were assessed to confirm whether there were position-specific amino acids adjacent to the acetyl lysine sites by motif model. Phenylalanine (F), tyrosine (Y), glycine (G), aspartate (D), leucine (L), lysine (K), threonine (T), glutamine (Q), and glutamate (E) were found overrepresented surrounding acetyl lysine sites. The presence of phenylalanine, tyrosine, glycine, leucine, and glutamate was particularly observed in the immediate neighbourhood (+/-1 or +/-2 position) while threonine was frequently represented in a more distant position (-9 position).

Table 11. Motif enriched analysis of INS-1E acetylome. Schematic representation and plot of motifs are shown; a dot stands for a generic amino acid. The motif score was calculated by taking the sum of the -Log$_{10}$ p-value used to fix each position of the motif. Higher motif scores typically correspond to motifs that are statistically more significant as well as more specific. Match represents the sequence frequency matching with this motif in the dataset. Fold is an indicator of

the enrichment level of the extracted motifs. It was calculated by using the following mathematical ratio, (Dataset matches/Dataset size)/(Background matches/Background size).

Motif	Plot	Score	Matches	Size	Fold
.........KY.........		3,06	15	232	2,59
........GK.........		2,52	15	93	2,21
........DK.........		2,42	14	150	2,27
.........KF.........		2,33	14	200	2,23
.......L.K.........		2,56	13	55	2,35
.........K..K.......		2,12	13	78	2,14

Motif				
D.........K..........		2,17	12	105	2,30
.........FK..........		2,35	11	131	2,53
.T........K..........		2,63	10	65	2,92
.......Q.EK..........		1,58	10	292	8,64

To complete the motif analysis, the percentage of variation of grouped amino acids in position from -5 to +5 was calculated as described above in the motive enriched analysis of human islet acetylome. As for the human islet acetylome, this analysis suggested an increased frequency of aromatic amino acids in +1 (93.72%) and -1 (38.46%) positions although with reduced percentages. Positively charged amino acids showed a 28.82% increase in +1 position and 69.46% and 52.04% decreases in -1 and -2 positions, respectively. Negatively charged amino acids showed a 108% frequency increase in -1 position while the percentage of variation decreased in +1 (37.11%) and +2 (17.02%) positions (Table 12).

Table 12. Percentage of amino acid variation in -5 to +5 positions around Nε-acetylated sites. Green and red colours indicate decreased (-) and increased (+) % of variation, respectively, while colour intensity correlates to the % value.

	-5	-4	-3	-2	-1	K	+1	+2	+3	+4	+5
AA +	-31,10	9,94	-33,86	-52,04	-69,46	/	28,82	10,71	25,26	3,70	-10,91
AA -	-27,27	18,10	-1,59	-23,72	108,28	/	-37,11	-17,02	-11,98	5,63	45,45
AA +/- polar	0,29	-9,93	25,26	-21,43	-22,44	/	-28,99	-14,44	-8,27	10,26	3,75
AA +/- apolar	21,00	1,47	3,46	37,35	-10,91	/	5,65	13,60	8,37	-4,26	-7,87
AA Aromatics	21,62	-43,48	-11,92	17,65	38,46	/	93,72	19,59	-10,47	11,72	9,24

Amino acid (AA), positively charged (+), negatively charged (-), neutral (+/-).

3.2.5. Effect of cytokines on protein thermal stability examined by PISA analysis

The novelty of this section of the work lies in the application of an innovative technique, PISA, which allows to study variations of protein thermal stability at a proteomic level.

Eight thousand three hundred three (8303) proteins were identified by at least 2 unique peptides and quantified through TMT™16. Protein amount was firstly normalized by the total amount of TMT for each channel used and then by the protein expression data. Four thousand fifty-one (4051) and 5854 proteins showed solubility and expression variations, respectively, in cytokine treated cells as compared to untreated cells. Among the former, 198 proteins displayed a solubility reduction while the solubility of 306 increased in cytokine treated cells (Figure 16A, Table 13). Among the differentially expressed proteins, 196 and 727 were upregulated and downregulated in cytokine treated cells, respectively (data not shown).

Protein solubility and expression (p-value, < 0.05) were correlated using their $\log_2$ Cyto/CTRL ratio values (Figure 16B). This analysis highlighted a major negative correlation and minor positive correlation for some proteins (Figure 16B).
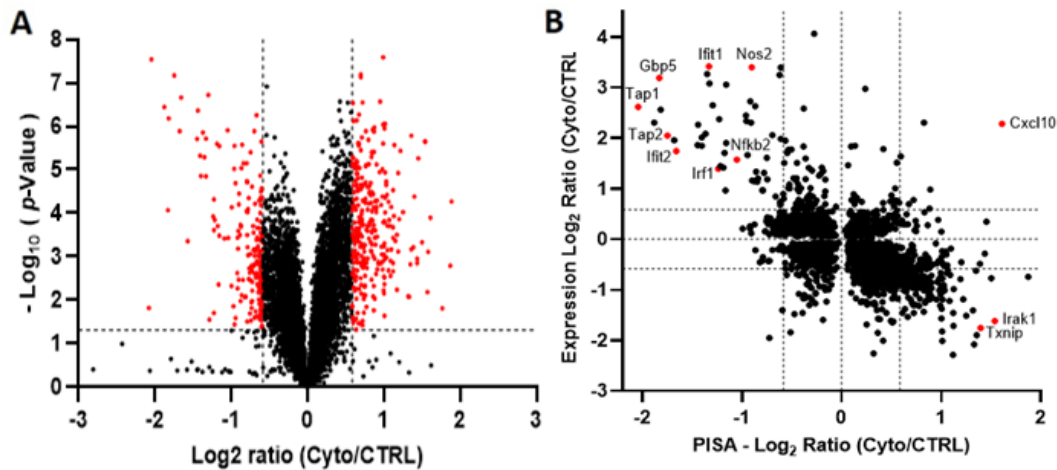
Figure 16. A) Volcano plot of differentially soluble proteins with a cut-off of 1.3 for -log$_{10}$ p-values and ± 0.584 for log$_2$ Cyto/CTRL ratio values. The red dots represent the curated list of proteins showing significant changes. B) Graphical representation of the correlation between significant variations of protein solubility and expression reported as log$_2$ Cyto/CTRL ratio values with a cut-off of ± 0.584.

Table 13. List of top 50 differentially soluble proteins (25 increased and 25 decreased solubility) ordered by log$_2$ Cyto/CTRL ratio values.

ID	Gene	Name	Cov.	Pept	Uniq	MW [kDa]	Log$_2$ Ratio	-Log$_{10}$ p-Value
G3V6I9	Rpl26	60S ribosomal protein L26	44	8	8	17.2	1.89	4.27
Q4V898	Rbmx	RNA-binding motif protein, X chromosome	45	21	3	42.2	1.87	2.79
D3ZY01	Znf48	RCG39517, isoform CRA_a	7	2	2	64.6	1.77	1.81
P48973	Cxcl10	C-X-C motif chemokine 10	24	2	2	10.7	1.61	3.90
D4A3K5	H1-1	Histone H1.1	39	8	6	22	1.58	3.11
D3ZIX4	H1fx	H1 histone family, member X	56	10	10	20.5	1.57	2.19
B2RYH5	Irak1	Interleukin-1 receptor-associated kinase 1	13	8	8	77.8	1.54	5.66
D4A720	Srsf7	RCG61762, isoform CRA_d	32	10	9	27.4	1.54	5.64
D3ZXH7	Alyref	Aly/REF export factor	36	5	5	19.9	1.45	5.26
Q00728		Histone H2A type 4	38	6	2	14.3	1.44	2.85
A0A0G2K654	Hist1h1c	Histone cluster 1 H1 family member c	38	8	6	21.3	1.44	2.95
Q5M7W1	Txnip	Thioredoxin-interacting protein	17	6	6	44	1.40	4.38
F1LT35	RGD1564606	Similar to 60S ribosomal protein L23a	40	7	7	17.7	1.39	3.22
Q6AYK5	Lyar	Cell growth-regulating nucleolar protein	34	12	12	43.7	1.36	3.17
D3ZGZ4	Rai2	RCG49718	12	4	4	57.1	1.36	5.78
P62919	Rpl8	60S ribosomal protein L8	27	6	6	28	1.35	2.83
D3ZPN3	Mlf2	Myeloid leukemia factor 2	16	3	3	28	1.33	2.07
D3ZSV8	Unc79	Unc-79 homolog, NALCN channel complex subunit	1	3	3	282.6	1.32	2.09
Q10758	Krt8	Keratin, type II cytoskeletal 8	49	24	15	54	1.25	4.03
D3Z8A4	Tcaf1	Similar to mKIAA0738 protein (Predicted), isoform CRA_a	5	5	5	102.3	1.22	5.44
M0RCH8	Rsl1d1l1	Ribosomal L1 domain-containing protein 1-like	38	11	11	52.2	1.20	3.87
Q6AYL9	Nuf2	Kinetochore protein Nuf2	27	13	13	54.5	1.19	4.92
P26801	Cebpg	CCAAT/enhancer-binding protein gamma	25	2	2	16.4	1.19	3.12
D3ZXP3	H2afx	Histone H2A	68	9	3	15.1	1.17	2.24
P61928	Rpl37	60S ribosomal protein L37	23	3	3	11.1	1.17	3.50

ID	gene	protein	Cov.	Pept.	Uniq.	MW	Log₂	-Log₁₀

Q6DGG4	Irf1	Interferon regulatory factor	15	4	4	37.1	-1.19	5.60
Q5MYT9	Oasl2	2'-5'-oligoadenylate synthase-like protein 2	6	2	2	59.4	-1.22	3.84
Q5BJS6	Tmem50b	Transmembrane protein 50B	20	3	3	17.9	-1.23	1.70
A0A0G2K2T4	Lrp4	Low-density lipoprotein receptor-related protein 4	1	2	2	201.3	-1.23	3.61
G3V9U5	Tmem243	Similar to chromosome 7 open reading frame 23 (Predicted), isoform CRA_b	22	2	2	13.4	-1.23	4.32
Z4YNI2	Hbp1	HMG box-containing protein 1	8	3	3	58.5	-1.24	3.92
P11608	Mt-atp8	ATP synthase protein 8	31	2	2	7.6	-1.29	1.55
D3ZLE6	Rt1-ce7	RT1 class I, CE7	32	10	2	39.3	-1.30	6.72
P18589	Mx2	Interferon-induced GTP-binding protein Mx2	64	36	7	75	-1.33	5.72
Q4V797	RGD1309362	Interferon-gamma-inducible GTPase Ifgga1 protein	39	14	7	48.2	-1.33	4.85
F1M115	LOC100364500	RT1 class I, locus CE11-like	18	5	3	39.4	-1.35	5.29
F1M512	Apol11a	Apolipoprotein L 11a	8	3	3	34.9	-1.37	5.86
G3V9A4	Oas1a	2'-5'-oligoadenylate synthase 1A	30	9	9	41.7	-1.40	4.86
Q6AYE7	Ifit3	Interferon-induced protein with tetratricopeptide repeats 3	29	9	9	48	-1.41	5.32
Q6AYC2	Irgm	Immunity-related GTPase family M protein	39	16	16	46.3	-1.44	6.36
Q4V8H9	Ifit2	Interferon-induced protein with tetratricopeptide repeats 2	23	11	11	53.9	-1.45	5.71
D3ZIJ5	Dpm3	Dolichol-phosphate mannosyltransferase subunit 3	24	2	2	10.1	-1.57	3.36
A0A0H2UHF4	Rsad2	RCG62278	30	7	7	41.4	-1.66	6.66
P36372	Tap2	Antigen peptide transporter 2	37	20	6	77.7	-1.68	5.89
F1LZ05	Parp14	Poly [ADP-ribose] polymerase	43	68	68	199.4	-1.75	7.17
F7F469	Igtp	Interferon gamma-induced GTPase	21	19	8	157	-1.82	6.18
F1M9F6	Gbp5	Guanylate-binding protein 5	31	14	14	66.9	-1.83	4.07
P18590	Mx3	Interferon-induced GTP-binding protein Mx3	55	31	2	74.9	-1.88	6.44
P36370	Tap1	Antigen peptide transporter 1	49	26	24	79.1	-2.05	7.54
D4A9I3	Cacfd1	Calcium channel flower homolog	30	5	5	18.4	-2.08	1.82

ID, protein accession number; gene, gene name; protein, protein name; Cov., coverage; Pept., number of identified peptides;

Uniq., unique peptides; MW, molecular weight; Log₂, Log₂ Cyto/CTRL ratio value; - Log₁₀, -Log₁₀ p-value.

The list of 504 proteins that showed consistent solubility changes was analysed by Metascape. The pathway enrichment analysis is shown in Figure 17. In the top positions, pathways such as "SRP-dependent co-translational protein targeting to membrane", "RAB geranylgeranylation" and "endoplasmic reticulum to Golgi vesicle-mediated transport" with -log₁₀ p-value of 12.38, 6.73, and 6.52, respectively, are found. Moreover, the "TNF-α NF-κB signalling pathway" (-log₁₀ p-value, 2.3) is also present in this list among other pathways, which can be related to β cell dysfunction and inflammatory responses.
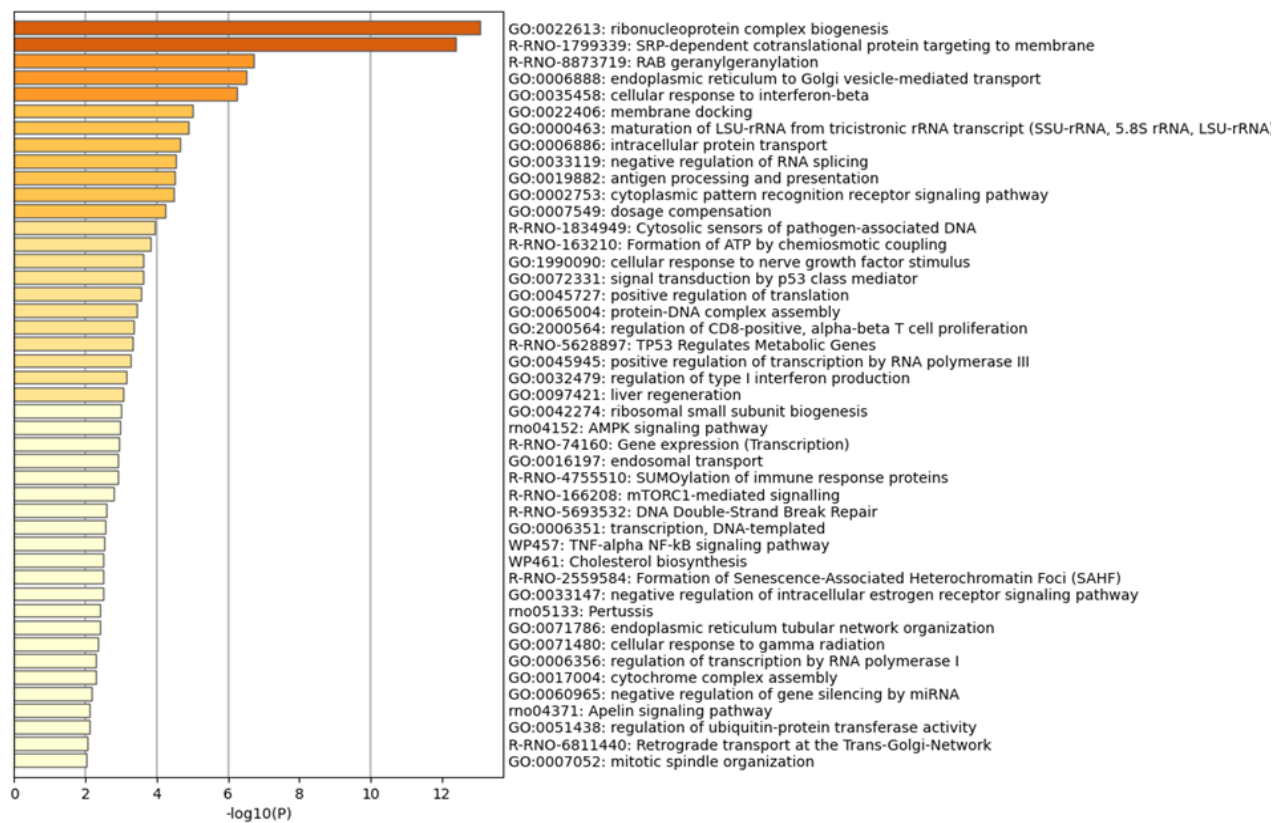
Figure 17. Metascape enrichment analysis. Bar graph of enriched terms coloured according to -Log₁₀ p-value.

3.3. References

[1] Eizirik DL, Sammeth M, Bouckenooghe T, Bottu G, Sisino G, Igoillo-Esteve M, Ortis F, Santin I, Colli ML, Barthson J, Bouwens L, Hughes L, Gregory L, Lunter G, Marselli L, Marchetti P, McCarthy MI, Cnop M. The human pancreatic islet transcriptome: expression of candidate genes for type 1 diabetes and the impact of pro-inflammatory cytokines. *PLoS Genet.* 2012; 8(3):e1002552. doi: 10.1371/journal.pgen.1002552.

[2] Kutlu B, Cardozo AK, Darville MI, Kruhøffer M, Magnusson N, Ørntoft T, Eizirik DL. Discovery of gene networks regulating cytokine-induced dysfunction and apoptosis in insulin-producing INS-1 cells. *Diabetes.* 2003; 52(11):2701-19. doi: 10.2337/diabetes.52.11.2701.

[3] Ramos-Rodríguez M, Raurell-Vila H, Colli ML, Alvelos MI, Subirana-Granés M, Juan-Mateu J, Norris R, Turatsinze JV, Nakayasu ES, Webb-Robertson BM, Inshaw JRJ, Marchetti P, Piemonti L, Esteller M, Todd JA, Metz TO, Eizirik DL, Pasquali L. The impact of proinflammatory cytokines on the β-cell regulatory landscape provides insights into the genetics of type 1 diabetes. *Nat Genet.* 2019; 51(11):1588-1595. doi: 10.1038/s41588-019-0524-6.

4. Discussion

An autoimmune attack targeting pancreatic β cells is the commonly recognised pathogenetic mechanism of β cells destruction, which leads to T1DM development. This immunological assault causes a strong inflammatory reaction mediated by lymphocytes and macrophages, which release ROS, NO and cytokines. Pro-inflammatory cytokines as well as physiological conditions requiring increased insulin production and release can induce stress of β cells, which respond trying to re-establish the lost physiological equilibrium. Indeed, a widely accepted recent view does not consider β cells as innocent spectators of their damage by the immune assault but active participants through their responses, which may stimulate and/or reinforce the immune reaction [1; 2; 3]. Under stressful conditions, the ER stress response can lead to HLA class 1 antigen and chemokine overexpression and generation of neoantigens, such as alternative splicing variants and PTMs of proteins. In the contest of T1DM, several neoantigens produced through PTMs have been described [4; 5]. For instance, oxidated insulin and deamidated proinsulin have been reported to act as neoantigens. In addition, the inflammatory stress induced by β cell (INS-1E cells) exposure to IL-1β and INF-γ leads to citrullination of GRP78, an ER chaperone, followed by translocation to the plasma membrane and secretion [6]. Citrullinated GPR78 is a neoantigens, which can induce an autoimmune response.

In all cell types, reversible PTMs dynamically modulate functions of a wide variety of protein and dysregulation can have pathological consequences. Sumoylation that is protein modification by ubiquitin-like modifiers (SUMO) has been linked to the pathogenesis of diverse human diseases including T1DM [7; 8]. On the other hand, lysine hyperacetylation of mitochondrial metabolic enzymes in β cells has been implicated in mitochondrial function impairment and T2DM development [9]. A pathogenetic role of other PTMs such as phosphorylation and glycosylation has been suggested while lysine acetylation of histones and metabolic enzymes is likely involved in DM complications [9; 10].

Transcriptomic, proteomic, and multi-omic approaches have allowed to analyze cytokines-induced expression changes of whole cell proteins in clonal β cells, rat, and human

pancreatic islets [11; 12; 13]. Proteomic studies addressing the role of PTMs in cytokine-induced β cell dysfunction are instead lacking.

In this study, proteome and lysine acetylome variations due to cytokine exposure were investigated in INS-1E cells and human pancreatic islets. These two models cannot be considered equivalents since different mechanisms are responsible for cytokine-induced ER stress in human β cells and INS-1E cells [14]. For the first time, the thermal stability of INS-1E proteins was also studied using an innovative proteomic approach, named PISA technique, which allows to observe the shift of proteins melting point through their residual solubility after a thermal treatment. Changes of protein thermal stability can suggest difference in PTMs.

4.1. Human pancreatic islets and INS-1E cells differential expression proteomics

Differential expression proteomics was performed using two different approaches. Label-free shotgun and TMT labelled proteomics were used to study human pancreatic islet and INS-1E cell proteome, respectively. Both sets of differentially expressed proteins are found in networks of similar molecular pathways, mainly cytokine signalling pathways, inflammatory and immune response pathways. Our results are in agreement with reported transcriptomic data, which have been obtained using similar conditions of cytokine exposure. The differential expression of 102 human and 50 rat proteins matched with the expression changes of corresponding genes found in human islets and rat INS-1E cells, respectively [12; 15]. Interestingly, transcriptome and proteome changes observed in a human β cell line have evidenced top 10 up-regulated proteins, which I also found overexpressed in human islets and INS-1E cells [16]. Among these top 10 proteins, the INFγ-inducible chemokine CXCL10, the immune-response protein HLA-B (an HLA class I histocompatibility antigen) and the cell surface glycoprotein bone marrow stromal antigen 2 (BST2) are included [16].

Several chemokines were strongly upregulated in both human islets and INS-1E cells (e.g. CXCL1, CXCL2, and CXCL10) confirming that IFNγ and IL-1β trigger synthesis and release of chemotactic cytokines in β cells. In human islets, HLA-C, an HLA class I histocompatibility antigen, is highly upregulated together with upregulation of HLA-DRB1 (HLA class II histocompatibility antigen) and downregulation of HLA-A (HLA class I histocompatibility antigen). HLA class I molecules expressed in nearly all cell types play a central role in the immune responses presenting peptides derived from the endoplasmic reticulum lumen to T cells. Instead, HLA class II molecules, which are normally expressed in antigen presenting cells (APCs), present antigenic peptides to a subclass of T cells. The concomitant upregulation of antigen peptide transporter 1 (TAP1) and 2 (TAP2), and proteasome subunit beta type-10 (PSMB10) indicates antigen processing and unidirectional transport of antigen peptides from cytosol to ER where they associate with HLA class I molecules. Gamma-interferon-inducible lysosomal thiol reductase (IFI30), which plays an important role in antigen processing, is also upregulated indicating the active reduction of disulphide bonds and unfolding of proteins addressed to lysosomal degradation [17]. These findings imply that β cells actively participate in stimulating and reinforcing the immune response as suggested by other studies [12; 15; 16]. The overexpression of HLA molecules, ER transporters, and a proteosome subunit suggest that cytokines stimulate the ER stress response by activating some transcription factors such as IRF1, STAT1, and RELA.

Pro-inflammatory cytokines stimulate β cells to produce micromolar levels of reactive nitrogen species (RNS) and ROS, which mediate some of cytokines-induced effects including inhibition of oxidative phosphorylation and insulin secretion, induction of ER stress, and DNA damage [1]. Curiously, peroxynitrite isomerase THAP4 expression was found slightly decreased in cytokine treated islets while other cytoplasmic antioxidants such as peroxiredoxin-1 (PRDX1) showed less than 10-fold increase (data not included in the table). The thiol-specific peroxidase PRDX1 and THAP4 catalyse the reduction of H_2O_2 to H_2O and conversion of peroxynitrite to nitrate, respectively. In cells, THAP4 plays a role as peroxynitrite sensor and participates to detoxification of both RNS and ROS [18; 19].

Recently, Stancil et al. have suggested that rat β cells rely on cytoplasmic PRDX1 and thioredoxin reductase 1 (TXNRD1) to protect themselves from the oxidative damage caused by an excessive production of RNS and ROS [20]. However, Prdx and Thap proteins did not show up in the list of differentially expressed proteins in INS-1E cells but a downregulation of thioredoxin interacting protein (Txnip) was observed (data not included in the table). TXNIP is considered as a redox rheostat, which control TRX1 activity and expression. The TRX1/TXNIP system has been implicated in T1DM and T2DM pathogenesis. Moreover, numerous observations have suggested that TXNIP promotes β cells apoptosis under various kinds of stresses while TRX1 protects [21]. Thus, Txnip downregulation can represent a self-defence mechanism of INS-1 cells against cytokine-induced apoptosis. Finally, the overexpression of NO synthase 2 (Nos2) in INS-1E cells exposed to cytokines confirm the activation of NF-κB and STAT1 signalling pathways.

Recent advances in the study of β cell response to pro-inflammatory cytokines have revealed a marked plasticity of the regulatory element landscape unveiling neo- and primed- Induced Regulatory Elements (IREs) [16]. A pro-inflammatory environment changes chromatin accessibility and induces the binding of inflammatory response transcription factors at IREs, which are pre-bound by islet-specific transcription factors. Interestingly, the results presented here suggest that the exposure of human islets and INS-1E cells to cytokines induce the expression of both inflammatory response (i.e. STAT1, NF-κB) and islets specific (i.e. MAFB, PDX1) transcription factors.

Many pathways related to peptide hormone synthesis, processing and response were revealed by canonical pathway analysis of dysregulated proteins in INS-1E cells. The downregulated expression of transcription factor MafA (Mafa), which is considered a master regulator of gene implicated in β cells function, insulin synthesis and glucose stimulated insulin secretion, correlates with cytokine-induced downregulation of insulin-1 and impairment of INSE-1E functional activity [22; 23].

Overall, these proteomic analyses have highlighted that both identical and diverse proteins are dysregulated in INS-1E cells and human islets upon cytokine exposure. More factors can

contribute to create discrepancies. First, the higher number of identified proteins in INS-1E cells than islets is likely due to the most sensitive proteomic technique that was used (TMT labelled versus label-free shotgun and different mass spectrometer). Second, these two *in vitro* models differ in many aspects including their origin from diverse species (rat versus human), a β cell line versus primary unselected β cells. Moreover, different mechanisms are involved in inducing ER stress in INS-1E and human β cells exposed to pro-inflammatory cytokines [14]. Nevertheless, the cellular models share some activated pathways such as cytokine signalling, inflammatory response, and immune response pathways.

4.2. Human pancreatic islet and INS-1E cell acetylome analysis

For the first time, the lysine acetylome profiles of INS-1E cells and human islets exposed to IL-1β and INF-γ were studied. Two different immune enrichment approaches were used that is multiple enrichment for each sample of human islets and a single enrichment for all INS-1E cell samples taking advantage of TMT labelling. The single enrichment led to identify a larger number of Nε-acetyl-sites because of TMT labelling more biological replicates and protein quantities could be used.

Many proteins were found hyper- or down-acetylated in cytokine-exposed INS-1E cells and human islets. However, the number of hyperacetylated proteins is greater in rat cells than human islets. Cytokine exposure induces changes of the Nε-acetylation status of various enzymes including those of metabolic pathways. Though, some metabolic enzymes (e.g. fructose-bisphosphate aldolase A, 3-ketoacyl-CoA thiolase mitochondrial), which are hyperacetylated in INS-1E, show decreased lysine acetylation in human islets.

Component ε of ATP synthase (Atp5f1e in rat cells and ATP5E in human islets) was found hyperacetylated both in INS-1E cells and human islets. ATP synthase complex contains multiple SIRT3-dependent Nε-acetyl sites, which are altered in several stress conditions [24]. Moreover, its acetylation is associated to a decrease of activity [25]. Ciregia et al, have reported hyperacetylation of ATP synthase in human islets and INS-1E cells exposed to palmitate-induced stress [26]. Therefore, the present finding suggests that β cells respond

to either metabolic or inflammatory stress by reducing ATP production in mitochondria. The reduction of ATP synthase activity may come first or after the initiation of mitochondrial dysfunction.

In human islets but not in INS-1E cells, voltage-dependent anion-selective channel protein 2 and 3 (VDAC2 and VDAC3) are hyperacetylated upon cytokine challenge. Similarly, INS-1E cells exposed to palmitate show hyperacetylation of Vdac2 [26]. However, VDAC1 acetylation decrease in human islets exposed to cytokines. VDACs are believed key players in mitochondria-mediated apoptosis, although the molecular mechanisms involved are not completely understood [27]. These transmembrane proteins can endure different types of PTMs including phosphorylation and acetylation at multiple sites but the relevance of these PTMs in regulating VDAC function is still unclear.

In all cell types under physiological conditions, mitochondrial SOD2 plays a pivotal role against the oxidative stress due to mitochondria production of ROS. Pancreatic β cells are particularly vulnerable to oxidative stress because of low expression of anti-oxidant enzymes and the need of ATP produced through oxidative phosphorylation. Surely, β cell exposure to cytokine cause further increase of ROS leading more pressure to the anti-oxidant system. SOD2 is post-translationally modified by nitration, succinylation, and acetylation. Acetylation at K122 empires its catalytic activity while acetylation at both K122 and K130 seems to be required for importation of SOD2 cytosolic precursor into mitochondria [28]. Nevertheless, only the SOD2 K122 site has been found acetylated and deacetylated by SIRT3 in the heart of wild-type rats compared to rats overexpressing SOD2. In the present study, SOD2 was discovered acetylated at multiple sites including K122 and K130 implying its inactivation in cytokine-exposed islets. This finding is quite surprising since islets were in a condition of oxidative stress requiring a catalytically active SOD2. I feel to speculate that a reduction of SIRT3 activity is unlikely because of decreased Nε-acetylation of other mitochondrial enzymes such as the trifunctional enzyme subunit alpha (HADHA), hydroxyacyl-CoA dehydrogenase (HADH), Succinate dehydrogenase flavoprotein subunit (SDHA) and ACAA2. SOD2 of human islets and INS-1E cells exposed

to a metabolic (palmitate) stress has been also found hyperacetylated [26]. Single nucleotide polymorphisms (SNP) of the SOD2 gene have been associated with protection or increased risk of DM and its complications.

HADHA and HADH, key enzymes of β oxidation pathways, have been found hyperacetylated in rat islets under high glucose concentrations resulting in decreased fatty acid oxidation and enhanced β cells functions [29]. A decrease of HADHA and HADH acetylation as occur in cytokine-exposed human islets may suggest an increase of β oxidation. However, it has been also reported that acetylation of HADHA acetylation does not modify its enzymatic activity in mouse liver [30].

Among the various hyperacetylated proteins in INS-1 cells exposed to cytokines, glutamate dehydrogenase 1 (Glud1 for rat and GLUD1 for human) merits a special mention. This enzyme catalyzes the oxidative deamination of endogenous glutamate, which is present at high concentrations in pancreatic β cells contributing to insulin secretion [31]. Glutamate dehydrogenase 1 is post-translationally modified at serine, threonine, tyrosine, and lysine residues. Nε-acetylation regulates the enzyme activity with progressive loss as the degree of acetylation increases [32]. SIRT3 deacetylates GLUD1 restoring the activity [33]. The impaired glutamate dehydrogenase 1 activity can contribute together with other dysregulated proteins to compromise insulin secretion in INS-1 cells. The enzyme is also hyperacetylated in INS-1E and human islets upon prolonged exposure to palmitate [26].

Although INS-1E cells and human islets show profiles of dysregulated protein Nε-acetylation which do not quite overlap, pathway analysis highlighted some shared pathways that are SIRT signaling, mitochondrial dysfunction, TCA cycle II and gluconeogenesis I. Apart from SIRT signaling pathway, which represents a key factor in acetylation/deacetylation cycle, mitochondrial dysfunction appears to be the main player in cytokine-induced INS-1E and human β cell functional impairment and death. Different molecular mechanisms can lead to the same final effect.

4.3. Protein integral solubility alteration analysis of INS-1E cells

The study of proteins thermal stability can be useful to analyse the molecular mechanisms involved in cytokine-induced β cell dysfunction and death by a different but complementary point of view. The melting point of proteins can be altered by various factors, such as drug-interaction [34], nucleic acid [35] and metabolite binding [36], as well as protein-protein interactions [37], and PTMs [38]. Therefore, the study of proteome thermal stability shows a list of proteins that can be involved in molecular pathways even if they do not change expression.

The increase of thermal stability of more than 30 ribosomal proteins and proteins related to protein synthesis was found. Proteins, which participate to ribonucleoprotein complex biogenesis, were included. Among them, the DEAD-box RNA helicases, Ddx18, Ddx20, and Ddx21 showed an increase of thermal stability. These proteins are vital for the regulation of various aspects of the RNA life cycle. Song et al. have shown that DDX21 can prevent R-loop-associated DNA damage and transcription-associated genomic instability [39]. The helicase activity that is triggered by SIRT7-mediated deacetylation overcomes R-loop-facilitated stalling of RNA polymerases [39]. Ddx21 was not found acetylated in cytokine treated INS-1E but Ddx18 acetylation at K98 and K415 was detected. Such acetylation can be responsible for both activity reduction and thermal stability increase. Various ribosomal proteins including 60S ribosomal protein L37 (Rpl37), L26 (Rpl26), and L8 (Rpl8) also show thermal stability increase upon INS-1E cell exposure to cytokines. The Rpl proteins undergo diverse types of PTM. RPL8 UFMylation by ubiquitin-fold modifier 1 (UFM1) is considered a way for cells with intense secretory activity to regulate ribosome turnover [40]. A dysregulated RPL8 UFMylation is involved in ER stress [41].

INS-1E cells exposed to cytokines overexpress proteins related to inflammatory and immune responses, oxidative and ER stress. Changes of protein thermal stability predict the involvement of similar cellular pathways although with some differences. A group of proteins shows changes of both expression and thermal stability and expression. Most of cytokine-responsive proteins such as Nos2 and Nfkb2 show negative correlations with

increased expression and decreased thermal stability while few others display positive correlations as the chemokine Cxcl10 of which both expression and thermal stability increase.

Numerous proteins of the immune response exhibit thermal shifts, such as Cxcl10, interferon-induced protein with tetratricopeptide repeats 2 (Ifit2), Tap1 and Tap2, and Rt1 class I CE7 (Rt1-ce7). Tap2 and Tap2, which are members of ATP-binding cassette (ABC) family and homologous to human TAP1 and TAP2, heterodimerize forming ER-resident transporters, which bind and drug cytosolic peptides into ER lumen where they are loaded into MHC class I binding grove. The thermal stability of Tap1 and Tap2 was found decreased in INS-1E cells exposed to cytokines whereas their expression increased (data not shown) suggesting an enhanced demand to bind neo-antigens. The reduction of thermal stability may be due to peptide binding or reduced interaction with other proteins of the transporter complex.

The thermal stability of Txnip, an inhibitor of Trx1, was found increased while the expression decreases. Numerous observations have suggested that Txnip promotes β cells apoptosis under various kinds of stresses while Trx1 protects [21]. In INS-1E cells overexpression of human TXNIP induces apoptosis while glucose stimulates its overexpression in rat and human islets suggesting a link between glucotoxicity and β cell apoptosis [42]. The increased thermal stability of Txnip may indicate PTM changes or binding to other proteins.

Overall, the study of proteome thermal stability allowed to expand the range of information on cytokine-induced changes in β cell proteome going beyond variations of protein expression and Nε-acetylation. Most proteins with modified thermal stability seem to be related to protein synthesis, vesicle transport, antigen processing and presentation.

4.4. Reference

[4] Eizirik DL, Pasquali L, Cnop M. Pancreatic β-cells in type 1 and type 2 diabetes mellitus: different pathways to failure. *Nat Rev Endocrinol.* 2020; 16(7):349-362. doi: 10.1038/s41574-020-0355-7.

[5] Powers AC. Type 1 diabetes mellitus: much progress, many opportunities. *J Clin Invest.* 2021; 15;131(8):e142242. doi: 10.1172/JCI142242.

[6] Eizirik DL, Szymczak F, Alvelos MI, Martin F. From Pancreatic β-Cell Gene Networks to Novel Therapies for Type 1 Diabetes. Diabetes. 2021; 70(9):1915-1925. doi: 10.2337/dbi20-0046.

[7] Balakrishnan S, Kumar P, Prabhakar BS. Post-translational modifications contribute to neoepitopes in Type-1 diabetes: Challenges for inducing antigen-specific tolerance. *Biochim Biophys Acta Proteins Proteom.* 2020; 1868(10):140478. doi: 10.1016/j.bbapap.2020.140478.

[8] Rodriguez-Calvo T, Johnson JD, Overbergh L, Dunne JL. Neoepitopes in Type 1 Diabetes: Etiological Insights, Biomarkers and Therapeutic Targets. *Front Immunol.* 2021; 12:667989. doi: 10.3389/fimmu.2021.667989.

[9] Rondas D, Crèvecoeur I, D'Hertog W, Ferreira GB, Staes A, Garg AD, Eizirik DL, Agostinis P, Gevaert K, Overbergh L, Mathieu C. Citrullinated glucose-regulated protein 78 is an autoantigen in type 1 diabetes. *Diabetes.* 2015; 64(2):573-86. doi: 10.2337/db14-0621.

[10] Zhang J, Chen Z, Zhou Z, Yang P, Wang CY. Sumoylation Modulates the Susceptibility to Type 1 Diabetes. *Adv Exp Med Biol.* 2017; 963:299-322. doi: 10.1007/978-3-319-50044-7_18.

[11] Li M, Guo D, Isales CM, Eizirik DL, Atkinson M, She JX, Wang CY. SUMO wrestling with type 1 diabetes. *J Mol Med (Berl).* 2005; 83(7):504-13. doi: 10.1007/s00109-005-0645-5. Epub 2005 Apr 2. PMID: 15806321.

[12] Santo-Domingo J, Dayon L, Wiederkehr A. Protein Lysine Acetylation: Grease or Sand in the Gears of β-Cell Mitochondria? *J Mol Biol.* 2020; 6;432(5):1446-1460. doi: 10.1016/j.jmb.2019.09.011.

[13] Chatterjee B, Thakur SS. Investigation of post-translational modifications in type 2 diabetes. *Clin Proteomics.* 2018; 24;15:32. doi: 10.1186/s12014-018-9208-y.

[14] Crèvecoeur I, Rondas D, Mathieu C, Overbergh L. The beta-cell in type 1 diabetes: What have we learned from proteomic studies? *Proteomics Clin Appl.* 2015; 9(7-8):755-66. doi: 10.1002/prca.201400135.

[15] Eizirik DL, Sammeth M, Bouckenooghe T, Bottu G, Sisino G, Igoillo-Esteve M, Ortis F, Santin I, Colli ML, Barthson J, Bouwens L, Hughes L, Gregory L, Lunter G, Marselli L, Marchetti P, McCarthy MI, Cnop M. The human pancreatic islet transcriptome: expression of candidate genes for type 1 diabetes and the impact of pro-inflammatory cytokines. *PLoS Genet.* 2012; 8(3):e1002552. doi: 10.1371/journal.pgen.1002552.

[16] Colli ML, Ramos-Rodríguez M, Nakayasu ES, Alvelos MI, Lopes M, Hill JLE, Turatsinze JV, Coomans de Brachène A, Russell MA, Raurell-Vila H, Castela A, Juan-Mateu J, Webb-Robertson BM, Krogvold L, Dahl-Jorgensen K, Marselli L, Marchetti P, Richardson SJ, Morgan NG, Metz TO, Pasquali L, Eizirik DL. An

integrated multi-omics approach identifies the landscape of interferon-α-mediated responses of human pancreatic beta cells. *Nat Commun.* 2020; 22;11(1):2584. doi: 10.1038/s41467-020-16327-0.

[17] Brozzi F, Nardelli TR, Lopes M, Millard I, Barthson J, Igoillo-Esteve M, Grieco FA, Villate O, Oliveira JM, Casimir M, Bugliani M, Engin F, Hotamisligil GS, Marchetti P, Eizirik DL. Cytokines induce endoplasmic reticulum stress in human, rat and mouse beta cells via different mechanisms. *Diabetologia.* 2015; 58(10):2307-16. doi: 10.1007/s00125-015-3669-6.

[18] Kutlu B, Cardozo AK, Darville MI, Kruhøffer M, Magnusson N, Ørntoft T, Eizirik DL. Discovery of gene networks regulating cytokine-induced dysfunction and apoptosis in insulin-producing INS-1 cells. *Diabetes.* 2003; 52(11):2701-19. doi: 10.2337/diabetes.52.11.2701.

[19] Ramos-Rodríguez M, Raurell-Vila H, Colli ML, Alvelos MI, Subirana-Granés M, Juan-Mateu J, Norris R, Turatsinze JV, Nakayasu ES, Webb-Robertson BM, Inshaw JRJ, Marchetti P, Piemonti L, Esteller M, Todd JA, Metz TO, Eizirik DL, Pasquali L. The impact of proinflammatory cytokines on the β-cell regulatory landscape provides insights into the genetics of type 1 diabetes. *Nat Genet.* 2019; 51(11):1588-1595. doi: 10.1038/s41588-019-0524-6.

[20] Ewanchuk BW, Yates RM. The phagosome and redox control of antigen processing. *Free Radic Biol Med.* 2018; 125:53-61. doi: 10.1016/j.freeradbiomed.2018.03.040.

[21] De Simone G, Ascenzi P, Polticelli F. Nitrobindin: An Ubiquitous Family of All β-Barrel Heme-proteins. *IUBMB Life.* 2016; 68(6):423-8. doi: 10.1002/iub.1500.

[22] De Simone G, di Masi A, Polticelli F, Ascenzi P. Human nitrobindin: the first example of an all-β-barrel ferric heme-protein that catalyzes peroxynitrite detoxification. *FEBS Open Bio.* 2018; 9;8(12):2002-2010. doi: 10.1002/2211-5463.12534.

[23] Stancill JS, Happ JT, Broniowska KA, Hogg N, Corbett JA. Peroxiredoxin 1 plays a primary role in protecting pancreatic β-cells from hydrogen peroxide and peroxynitrite. *Am J Physiol Regul Integr Comp Physiol.* 2020; 1;318(5):R1004-R1013. doi: 10.1152/ajpregu.00011.2020.

[24] Yoshihara E, Masaki S, Matsuo Y, Chen Z, Tian H, Yodoi J. Thioredoxin/Txnip: redoxisome, as a redox switch for the pathogenesis of diseases. *Front Immunol.* 2014; 9;4:514. doi: 10.3389/fimmu.2013.00514.

[25] Zhang C, Moriguchi T, Kajihara M, Esaki R, Harada A, Shimohata H, Oishi H, Hamada M, Morito N, Hasegawa K, Kudo T, Engel JD, Yamamoto M, Takahashi S. MafA is a key regulator of glucose-stimulated insulin secretion. *Mol Cell Biol.* 2005; 25(12):4969-76. doi: 10.1128/MCB.25.12.4969-4976.2005.

[26] Wang H, Brun T, Kataoka K, Sharma AJ, Wollheim CB. MAFA controls genes implicated in insulin biosynthesis and secretion. *Diabetologia.* 2007; 50(2):348-58. doi: 10.1007/s00125-006-0490-2.

[27] Vassilopoulos A, Pennington JD, Andresson T, Rees DM, Bosley AD, Fearnley IM, Ham A, Flynn CR, Hill S, Rose KL, Kim HS, Deng CX, Walker JE, Gius D. SIRT3 deacetylates ATP synthase F1 complex proteins

in response to nutrient- and exercise-induced stress. *Antioxid Redox Signal.* 2014; 1;21(4):551-64. doi: 10.1089/ars.2013.5420.

[28] Hosp F, Lassowskat I, Santoro V, De Vleesschauwer D, Fliegner D, Redestig H, Mann M, Christian S, Hannah MA, Finkemeier I. Lysine acetylation in mitochondria: From inventory to function. *Mitochondrion.* 2017; 33:58-71. doi: 10.1016/j.mito.2016.07.012.

[29] Ciregia F, Bugliani M, Ronci M, Giusti L, Boldrini C, Mazzoni MR, Mossuto S, Grano F, Cnop M, Marselli L, Giannaccini G, Urbani A, Lucacchini A, Marchetti P. Palmitate-induced lipotoxicity alters acetylation of multiple proteins in clonal β cells and human pancreatic islets. *Sci Rep.* 2017; 18;7(1):13445. doi: 10.1038/s41598-017-13908-w.

[30] Martel C, Wang Z, Brenner C. VDAC phosphorylation, a lipid sensor influencing the cell fate. *Mitochondrion.* 2014; 19 Pt A:69-77. doi: 10.1016/j.mito.2014.07.009.

[31] Zhang L, Chen CL, Kang PT, Jin Z, Chen YR. Differential protein acetylation assists import of excess SOD2 into mitochondria and mediates SOD2 aggregation associated with cardiac hypertrophy in the murine SOD2-tg heart. *Free Radic Biol Med.* 2017; 108:595-609. doi: 10.1016/j.freeradbiomed.2017.04.022.

[32] Zhang Y, Zhou F, Bai M, Liu Y, Zhang L, Zhu Q, Bi Y, Ning G, Zhou L, Wang X. The pivotal role of protein acetylation in linking glucose and fatty acid metabolism to β-cell function. *Cell Death Dis.* 2019; 25;10(2):66. doi: 10.1038/s41419-019-1349-z.

[33] Zhang Y, Goetzman E. The enzyme activity of mitochondrial trifunctional protein is not altered by lysine acetylation or lysine succinylation. *PLoS One.* 2021; 13;16(10):e0256619. doi: 10.1371/journal.pone.0256619.

[34] Fahien LA, Macdonald MJ. The complex mechanism of glutamate dehydrogenase in insulin secretion. *Diabetes.* 2011; 60(10):2450-4. doi: 10.2337/db10-1150.

[35] Colman RF, Frieden C. On the role of amino groups in the structure and function of glutamate dehydrogenase. II. Effect of acetylation on molecular properties. *J Biol Chem.* 1966; 25;241(16):3661-70.

[36] Schlicker C, Gertz M, Papatheodorou P, Kachholz B, Becker CF, Steegborn C. Substrates and regulation mechanisms for the human mitochondrial sirtuins Sirt3 and Sirt5. *J Mol Biol.* 2008; 10;382(3):790-801. doi: 10.1016/j.jmb.2008.07.048.

[37] Gaetani M, Sabatier P, Saei AA, Beusch CM, Yang Z, Lundström SL, Zubarev RA. Proteome Integral Solubility Alteration: A High-Throughput Proteomics Assay for Target Deconvolution. *J Proteome Res.* 2019; 1;18(11):4027-4037. doi: 10.1021/acs.jproteome.9b00500.

[38] Becher I, Andrés-Pons A, Romanov N, Stein F, Schramm M, Baudin F, Helm D, Kurzawa N, Mateus A, Mackmull MT, Typas A, Müller CW, Bork P, Beck M, Savitski MM. Pervasive Protein Thermal Stability Variation during the Cell Cycle. *Cell.* 2018; 31;173(6):1495-1507.e18. doi: 10.1016/j.cell.2018.03.053.

[39] Sridharan S, Kurzawa N, Werner T, Günthner I, Helm D, Huber W, Bantscheff M, Savitski MM. Proteome-wide solubility and thermal stability profiling reveals distinct regulatory roles for ATP. *Nat Commun.* 2019; 11;10(1):1155. doi: 10.1038/s41467-019-09107-y.

[40] an CSH, Go KD, Bisteau X, Dai L, Yong CH, Prabhu N, Ozturk MB, Lim YT, Sreekumar L, Lengqvist J, Tergaonkar V, Kaldis P, Sobota RM, Nordlund P. Thermal proximity coaggregation for system-wide profiling of protein complex dynamics in cells. *Science.* 2018; 9;359(6380):1170-1177. doi: 10.1126/science.aan0346.

[41] Huang JX, Lee G, Cavanaugh KE, Chang JW, Gardel ML, Moellering RE. High throughput discovery of functional protein modifications by Hotspot Thermal Profiling. *Nat Methods.* 2019; 16(9):894-901. doi: 10.1038/s41592-019-0499-3.

[42] Song C, Hotz-Wagenblatt A, Voit R, Grummt I. SIRT7 and the DEAD-box helicase DDX21 cooperate to resolve genomic R loops and safeguard genome stability. *Genes Dev.* 2017; 1;31(13):1370-1381. doi: 10.1101/gad.300624.117.

[43] Gerakis Y, Quintero M, Li H, Hetz C. The UFMylation System in Proteostasis and Beyond. *Trends Cell Biol.* 2019; 29(12):974-986. doi: 10.1016/j.tcb.2019.09.005.

[44] Liang JR, Lingeman E, Luong T, Ahmed S, Muhar M, Nguyen T, Olzmann JA, Corn JE. A Genome-wide ER-phagy Screen Highlights Key Roles of Mitochondrial Metabolism and ER-Resident UFMylation. *Cell.* 2020; 19;180(6):1160-1177.e20. doi: 10.1016/j.cell.2020.02.017.

[45] Minn AH, Hafele C, Shalev A. Thioredoxin-interacting protein is stimulated by glucose through a carbohydrate response element and induces beta-cell apoptosis. *Endocrinology.* 2005; 146(5):2397-405. doi: 10.1210/en.2004-1378.

5. Conclusions

This multi-level proteomic approach provided a broader view of how β cell proteins participate to build "a response" against a stressful stimulus such as exposure to pro-inflammatory cytokines. Complex networks of proteins are activated, which can lead to initiation and reinforcement of immune response as well as β cell dysfunction and death. Both extent and intensity of pro-inflammatory stimuli play important roles in addressing β cell destiny but structural and functional properties of β cell proteins are as well crucial. Under prolonged cytokine exposure, numerous proteins with different functions change expression, lysin acetylation and/or thermal stability providing information of their active role in β cell destiny. To address the impact of observed changes in β cell economy, functional studies are required even though information for some proteins already exist.

6. Curriculum

Lorenzo Zallocco was born on July 28th 1990 in Livorno, Italy. In 2009, after completing his studies at a scientific high school in Livorno, he continued his education in Pharmaceutical Chemistry and Technology at the University of Pisa. He obtained his master's degree with a thesis titled "Evaluation of the cardioprotective properties of novel synthetic and natural agents in an acute myocardial infarct model and investigation of the mitochondrial targets." carried out with Pharmacologist unit, department of pharmacy, Pisa University, under the supervision of Prof. Vincenzo Calderone and Prof. Lara Testai. After the graduation, in 2018 he continued his education in the regional PhD School in Biochemistry and Molecular Biology at the University of Siena. He started his PhD studies in the laboratory of proteomics at the Department of Clinical and Experimental Medicine, University of Pisa, Italy, under the supervision of Prof. Maria Rosa Mazzoni and Prof. Laura Giusti. As part of his PhD program, in 2021 he started working at the Chemical Proteomics Facility of Karolinska Institute, Stockholm, Sweden under the supervision of Prof. Roman Zubarev and Dr. Massimiliano Gaetani. His research work resulted in this thesis entitled "Protein post translational modifications and diabetes.

Pro-inflammatory cytokines reshape lysin acetylome of human pancreatic islets".

6.1. School and seminars

11/05/18 "Corso base in materia di protezione degli animali utilizzati ai fini scientifici" Pole Le Benedettine, University of Pisa, Pisa, Italy

11/12/18 "New opportunities of research in materials and life science at Elettra and Fermi" Pole Fibonacci, University of Pisa, Pisa, Italy

02/01/19 "Therapeutics targhet whitin the coagulation cascade" Pole Le Benedettine, University of Pisa, Pisa, Italy

02/01/19 "Interfering with protein-protein interactions: the promise of exosite inhibitors" Pole Le Benedettine, University of Pisa, Pisa, Italy

03/22/19 "Cellule staminali neuroepiteliali umane nella terapia delle lesioni spinali" Department of Pharmacy, University of Pisa, Pisa, Italy

06/13/19 "Does pharma-biotech public private multicompetence HUB from drug design to the end of preclinical phase" Certosa di Pontignano, University of Siena, Siena, Italy

09/02/19 "Scientific writing and presentation – Complementary skills" University of Siena, Siena, Italy

02/18/20 "Scuola teorico-pratica di proteomica" CEINGE Avanced Biotecnology, Napoli, Italy

02/21/20 "English for research pubblication and presentation purpose" (Level C1 certificated) Interdepartment linguistic center, University of Pisa, Pisa, Italy

05/11/20 "Diritto dei brevetti – Complementary skills" University of Siena, Siena, Italy

05/29/20 "Applicazione della spettrometria di massa" University of Pisa, Pisa, Italy

06/17/20 "I rapporti tra scienza e società – Complementary skills" University of Siena, Siena, Italy

06/23/20 "How to exploit your research idea, a quick introduction to EU project design and management – Complementary skills" University of Siena, Siena, Italy

01/29/21 "Neuroprotective and cardioprotective strategies by nutraceutical compounds" Italian Biochemistry Society

02/26/21 "Progressively de-differentiated pancreatic cancer cells shift from glycolysis to oxidative metabolism and gain a quiescent steam state" Italian Biochemistry Society

04/30/21 "Young investigators virtual day" Italian Proteomics Associacion

6.2. Conference

2019   TUM - Interregional mapping of SIB issues between Tuscany, Umbria and Marche
Politecnical University of Marche, Ancona, Italy.
Oral Presentation - Proteomic analysis of tumors of the major salivary glands.

2019   ItPA – XIV Conference of Italian Proteomic Association with Hellenic Proteomics Society
"Magna Graecia" University, Catanzaro, Italy.
Poster Presentation - Neuroprotective effects of extra virgin oils: a multidisciplinary approach.
Oral Presentation for Poster Prize.

2019   SIB – Italian Society of Biochemistry and Molecular Biology - 60th Congress
University of Salento, Lecce, Italy.
Poster Presentation - Salivary proteome changes in response to stress and sensory stimuli.
Poster Presentation - Neuroprotective effects of extra virgin oils: a proteomic approach.

2020   HUPO Connect - 19th Human Proteome Organization World Congress
Virtual congress

2020   SIPF - Italian Society of Psychophysiology and Cognitive Neuroscience - 28th Congress
Virtual Congress

Poster Presentation - Salivary proteome changes in response to social anxiety and sensory stimuli.

2021   ItPA – XV Conference of Italian Proteomic Association with Hellenic and Serbian Proteomics Society
The Catholic University, Roma, Italy.

Poster Presentation - Salivary proteome changes in response to acute stress in students performing an exam simulation with and without olfactory stimulation.

2021   SIB – Italian Society of Biochemistry and Molecular Biology - 60th Congress
University of Salento, Lecce, Italy.

Poster Presentation - Proteomic analysis of thyrocytes carrying H64 (rs4644) homo-zygotes polymorphism within galectin-3 unveils a carcinogenic profile.

6.3. List of Publications

[1] **Pterostilbene promotes mean lifespan in both male and female Drosophila melanogaster modulating different proteins in the two sexes.** D. Beghelli, *L. Zallocco*, M.C. Barbalace, S. Paglia, S. Strocchi, I. Cirilli, V. Marzano, L. Putignani, G. Lupidi, S. Hrelia, L. Giusti, C. Angeloni. *Oxid Med Cell Longev – Accepted for publication*

[2] **Comparative Proteomic Profile of Parathyroid Carcinoma and Adenoma: a Case Report.** F. Ciregia, F. Cetani, E. Pardi, A. Soggiu, C. Piras, *L. Zallocco*, S. Borsari, M. Ronci, V. Caruso, C. Marcocci, M.R. Mazzoni, A. Lucacchini, L. Giusti. *Canc Gen Pro – 2021, 18(6), 781-796.*

[3] **Age-related changes in the primary motor cortex of newborn to adult domestic pig Sus scrofa domesticus.** S. Desantis, S. Minervini, *L. Zallocco*, B. Cozzi, A. Pirone. *Animals – 2021, 11(7), 2019.*

[4] **Preclinical development of FA5, a novel AMP-activated protein kinase (AMPK) activator as innovative drug for the management of bowel inflammation.** L. Antonioli, C. Pellegrini, M. Fornai, L. Benvenuti, V. D'Antongiovanni, R Colucci, L. Bertani, C. Di Salvo, G. Semeghini, C. La Motta, L. Giusti, *L. Zallocco*, M. Ronci, L. Quattrini, F. Angelucci, V. Coviello, W.K. Oh, T.K.Q. Ha, Z.H. Németh, G. Haskó, C. Blandizzi. *Int J Mol Sci – 2021, 22(12), 6325.*

[5] **Salivary proteome changes in response to acute psychological stress due to an oral exam simulation in university students: effect of an olfactory stimulus.** *L. Zallocco*, L. Giusti, M. Ronci, A. Mussini, M. Trerotola, M.R. Mazzoni, A. Lucacchini, L. Sebastiani. *Int J Mol Sci – Molecular Biology, 2021, 22(9), 4295.*

[6] **Antioxidant and neuroprotective activity of extra virgin olive oil extracts obtained from Quercetano cultivar trees grown in different areas of the Tuscany region (Italy)** M.C. Barbalace, *L. Zallocco*, D. Beghelli, M. Ronci, S. Scortichini, M. Digiacomo, M. Macchia, M.R. Mazzoni, D. Fiorini, A. Lucacchini, S. Hrelia, L. Giusti, C. Angelonii. *Int J Mol Sci – Antioxidants, 2021, 10(3), 421.*

[7] **Pro64His (rs4644) polymorphism within galectin-3 is a risk factor of differentiated thyroid carcinoma and affects the transcriptome of thyrocytes engineered via CRISPR/Cas9 system.** A. Corrado, R. Aceto, R. Silvestri, I. Dell'Anno, B. Ricci, S. Miglietta, C. Romei, R. Giovannoni, L. Poliseno, M. Evangelista, M. Vitiello, M. Cipollini, S. Garritano, L. Giusti, *L. Zallocco*, R. Elisei, S. Landi, F. Gemignani. *Thyroid J, 2020 Dec 14.*

[8] **Toward Patient-Tailored Therapy in Agonist Opioid Treatment: The Role of Psychopathology, Craving Behavioural Covariates, Stress Reaction and Methadone Blood Concentration. A Case Series** A.G.I Maremmani, S. Bacciardi, I. Maremmani, F. Della Rocca, F. Lamanna, C. Socci, E. Cerrai, *L. Zallocco*, L. Cerniglia, S. Cimino, L. Giusti, A. Lucacchini, M. Protti, L. Mercolini, G. Perugi, and M.R. Mazzoni. *Heroin Addict Relat Clin Probl, 2020, 22(6), 57-72.*

ACKNOWLEDGEMENTS